
UNIVERSITÀ DEGLI STUDI DI SALERNO


**UNIVERSITÀ DEGLI STUDI DI SALERNO**
**Dipartimento di Farmacia**

PhD Program
in **Drug Discovery and Development**
XXX Cycle — Academic Year 2017/2018

# *PhD Thesis in*

# *Design, synthesis and biological evaluation of new small-molecule modulators of protein lysine methyltransferases (PKMTs)*

Candidate

*Donatella Rescigno*

Supervisor

Prof. Dr. *Sabrina Castellano*

PhD Program Coordinator: Prof. Dr. *Gianluca Sbardella*

# INDEX

# ABSTRACT

Histone lysine methyltransferases have crucial roles in a number of biological processes and human diseases by controlling gene expression and chromatin state. Within this family, the lysine methyltransferase G9a has emerged as critical player in several pathologic states, particularly because of its important role in the silencing of tumor suppressor genes and in the regulation of other chromatin events. The low number of G9a chemical probes suitable for cell-based and animal studies, as well as the limited chemical diversity demand for the development of new modulators.

In this thesis, two different approaches aimed at the identification of novel chemotypes for the modulation of G9a are presented. On one hand, from a medicinal chemistry prospective, we considered the modification of the central core of the potent and selective inhibitor UNC0638, resulting in a 1,4-benzodiazepine derivative **EML741**. To validate the approach, we designed and synthesized a small set of ring-expanded derivatives and tested their activity *in vitro*. Peptide-based biochemical assays (AlphaLISA) validated our design, as compound **EML741** preserves the activity of the parent compound. In fact, **EML741** is a G9a competitive inhibitor with respect to substrate endowed with potent activity and selectivity. In addition, **EML741** showed favorable physico-chemical properties as it is quite soluble and chemical stable in aqueous media, and exhibited a membrane permeability profile (PAMPA and PAMPA-BBB) better than the parent compound UNC0638.

The second approach was aimed to explore a high-diversity chemical space, generating a reporter cell line that enhance the expression of a fluorescent protein as result of chromatin changes provoked by G9a inhibition. By means of lentiviral infection, a construct encoding for a blue fluorescent protein (BFP) was integrated in the background of the human KBM7 cell line, in genomic *loci* whose chromatin organization is regulated by G9a activity. Two cell lines were selected and their specificity to detect G9a inhibition was preliminary evaluated. The validation of

these cell lines is still ongoing. When completed, this reporter could be used both in chemical and genetic screens.

# CHAPTER 1

# INTRODUCTION

## 1.1 Epigenetic

Genetic mechanisms alone cannot explain why cells of multicellular organisms, that have the same set of genetic instructions, become highly specialized to perform different functions.

In 1942, Conrad Waddington coined the term *epigenetics* to define the "causal interactions between genes and their products which bring the phenotype into being".[1] The word etymologically derives from the Greek επί (epì) γεννετικός (genetikòs) and literally means "above or beyond genetics". Over the years, the concept of *epigenetic* has been continuously expanded and revised.[2] To date, *epigenetics* refers to all the mechanisms that work in addition to the DNA template to regulate and perpetuate gene expression programs and thereby canalize cell-type identities.[3] Epigenetic modifications can be accumulated during a lifetime, but also transmitted to the offspring, even if mechanisms behind such heritability are often unclear.[4] In addition to stable marks, some epigenetic modifications are highly flexible and easily reversed to respond to environmental stimuli.[5]

## 1.2 The genome organization

Eukaryotic cells package their genome in the form of a DNA-protein complex known as *chromatin*. Besides the packaging role, the chromatin organization allows a cell to fine control the accessibility of different genomic regions for transcription, recombination, DNA repair and replication.[6] The basic packaging element of chromatin is the *nucleosome*, which consists of 146 base pairs of DNA wrapped around an octameric protein complex, made up of four highly basic proteins named histones (H2A, H2B, H3, and H4). Histones, bearing positively charged residues, are able to interact with the negatively charged DNA phosphate backbone (Figure 1.1).[6-7]

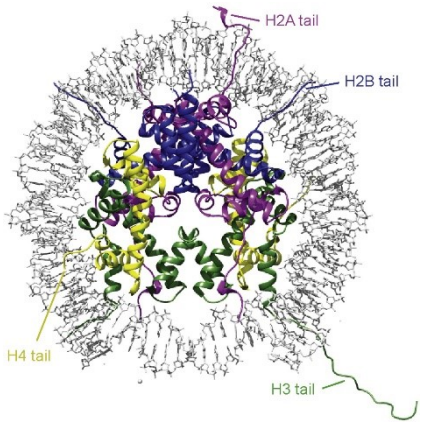


**Figure 1.1** Structure of the nucleosome core particle. Picture adapted from Setiaputra, D. *et al*., *BBA-Proteins Proteomics* **2017**, *1865*, 1613-1622.

At the molecular level, epigenetic control of gene expression involves covalent and reversible post-synthetic modifications of DNA and histone proteins. These modifications, together with non-coding RNAs (ncRNAs), histone variants and nucleosome remodelers, can induce changes in chromatin structure, resulting in transcriptional regulation without altering the underlying DNA sequence.[8] In other terms, epigenetic modifications label specific genomic regions to recruit different chromatin-binding proteins, ultimately resulting in cellular reprogramming and response to the environment (cellular plasticity).[3]

## 1.3 Histone modifications

Since Allfrey's pioneering studies in the mid-1960s highlighted histones post-translational modifications (PTMs), major discoveries have uncovered their key role, in addition to DNA methylation, in carrying information that can distinguish transcriptionally active or silent chromatin states.[9]

Histone PTMs include acetylation, methylation, phosphorylation, ubiquitinylation, sumoylation, ADP ribosylation, and deamination. These modifications mainly occur on the N-terminal regions (tails) of the histones, which protrude from the nucleosome and are accessible to the epigenetic machinery (Figure 1.2). Epigenetic marks can either affect the chromatin structure by merely

being there, but also influencing inter-nucleosomal interactions and recruiting remodeling enzymes, thus changing the overall chromatin architecture.[10]

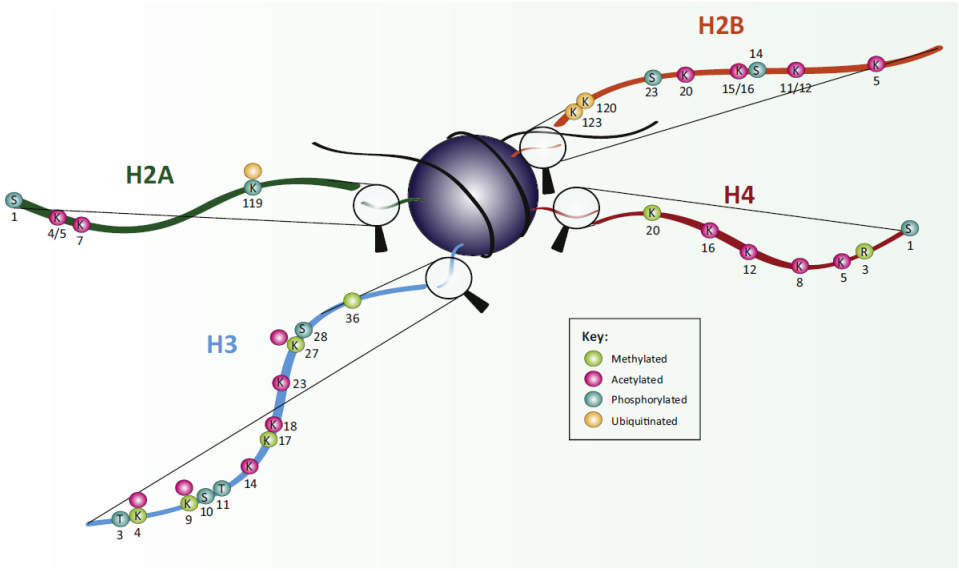


**Figure 1.2** Post translational modifications on the histone tails. Picture adapted from Lawrence, M. *et al*., *Trends Genet.* **2016**, *32*, 42-56.

Histone modifying proteins are usually categorized as *writers*, *readers* and *erasers* (Figure 1.3).[11] Epigenetic writers, such as histone acetyltransferases (HATs), histone methyltransferases (HMTs) and kinases, catalyze the addition of epigenetic marks on amino acid residues on histone tails. Epigenetic readers, such as proteins containing bromodomains, chromodomains and Tudor domains, are "effector proteins" that recognize and bind to epigenetic marks, and consequently recruit various components of the nuclear signaling network to chromatin. Lastly, when epigenetic marks are no longer needed, they can be removed by epigenetic erasers, such as histone deacetylases (HDACs), histone demethylases (HDMs) and phosphatases. The complex interplay of these three classes of proteins results in a tight regulation of gene activity and expression during development and differentiation, or in response to intra- or extracellular events.[7, 11]

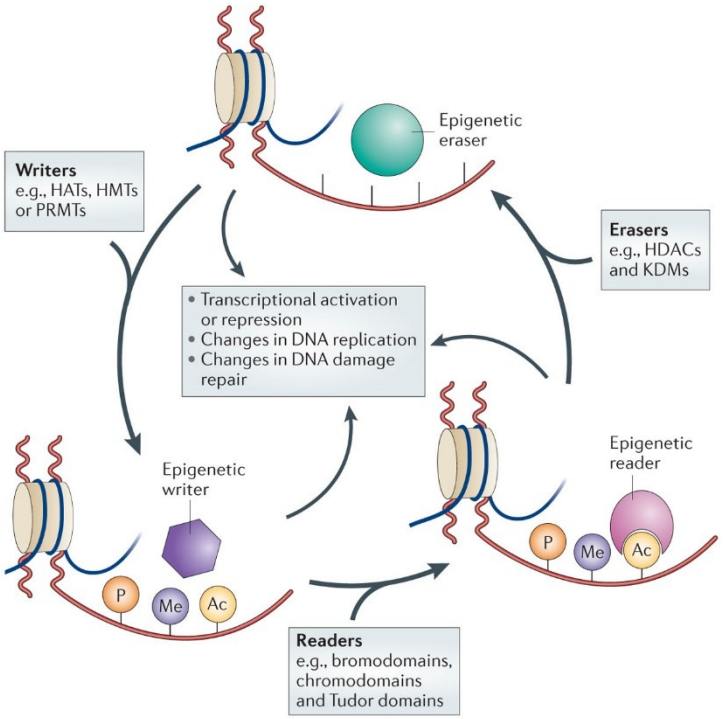


**Figure 1.3** Epigenetic writers, readers and erasers. Picture adapted from Falkenberg, K. J. *et al*., *Nat. Rev. Drug Discovery* **2014**, *13*, 673-691.

## 1.4 Histone methylation

Among epigenetic marks, methylation of histone proteins constitutes a highly complex control system directing diverse functions of the genome. Histone methylation state is tightly regulated by an intricate system made up by a large number of site-specific methylases (HMTs), demethylases (HDMs) and methyl reader proteins.[12]

Histone methylation mainly occurs at lysine and arginine side chains. For this reason, HMTs are generally classified as protein Lysine Methyltransferases (KMTs) and protein Arginine Methyltransferases (RMTs). The number of methyl groups that can be incorporated into a specific residue is different and can confer unique transcriptional, and therefore phenotypic, effects on cells. Thus, the ε-amino group of lysines can be mono-, di-, or trimethylated, while the guanidine nitrogen of arginine residues can accommodate one (ω-$N^G$-monomethyl arginine (MMA)) or two methyl groups in an asymmetric or symmetric manner (ω-$N^G$,$N^G$-

asymmetric dimethyl arginine (ADMA) and ω-$N^{G}$,$N'^{G}$-symmetric dimethyl arginine (SDMA)) (Figure 1.4). According to the case, the addition of more than one methyl group can be carried out in a processive or distributive manner.[13]

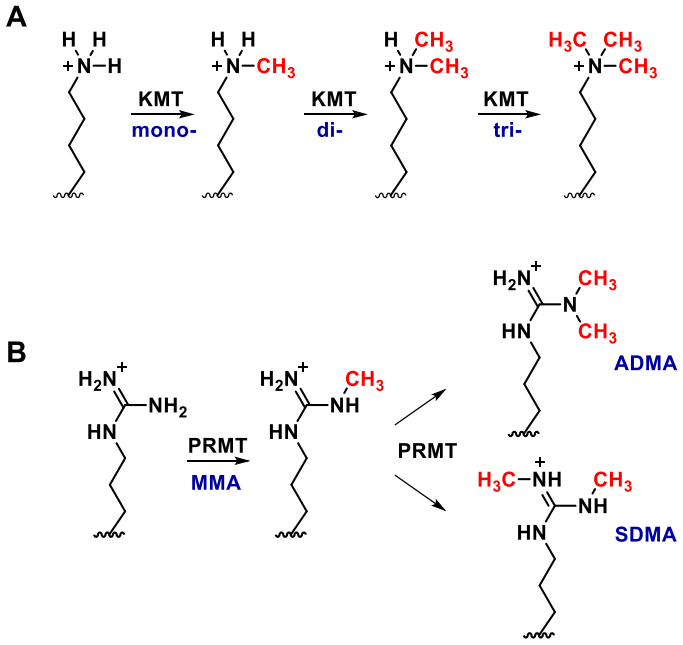


**Figure 1.4** Lysine (A) and arginine (B) methylation states.

The human genome encodes more than 60 PMTs including 9 known protein arginine methyltransferases (PRMTs) and >50 protein lysine methyltransferases (PKMTs).

The catalytic mechanism is common to both families and consists of $S_N2$ transfer of a methyl group from the universal methyl donor S-adenosyl-L-methionine (SAM or AdoMet) to the nitrogen atom(s) of a lysine or arginine residue, generating the methylated histone product and S-adenosyl-L-homocysteine (SAH or AdoHcy, Figure 1.5).[13-14]

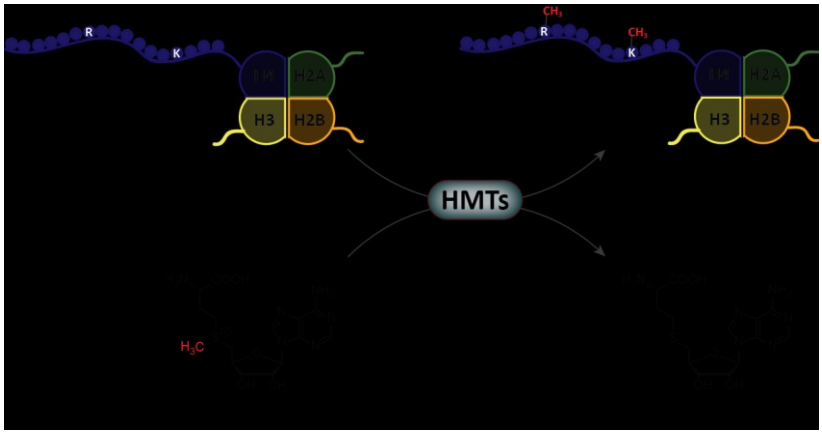


**Figure 1.5** Generic $S_N2$ methyl transfer reaction from SAM to the amino-acid side-chain nitrogen of a lysine/arginine residue on histones tails.

Unlike other epigenetic modifications, such as acetylation or phosphorylation, methylation of both arginine and lysine residues does not neutralize or alter the amino acid charge. Therefore, the effect of chromatin remodeling is not due to an alteration of the electrostatic interactions between DNA and histone proteins. Instead, methyl marks act as recruiting sites for proteins that compact nucleosomes together or engage additional regulatory proteins to the methylation site, mediating a variety of downstream effects. Hence, each type of mark is a specific signal that is recognized by highly evolved methyl binding domains, resulting in either transcriptional activation or repression.[15-16]

Additionally, it has been now widely demonstrated that arginine/lysine methylation also occurs on various non-histone substrates, resulting crucial for the regulation of their activities. Among these, there are key components of several cellular signaling pathways, such as nuclear factor-kappa B (NF-κB), the epidermal growth factor receptor (EGFR), as well as the tumor suppressor p53 or the estrogen receptor (ER).[17-20]

Hence, a dysregulated activity of histone methylation modifiers can lead to altered expression patterns of oncogenes or tumor suppressor genes, as well as to an altered methylation state of effector proteins, thus resulting in aberrant cellular signaling cascades and cellular transformation.[17] Therefore, proteins governing this

modification are of substantial interest from the perspective of medicinal chemistry and drug discovery.[12, 15]

### 1.5 Protein lysine methyltransferases (PKMTs)

In 2000, Jenuwein and co-workers reported the identification of the first histone lysine methyltransferase. Since then, many other relevant discoveries, together with technological advances, have deeply elucidated the biological importance of histone lysine methylation, and, therefore, of proteins governing this modification.[21]

With the exception of DOT1L (*Disruptor of telomeric silencing 1-like*), the catalytic activity of lysine methyltransferases is located in an approximately 130 amino acid-long conserved domain called the SET domain. The SET domain was first recognized as a conserved sequence in three *Drosophila melanogaster* proteins: a modifier of position-effect variegation, *Su(var.)3−9* (the suppressor of position-effect variegation 3−9),[22] the Polycomb-group chromatin regulator *En(zeste)* (Enhancer of zeste),[23] and the homeotic gene regulator *Trithorax*.[24] Differently from other SAM-dependent enzymes, in SET domain-containing proteins the binding sites for the histone substrate and the cofactor are located on opposite sides of the domain and are connected through a deep channel. It has been proposed that this particular arrangement consent the processive methylation lysine residues.[25]

Besides this common feature, SET domain KMTs display low sequence similarity and the residues at the active site are not all conserved, thus explaining their high substrate specificities.[26] Moreover, these enzymes exhibit a different product specificity, defined as the number of methyl group transferred to the substrate (Figure 1.6).[27] Importantly, have been recently identified many other SET domain-containing proteins that exclusively methylate non-histone substrates and do not appear to target histones directly. Moreover, in many proteins the SET domain co-occurs with multiple other domains.[28]

Histone lysine methylation mainly arises on histones H3 and H4. In particular, five lysine residues are located on H3/H4 tails, while one site of methylation is placed on H3 globular core.[16] Lysine methylation has been implicated in both transcriptional activation (H3K4, H3K36, H3K79) and silencing (H3K9, H3K27, H4K20). Apart from the residue modified, also the degree of methylation is responsible of the different outcomes.[29]

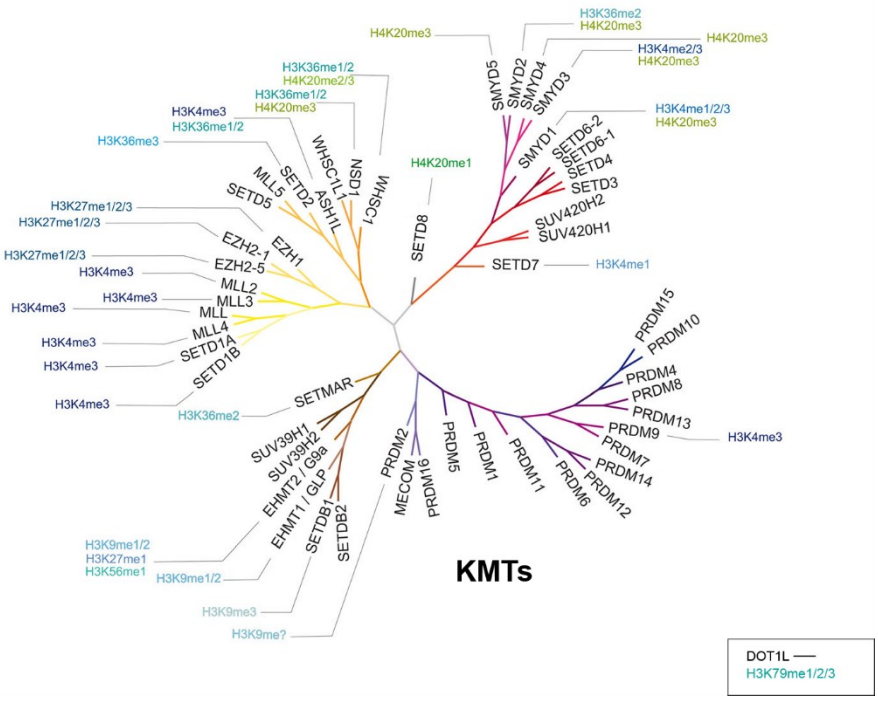


**Figure 1.6** Phylogenetic tree of KMTs. Picture modified from Milite, C. *et al*., *Clinical Epigenetics* **2016**, *8,* 1-15.

## 1.6 KMTs in health and disease

In the wide *scenario* of histone modifications, lysine methylation has attracted increasing attention because of its crucial regulatory role in important nuclear processes including transcription, cell cycle control and DNA damage response.[30-32] The physiological roles and the links to disease states of this epigenetic mark will be examined below.

### *1.6.1 The physiological role of KMTs*

The number of targetable histone lysine residues and the degree of methylation on each methylation site generate an extremely complex collection of potential functional outputs. This picture is actually even more complex, because histone methylation marks exert their activity cooperatively with other types of histone modifications (epigenetic cross-talk).[33]

Repressive methylation marks (H3K9, H3K27, H4K20) are essential for the X chromosome inactivation process,[34] transcriptional silencing of euchromatic genes,[35] as well as for the establishment and maintenance of highly condensed (heterochromatic) regions, such as centromeres.[36]

Instead, transcriptionally competent euchromatin is characterized by methylation on different residues, e.g. H3K4, H3K36 and H3K79. At chromosome level, specific histone methylation marks accomplish the establishment of permissive euchromatin by preventing silencing mechanisms to be carried out, such as binding of repressive complex or deposition of silencing marks. Furthermore, at gene level, lysine methylation is associated with the transition from transcription initiation to productive elongation stage.[32, 37]

Moreover, lysine methylation is important for the regulation of early steps in the replication processes,[38] as well as in DNA damage response.[39]

The biological importance of lysine modifying enzymes is even greater considering as their role in the regulation a number of non-histone proteins has a wide-ranging impact over a growing amount of cellular processes and disease states. Mono-, di- or trimethylation of non-histone substrates can positively or negatively affect protein stability, influence protein-protein interaction or, in some cases, subcellular localization.[20] In addition, again the crosstalk with other PTMs has to be taken into account. For example, one of the most studied non-histone protein that is regulated by lysine methylation is the well-known tumor suppressor p53. This protein bears at least four distinct lysine methylation sites in the C-terminal region (K370, K372, K373 and K382). Both the position of the methylated lysine residues and the methylation state (e.g., mono- or dimethylation) influence

p53 activity, allowing the fine-tuning of p53 functions in homeostatic conditions or stress responses.[40]

### *1.6.2 The pathological role of KMTs*

Is now clear that dynamic chromatin modifications are a mean by which cells establish the appropriate epigenetic homeostasis. Thus, the importance of the fine regulation of histone methylation is continuously evidenced by emerging links between histone methylation and disease states or ageing.[41-43] In fact, a growing amount of evidences indicates that the alteration of global histone methylation as well as the loss or gain of specific methyl marks have a role in a number of cancers, correlating with tumor phenotype, patient outcome and prognostic factors.[44-46] For example, the H3K27me3 methyltransferase EZH2 is up-regulated in a number of cancers, including breast and prostate cancer.[47] In the same way, activating point mutations in EZH2 have recently been identified and are associated with B cell lymphomas.[48] On the other hand, mutations that cause a loss of methyltransferase activity of EZH2 have been recognized in myelodysplastic syndromes, supporting the view that EZH2 functions as a tumor suppressor in that cancer type.[49]

Another noteworthy example of a histone methyltransferase involved in tumorigenesis is the H3K4 methyltransferase MLL1 (*Mixed-Lineage Leukaemia 1*). Thus, the *MLL* (also known as *ALL-1* and *KMT2A*) gene rearrangement is one of the most common chromosomal abnormalities in human leukaemia, resulting mutated in almost 80% of infant leukaemia and 5-10% of adult acute myeloid and lymphoid leukaemia.[50]

Dysregulation of histone methylation is also implicated in a number of neurodevelopmental disorders, including intellectual disabilities, autism, schizophrenia, and other conditions of importance, for instance Huntington's disease.[51-54]

Furthermore, aberrant activity of lysine modifying enzymes is associated with inflammation[55] and autoimmune diseases,[56] cardiovascular diseases[57-58] and diabetes complications.[59]

## 1.7 Euchromatin histone methyltransferase 2: G9a

The *Euchromatin Histone Methyltransferases* (EHMTs) are a subfamily of KMTs responsible of mono- and dimethylation of lysine 9 on histone H3 (H3K9me1, H3K9me2). In mammals, there are two EHMT proteins: G9a, encoded by *EHMT2*, and GLP (*G9a-like protein*), encoded by *EHMT1*. The name comes from the fact that H3K9me2 is frequently associated with repression of genes located in euchromatic regions.

EHMTs G9a and GLP share 80% sequence identity in their respective SET domains. They are characterized by the presence of an N-terminal SET and Pre-SET domain, preceded by a series of ankyrin (ANK) repeats, that serve as methyllysine binding module (protein-protein interaction).[60-61]

Initial studies showed that *in vivo* G9a and GLP form a stoichiometric heteromeric complex, *via* their SET domain, cooperatively carrying out H3K9 methyltransferase function.[62] Nevertheless, further surveys revealed that G9a and GLP have different pathophysiological functions, also displaying distinct tissue-specific expression profiles.[61, 63-64] Moreover, transcriptomic analysis shows that these two proteins regulate different sets of genes.[65]

### *1.7.1 The physiological role of G9a*

As mentioned above, G9a (EHMT2 or KMT1C) catalyze mono- and dimethylation of lysine 9 of histone H3 and, to a lesser extent, monomethylation of lysine 27 of histone H3 (H3K27me1). In particular, two residues of tyrosine are of essential for the catalytic activity (Tyr1154) and H3K9 substrate specificity (Tyr1067).[66] Moreover, recently G9a was reported as the enzyme responsible of the monomethylation of the lysine 56 of histone 3 (H3K56me1). This mark serves as

chromatin docking site for the replication processivity factor PCNA, preceding its function in DNA replication.[67]

During the development, G9a is ubiquitously expressed in all cell types and carries out important functions in the biological processes associated with gene regulation, including embryogenesis,[68] germ cell development,[69] immune response,[70] neural development and brain function.[71-72] At a molecular level, G9a is essential for transcriptional repression,[73-74] gene imprinting,[75] provirus silencing,[76] and DNA methylation.[76-78]

Almost all these functions are dependent on H3K9 methylation, nevertheless, like other methyltransferases, G9a methylates also a *plethora* of non-histone targets.[79-80] The first identified non-histone substrate of G9a was G9a itself: autocatalytic G9a methylation recruits the epigenetic regulator heterochromatin protein 1 (HP1), thus enhancing the silencing of gene transcription.[81] Among G9a non-histone substrates, there are several transcription factors, whose methylation usually results in their inactivation and consequent silencing of the target genes.[82-83] Of note, dimethylation of lysine 373 by G9a/GLP maintains the transcription factor p53 in an inactive state, thus inhibiting its function as tumor-suppressor.[84]

### *1.7.2 The pathological role of G9a*

As mentioned above, mutations in the epigenetic machinery and the resulting altered placement of epigenetic marks are frequently involved in various pathological conditions. Therefore, a deep understanding of epigenetic phenomena and their alterations in diseases has become a priority in biomedical research, especially because, unlike genetic alterations, epigenetic aberrations are reversible.[15, 85]

In the past years, numerous studies have provided evidences that link an aberrant activity of G9a to human diseases. Primarily, G9a is overexpressed in various human cancers, including leukaemia,[86-87] prostate carcinoma,[84] hepatocellular carcinoma[88] and lung cancer.[89]

Moreover, G9a plays a role in neurodegeneration induced by either ethanol and cocaine addiction,[90-91] mental retardation,[92-93] inflammatory diseases[94-95] and maintenance of HIV-1 (Human Immunodeficiency Virus type 1) latency.[96]

### *1.7.2.1 A specific role for G9a in medulloblastoma (MB)*

Of particular interest, a recent work by the group of Prof. Vidya Gopalakrishnan (University of Texas, MD Anderson Cancer Center, Houston, Texas) in collaboration with our research group, proved the role of G9a in human medulloblastoma (MB).[97] MB is the most malignant pediatric brain tumor, also named *cerebellar primitive neuroectodermal tumor* (PNET) because it origins in a region of the brain at the base of the skull, called the *posterior fossa*. Unlike most brain tumors, MB rapidly metastasizes *via* the cerebrospinal fluid.[98] To date, it is still a leading cause of cancer-related deaths in children. Current therapy is not specific for this tumor, basically relying on chemotherapy, craniospinal irradiation and surgery. More importantly, whilst the number of survivors after diagnosis and treatment is growing, the well-documented poor quality of that survivorship has extended the concept of cure to include improvements of long-term cognitive outcome.[99-100] The aforementioned study pointed out that G9a inhibition has the potential for therapeutic applications in MB. In fact, previous works had shown that the *RE1* Silencing Transcription Factor (REST) signaling pathway was aberrantly activated in over 80% of MBs and associated with poor prognostic significance in patients.[101] REST-dependent maintenance of tumor cell proliferation is mediated by an ubiquitin-specific protease (USP), USP37, that is downregulated in high-REST expressing MBs as result of REST aberrant activity. USP37 is essential for the stabilization of the cyclin-dependent kinase inhibitor (CDKI), p27. The failure to stabilize p27 directly endorse deregulated cell proliferation.[102] USP37 silencing is mediated by a significative increase of level of trimethylation of histone H3K9 at *USP37* promoter, a mark deposited by G9a following REST recruitment. It has been demonstrated that inhibition of G9a activity by means of small-molecules restores USP37 expression and its tumor-suppressive activity, resulting in medulloblastoma growth arrest in mouse orthotopic models (Figure 1.7).

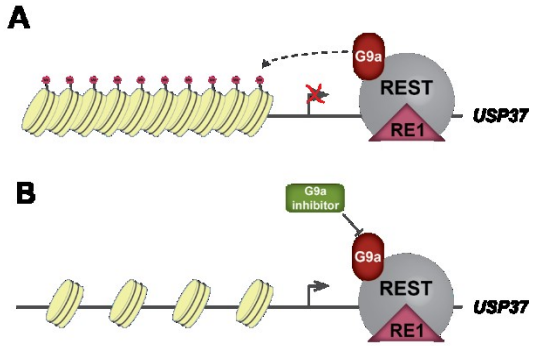


**Figure 1.7** Model to summarize the effect of G9a inhibition on USP37 gene expression. **A**, REST binds to a *RE1*-binding site on the *USP37* promoter and recruits G9a that catalyze di- and trimethylation of histone H3K9, resulting in gene silencing; **B**, G9a inhibition by means of small-molecule reestablishes USP37 expression. Picture modified from Dobson, T. *et al*., *Mol Cancer Res* **2017,** *15*, 1073-1084.

## 1.8 G9a as relevant drug target

Given the role of G9a in diverse biological processes, the development of specific G9a inhibitors has been increasingly pursued over the years and is currently the focus of many research groups.[103]

G9a inhibitors so far described in literature are usually categorized in two classes: molecules belonging to the Class I bind to the substrate pocket while Class II inhibitors are binders of the SAM pocket. In the following sections, these two classes will be briefly reviewed.

### *1.8.1 Binders of the SAM pocket (Class II)*

A small number of compounds bears to the Class II inhibitors. In fact, there has been restricted focus on developing SAM competitive inhibitors because of the intrinsic limit of these compounds to be able to bind others SAM-dependent enzymes.

The first inhibitor of the class is a member in an epidithiodiketopiperazine (ETP) family of alkaloids, named chaetocin (Figure 1.8). Originally, chaetocin was

reported as the first inhibitor of a lysine-specific histone methyltransferase and specific for the methyltransferase SU(VAR)3−9 both *in vitro* and *in vivo*.[104] Some years later, Iwasa *et al.* published the first total synthesis of natural (+)-chaetocin and its enantiomer and reported that both compounds effectively inhibited G9a ($IC_{50}$ = 2.5 and 1.7 μM, respectively).[105] Subsequently, simplified analogues of chaetocin have also been reported, such as PS-ETP-1 (Figure 1.8).[106] Nevertheless, the low selectivity, together with the hypothesized covalent mechanism of inhibition,[107] support the view that chaetocin and its related compounds are not suitable for investigating biological functions of G9a.

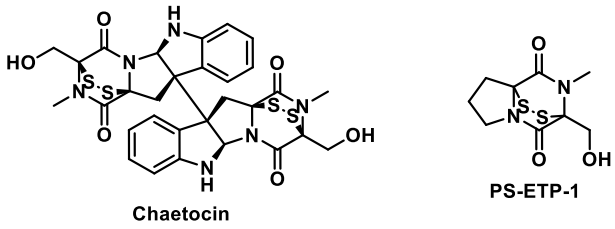


**Figure 1.8** Class II G9a inhibitors: Chaetocin and a simplified analogue.

In 2012, Yuan and co-workers reported the discovery of BRD9539 (Figure 1.9) by synthesizing a focused library of 2-substituted benzimidazoles inspired by the isoform selectivity exhibited by certain inhibitors of kinases and histone deacetylases.[108] BRD9539 inhibits G9a with an $IC_{50}$ of 6.3 μM, while no data were reported for GLP. Moreover, they also described the methyl ester BRD4770 (Figure 1.9) as "pro-drug" form of BRD9539 for cell-based assays.

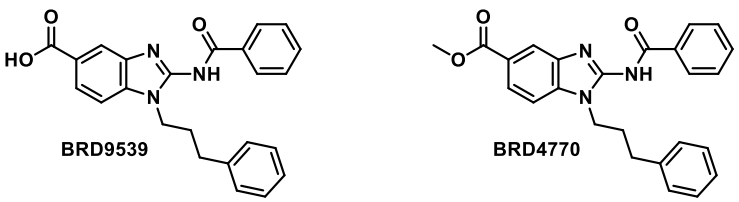


**Figure 1.9** Class II G9a inhibitors: Benzimidazoles.

The last subgroup of Class II inhibitors consists of sinefungin analogues (Figure 1.10). Sinefungin is a natural product, isolated from *Streptomyces incamatus* and *S. griseolus*, structurally closely related to SAM (it has an amino methylene group instead of the methylated sulfonium group) and known as broad-spectrum "pan" methyltransferase inhibitor.[109-111] Some cycloalkane sinefungin analogues are able to inhibit both G9a and GLP at micromolar potency, also effecting on three other methyltransferases (DNMT1, PRMT1 and SET7/9).[112-113] The effect on other methyltransferases was not evaluated.

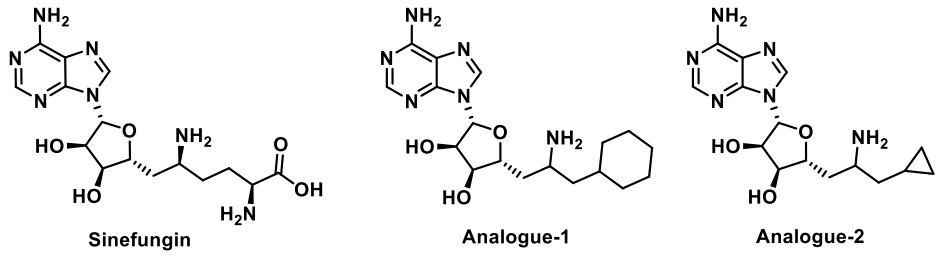


**Figure 1.10** Class II G9a inhibitors: Sinefungin and its analogues.

### *1.8.2 Binders of the substrate pocket (Class I)*

In 2007, Kubicek and co-workers identified, by a high-throughput screening (HTS) campaign, the first selective small-molecule inhibitor of G9a and GLP, BIX01294, and it was considered a major advancement in the PKMT inhibitor field (Figure 1.11 A).[114] In fact, BIX01294 was the first inhibitor with an interesting potency *in vitro* ($IC_{50}$ of 1.7 μM towards G9a and 38 μM towards GLP), combined with a good selectivity profile against several HMTs (up to 45 μM). Importantly, it was non-competitive for the cofactor and was also able in reducing H3K9me2 levels *in vivo*. In their study, the inhibition of GLP by BIX01294 was measured under oversaturated reaction conditions, where almost all the substrate was converted into the trimethylated product (H3K9me3). In a following study by Chang and co-workers, using the same linear assay conditions for both G9a and GLP, BIX01294 resulted slightly more potent for GLP ($IC_{50}$ = 0.7 μM) than for G9a ($IC_{50}$ = 1.9 μM). Moreover, they also report the crystal structure of the GLP

SET domain in complex with BIX01294 and SAH (PDB code 3FPD), which confirm that the inhibitor binds to the substrate binding groove.[115]

The main drawback of BIX01294 was the low activity-toxicity *ratio* in cells, that limited its use as chemical probe. Using BIX01294 as lead compound, Liu *et al.* extensively explored multiple regions of the quinazoline core, discovering, in 2009, a derivative named UNC0224 (Figure 1.11 A),[116] which was markedly more potent in several biochemical and biophysical assays ($IC_{50}$= 15 nM). In fact, the 7-dimethylaminopropoxy chain of UNC0224 interacts with the lysine binding channel, strongly increasing the potency. Focused efforts of structure-based design led to the identification of E67[117], E72,[117] UNC0321[118] and UNC0646 (Figure 1.11 A).[119] Despite the strongly improved G9a enzymatic inhibition profile ($IC_{50}$ in the *low* nM range), these molecules suffer of a poor cellular activity, mostly due to the relatively high polarity and consequent low cell membrane permeability.

Further efforts, in order to improve physicochemical properties while preserving high *in vitro* potency, led to the discovery of UNC0638 (Figure 1.11 A), by Vedadi and co-workers, in 2011. This compound was described as the first G9a and GLP cellular chemical probe, characterized by balanced *in vitro* potency, aqueous solubility, and cell membrane permeability.[120] UNC0638 has an excellent selectivity profile, resulting more than 200-fold selective for G9a and GLP over 16 other methyltransferases and epigenetic targets and at least 100-fold selective over other non-epigenetic proteins. More interestingly, UNC0638 retains the good activity in cell-based assays, together with an excellent functional potency/toxicity *ratio*.

Finally, another optimization attempt of this chemical series resulted in the discovery of UNC0642 (Figure 1.11 A), a close analogue of UNC0638, that similarly exhibited high *in vitro* potency, excellent selectivity and robust on-target activities, and also showed good *in vivo* pharmacokinetics properties in mouse model. Nevertheless, to date UNC0638 is the most used G9a chemical probe both in biological and pharmacological studies.[97, 121-126]

Despite scientific advancements, these remarkable efforts in improving quinazoline derivatives have not been combined with the identification of new

valuable scaffolds as G9a inhibitors. Besides the bioisosteric replacement of the central quinazoline ring of with a quinoline one (Figure 1.11 B),[127-128] only the spiro(cyclobutane-1,3′-indol)-2′-amine derivative A366 (Figure 1.11 C) shares the same potency and mechanism of inhibition of the BIX-derivatives, despite its low structure similarity.[129] However, this scaffold was not further developed and also any structural modification described in the same paper led to substantial decrease in potency.[129] Furthermore, A366 has recently been reported as inhibitor of the epigenetic reader protein Spindlin1-H3K4me3 interaction and also in this case even minor structural modifications of A366 entail activity reduction.[130] These data hang a question mark over A366 reliability as valuable lead compound.

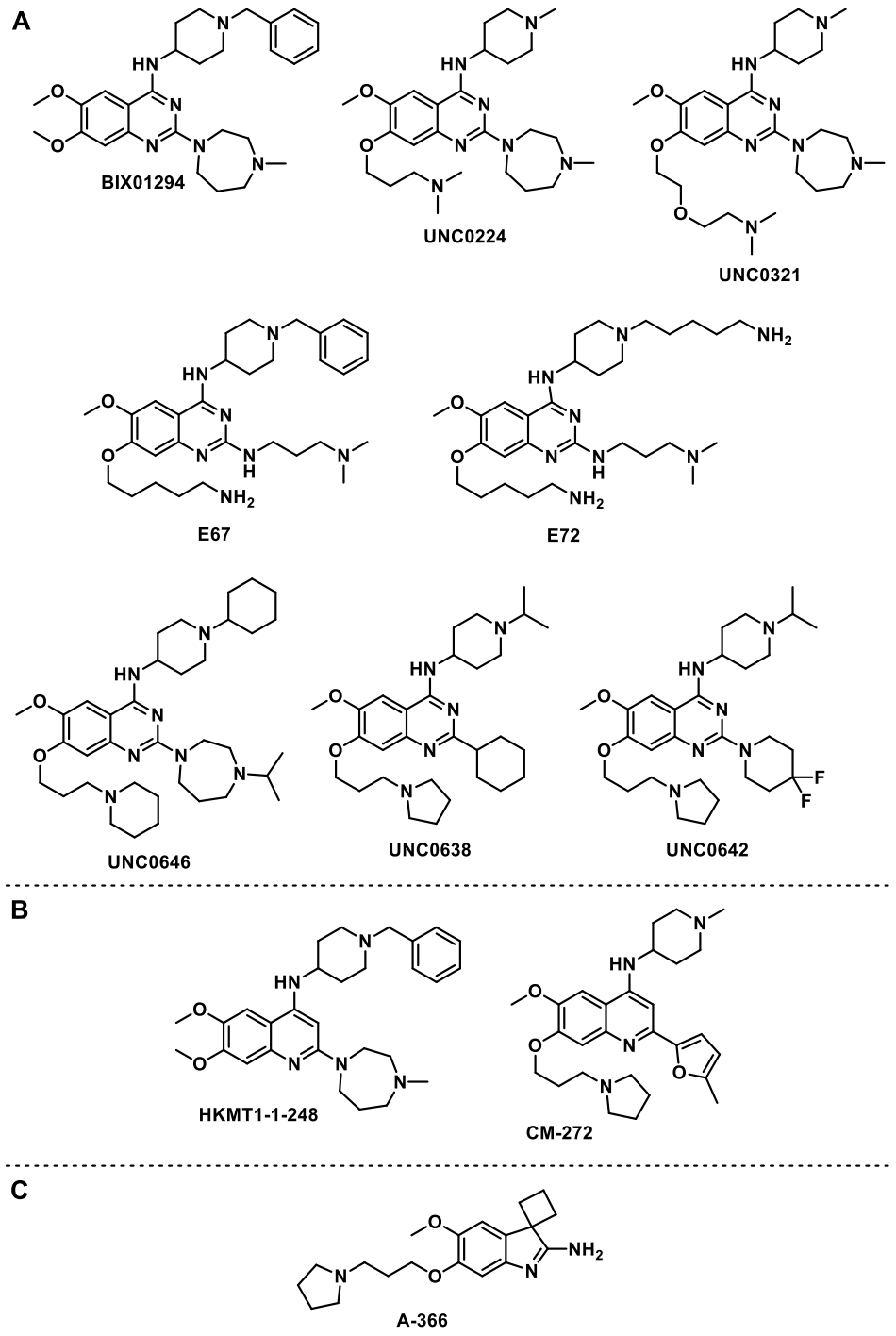


**Figure 1.11** Class I G9a inhibitors.

# CHAPTER 2

# AIM OF THE WORK

As described in Paragraph 1.8, several G9a/GLP inhibitors have been identified over the last few years. Nevertheless, the number of compounds that meets the requisite of a good chemical probe is very low.[103, 131]

Above all, the chemical diversity of current available G9a inhibitors is extremely limited. A successful drug discovery strategy relies on the optimization of a large number of variables ranging from strictly physicochemical parameters (e.g. solubility, hydrogen bonding, logP), to more complex factors, for instance related to toxicity and bioavailability among others.[132] Therefore, it is essential to start with a broad set of promising leads in order to identify drug candidates with the desired properties.

In this regard, my PhD project was aimed to identify novel chemical entities endowed with good affinity towards G9a by means of two different approaches, the first relying basically on a medicinal chemistry perspective and the second on a biological one. The latter was performed at the Research Center of Molecular Medicine (CEMM), in Vienna, during a 6-month period abroad entailed by my PhD Program.

## 2.1 Scaffold-repositioning approach

A common medicinal chemistry strategy for discovering structurally novel chemotypes is the modification of the central core structure of a known active compound, while conserving key substituents.[133-134] A change of the central chemical template is often a means to overcome any undesirable property associated with the parent molecule (e.g., potency plateau, selectivity, pharmacokinetics, etc.). This approach resembles the principles of the so-called *scaffold hopping*. Commonly, the concept of *scaffold hopping* has consistently been linked to computational methods and virtual screening,[135] nevertheless meaningful scaffold replacements have been accomplished on the basis of chemical knowledge and intuition.[133]

Therefore, pursuing our efforts toward the identification of potent and selective histone lysine methyltransferases inhibitors, we chose the well-validated

chemical probe UNC0638 as lead compound and replaced the quinazoline moiety with a benzodiazepine framework (Figure 2.1). In particular, the insertion of a methylene unit into the quinazoline ring resulted in the ring-expanded 1,4-benzodiazepine derivative (**EML741**). It is worthwhile noting that the chemistry of the 3H-benzo[*e*][1,4]diazepine scaffold, which could be considered a "privileged structure motif",[136] had been only rarely investigated and, to best of our knowledge, never exploited in medicinal chemistry.

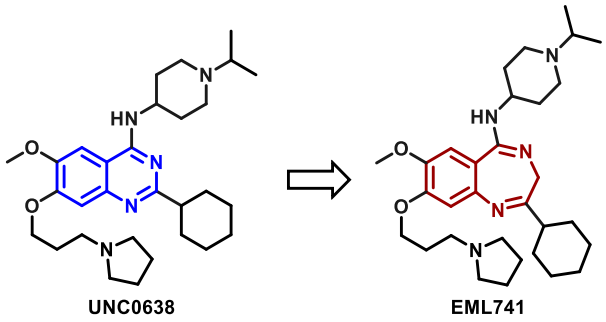


**Figure 2.1** Scaffold-repositioning hypothesis.

Before synthesis and screening, *in silico* pre-evaluation of our scaffold-repositioning hypothesis was performed in collaboration with Prof. Sandro Cosconati (DiSTABiF, University of Campania "Luigi Vanvitelli", Caserta, Italy).

### *2.1.1 Molecular Modeling Studies*

**EML741** was docked (AutoDock4)[137-138] into the structure of G9a to see whether it is able to recapitulate the interactions established by its parent compound (UNC0638) into the protein binding cavity (PDB code 3K5K). The docking study shows that, in principle, **EML741** is able to recapitulate the binding mode observed for UNC0638 at the G9a active site (PDB code 3RJW) and, in particular, the central 1,4-benzodiazepine scaffold may occupy the so-called "peptide binding groove", establishing a number of favorable hydrophobic interactions with the side chains of Leu1086, Ile1161, and Ala1077, with the cyclohexyl group pointing towards a negatively charged region (Asp1074 and Asp1078). The secondary amino group at the 4-position establishes a charged-reinforced H-bond with Asp1083. This

interaction is known to play a crucial role in increasing the inhibitory potency.[120] In addition, the aminoalkoxy moiety may fit into the lysine binding channel forming a H-bond with the backbone of Leu1086 and cation-π interactions with the aromatic side chains of Phe1087, Phe1152 and Tyr1154 (Figure 2.2).

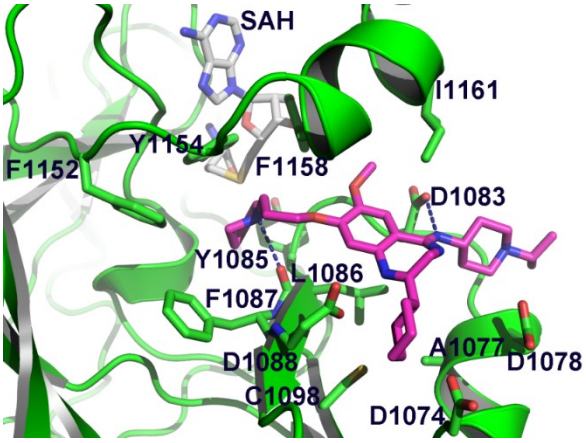


**Figure 2.2 EML741** docked conformation (pink) in G9a active site (green, PDB 3K5K). Important residues are labeled. H-bonds are shown in grey dashed lines.

These data are in agreement with those obtained with the recent published structure of G9a SET-domain PDB code 5VSE.[139] The Figure 2.3 A shows the G9a/**EML741** complex, while the superimposition of cocrystal ligand UNC0638 (pink) and **EML741** docked conformation (green) is depicted in panel B.

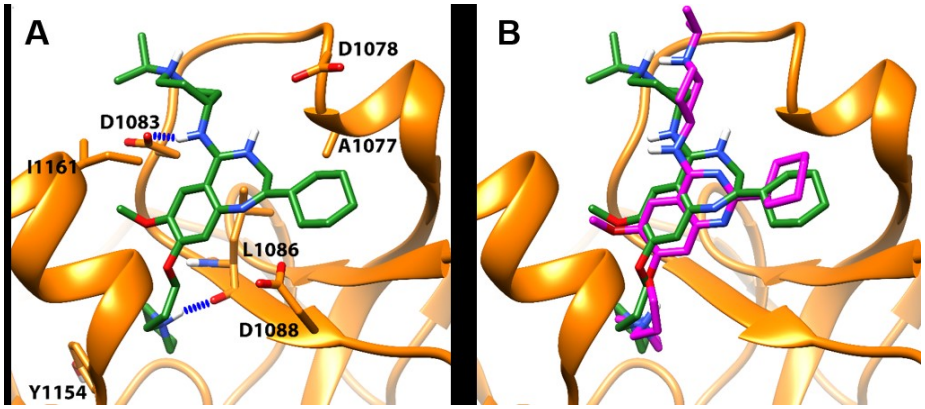


**Figure 2.3 A**, Superimposition of cocrystal ligand UNC0638 (pink) and **EML741** docked conformation (green) in G9a active site (orange, PDB 5VSE). **B**, G9a/**EML741** complex. Important residues are labeled. H-bonds are shown in blue dashed lines.

### *2.1.2 Ring-expanded 1,4-benzodiazepine derivatives*

Encouraged by the molecular modeling results, to validate the scaffold-repositioning hypothesis and to obtain early structure-activity relationships, we designed a small set of ring-expanded 1,4-benzodiazepine derivatives (Figure 2.4). In particular, the cyclohexyl moiety of **EML741** was replaced by a phenyl group (**EML693**), and to assess the importance of the central core geometry, 1,2-dihydro analogues were also considered (**EML698** and **EML696**).

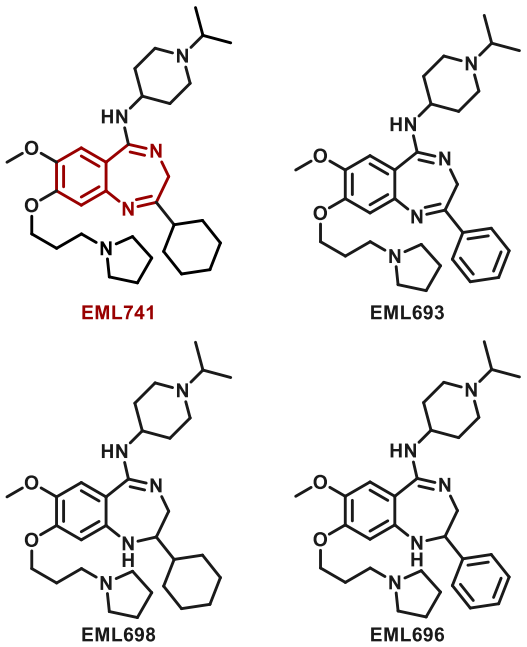


**Figure 2.4** Ring-expanded 1,4-benzodiazepine derivatives designed.

## 2.2 A cellular reporter for functional G9a inhibition

Systems cell biology has opened up the opportunity to study individual molecular targets in the context of their signaling and functional networks, giving the possibility of highlighting unknown links between molecular targets and disease. Advances in imaging technologies, as well as automated data processing and analysis, facilitated the implementation of biology approaches within HTS platforms.[140] In particular, the screening of libraries of small molecules, peptides or RNAi aimed to the identification of those that are able to modify the phenotype of a cell in a desired manner (High Content Screening, HCS) is a powerful tool for the modern drug discovery. In the past few years, the use of HCS increased in several stages of the drug discovery pipeline. Indeed, of the 22 drugs approved by the FDA (U.S. Food & Drug Administration) in 2016, 6 have been identified using HCS.[141]

The introduction of a DNA construct into a cell or an organism encoding, for example, for fluorescent or luminescent proteins (reporter gene) is widely used to monitor the cellular events associated with signal transduction and gene expression, both at the transcriptional or translational level.[142-143] In the contest of HCS,

fluorescent reporters can be a valuable tool to look for small molecules that alter gene expression patterns in a non-invasive manner, as the fluorescent signal can be real-time monitored.

For these reasons, we decided to establish a reporter cell line for the detection of G9a inhibition. Thus, I planned to spend my period abroad at the Research Center of Molecular Medicine of the Austrian Academy of Science, in the group of Dr. Stefan Kubicek, to learn the know-how and develop a cellular reporter able to activate the expression of a fluorescent marker following the chromatin remodeling induced by G9a inhibition (Figure 2.5).

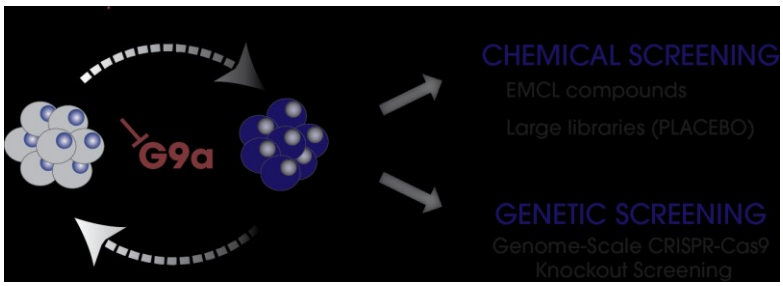


**Figure 2.5** Experimental model and applications.

In fact, as proven by Kubicek and co-workers with their reporter cell line for BRD4 inhibitors,[144] this type of system consents the high throughput screening of small molecule libraries in order to identify novel and diverse G9a direct or functional inhibitors. The new hits, with already good ability to inhibit G9a in cells, could then be further optimized providing novel lead compounds. Furthermore, performing genome-wide genetic screening, such cell line could allow the identification of G9a unknown biological partners, thus deeply elucidating its biological functions.

# CHAPTER 3

# CHEMISTRY

### 3.1 Optimization of the synthetic route to 1,4-benzodiazepin-5-ones

The retrosynthetic analysis for the preparation of the target compounds (Paragraph 2.1.2) leads to a 3,4-dihydro-5*H*-benzo[*e*][1,4]diazepin-5-one scaffold (**II**), depicted in Scheme 3.1.

**Scheme 3.1** General retrosynthesis of target compounds.

Despite the large number of publications describing the preparation of variously decorated benzodiazepine scaffolds, the synthesis of the 3,4-dihydro-5*H*-benzo[*e*][1,4]diazepin-5-one nucleus has been only rarely explored. The most relevant synthetic strategies for the preparation of this isomer were based on the ring closure of properly substituted keto-anthranilamides (**IV**, Scheme 3.2), which can be obtained by reduction of the corresponding nitro derivatives (**V**)[145-147] or through the reaction of an isatoic anhydride (**VI**) with proper α-aminoketones (**VII**).[148-149]

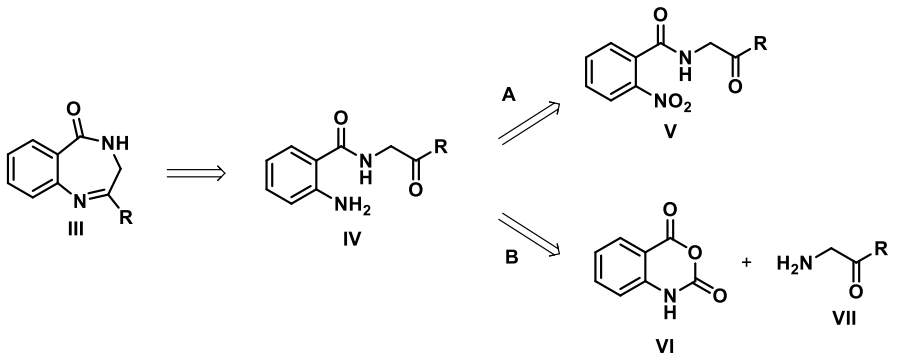

**Scheme 3.2** Reported synthetic strategies to 3,4-dihydro-5*H*-benzo[*e*][1,4]diazepin-5-one scaffold.

However, these procedures suffer the formation of undesired byproducts and/or are characterized by low to moderate yields. Moreover, the need for costly and time-consuming purification procedures makes these approaches inadequate to be run on larger scale, as necessary for the preparation of a key scaffold for a new library. For these reasons, we decided to optimize the synthesis of the 3,4-dihydro-5*H*-benzo[*e*][1,4]diazepin-5-one scaffold based on the reduction and simultaneous cyclization of the corresponding 2-nitrobenzamide (Scheme 3.3). We studied the proposed reaction using three model substrates, choosing as substituents phenyl- and cyclohexyl-, that would be used for the preparation of the designed compounds, and another less sterically hindered aliphatic substituent (isopropyl-) to further verify the robustness and versatility of the method.

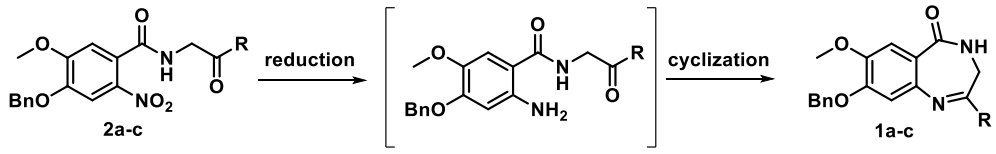


**Scheme 3.3** Reaction model.

### *3.1.1 Preparation of 2-nitrobenzamides 2a-c*

The 2-nitrobenzamides **2a-c** were obtained by condensation of 4-(benzyloxy)-5-methoxy-2-nitrobenzoic acid (**3**) with properly substituted α-aminoketones (Scheme 3.4). The synthesis of these derivatives will be illustrated below.

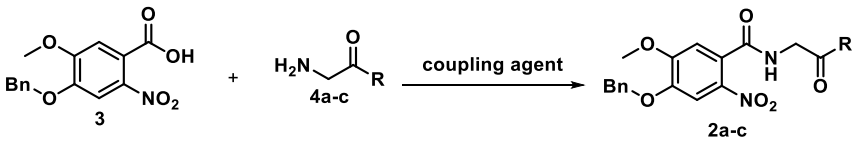


**Scheme 3.4** General synthetic strategy for nitrobenzamides **2a-c**.

*3.1.1.1 Synthesis of 4-(benzyloxy)-5-methoxy-2-nitrobenzoic acid (3)*

The synthetic strategy for the preparation of 4-(benzyloxy)-5-methoxy-2-nitrobenzoic acid (**3**) is depicted in Scheme 3.5.

Vanillic acid (**5**) was converted into the corresponding ethyl ester derivative **6** using a classic Fischer esterification. Subsequent benzylation using benzyl bromide and potassium carbonate, followed by regio-specific nitration, provided the 2-nitrobenzoate derivative (**8**) in good yield. The ethyl ester **8** was then hydrolyzed using an aqueous sodium hydroxide solution in THF to afford the 4-(benzyloxy)-5-methoxy-2-nitrobenzoic acid (**3**).

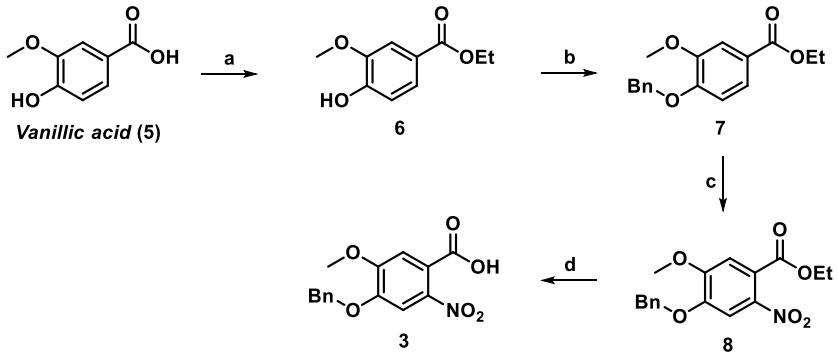


**Scheme 3.5** *Reagents and conditions*: **a)** $H_2SO_4$, EtOH, reflux, 8 h (99%); **b)** benzyl bromide, $K_2CO_3$, DMF, r.t., overnight (90%); **c)** $HNO_3$, $Ac_2O$, 0 °C to r.t., overnight (92%); **d)** NaOH, THF/$H_2O$, r.t. (98%).

*3.1.1.2 Synthesis of α-aminoketones 4a-c*

The 2-amino-1-phenylethan-1-one (**4a**) was conveniently prepared starting from the 2-bromoacetophenone (**9**). The bromine was replaced by azide (**10**) that was subsequently reduced via Staudinger procedure, in presence of hydrochloric acid, to afford the desired product (**4a**) (Scheme 3.6).

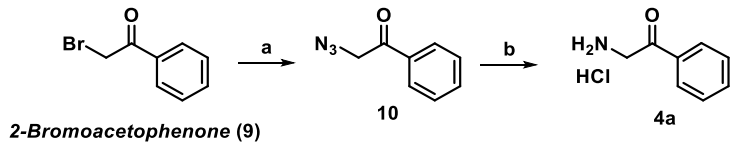


**Scheme 3.6** *Reagents and conditions* **a)** sodium azide, DMF, 0 °C, 30 min (98%), **b)** triphenylphosphine, MeOH, 37% HCl, 0 °C to r.t., overnight (quant.).

A different procedure was used for the preparation of the α-aminoketones **4b** and **4c** (Scheme 3.7). The Weinreb amide **12** was prepared starting from Boc-glycine (**11**), which was subjected to amide coupling with *N,O*-dimethylhydroxylamine under mild conditions using carbonyl diimidazole (CDI). Addition of the proper Grignard reagent to **12** afforded the corresponding N-Boc protected derivatives **13b** and **13c**, which were straightforwardly converted into the corresponding α-aminoketones **4b** and **4c** by treatment with trifluoracetic acid in dichloromethane.

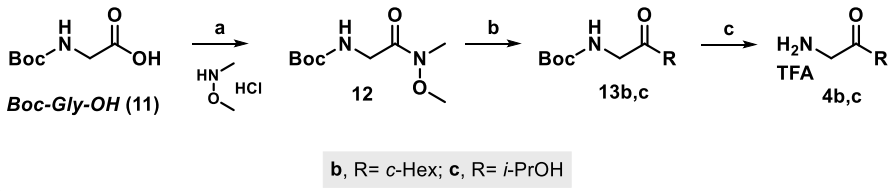


.

**Scheme 3.7** *Reagents and conditions*: **a)** *N,O*-dimethylhydroxylamine hydrochloride, CDI, triethylamine, dry THF, 0 °C to r.t., overnight (80%) **b)** cyclohexylmagnesium chloride (or isopropylmagnesium chloride), dry THF, -15 °C 1 h, then r.t. 1 h (45-50%) **c)** DCM/TFA 1:1, r.t. 2 h (quant.).

### *3.1.1.3 Coupling reaction*

Finally, as reported in Scheme 3.8, the 2-nitrobenzamides **2a-c** were prepared in good yields by treating 4-(benzyloxy)-5-methoxy-2-nitrobenzoic acid **3** with proper α-aminoketones **4a-c**, using HOBt and HBTU as amide-coupling reagents.

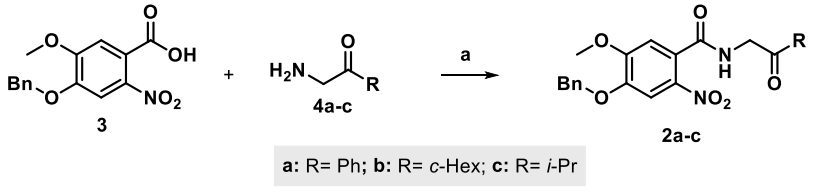


**Scheme 3.8** *Reagents and conditions*: **a)** HOBt, HBTU, DIPEA, dry THF/DMF 4:1, 0 °C to r.t., 12 h (70-85%).

### *3.1.2 Exploration of batch reduction procedures*

We therefore tested and compared different reaction conditions, starting from the classical batch procedures, as summarized in Table 3.1. The main byproducts

recovered from the reduction of the 2-nitrobenzamides **2a-c** are depicted in Figure 3.1.

The catalytic hydrogenation of the 2-nitrobenzamides always resulted in the cleavage of the benzyl group and yielded different byproducts depending on the starting compound. In particular, reduction of substrate **2a** using palladium on carbon (10% Pd/C) afforded derivative **14a**, in which the nitro- and the keto-groups were reduced (Table 3.1, entry 1). Instead, in the same conditions, the nitrobenzamide **2b** afforded the tetrahydrobenzodiazepinone **15b** (Table 3.1, entry 2). For the phenyl derivative **2a**, the conversion to the tetrahydrobenzodiazepinone **15a** was observed under microwave-assisted catalytic transfer hydrogenation conditions, using 1,4-cyclohexadiene as hydrogen donor and palladium on carbon as catalyst (Table 3.1, entry 3).[150]

Conversely, the traditional non-catalytic reduction of the substrates with iron sulfate heptahydrate (Table 3.1, entries 4-6) gave the desired 3,4-dihydro-5*H*-benzo[*e*][1,4]diazepin-5-ones **1a-c**, although in moderate yields (53-61%). A slight yield improvement was obtained only for the phenyl derivative **1a** using iron powder in acetic acid (Table 3.1, entry 7). Nevertheless, these conditions were hardly satisfactory. In fact, besides the not excellent yields, these methods suffer from various practical drawbacks. For example, the large excess of reagents implies the generation of big amounts of waste and therefore requires tedious work-up and time-consuming purification procedures.

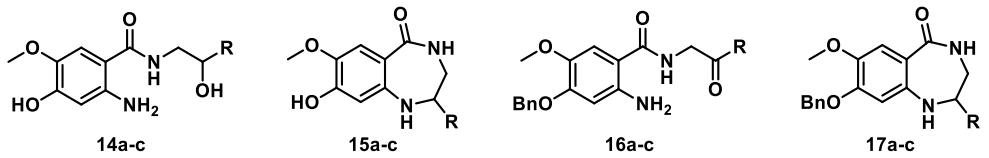


**Figure 3.1** Main byproducts obtained from of 2-nitrobenzamides **2** under reduction conditions.

**Table 3.1** Reduction of 2-nitrobenzamides **2a-c** under different batch conditions.[a]

| Entry | R | Reducing agent | method[a] | time | Yield 1[b] (%) | Main product[b] (%) |
|---|---|---|---|---|---|---|
| 1 | Ph | $H_2$, Pd/C | A | 1 h | - | **14a** (54) |
| 2 | *c*-Hex | $H_2$, Pd/C | A | 1 h | - | **15b** (88) |
| 3 | Ph | 1,4-CHDN, Pd/C | B | 10 min | - | **15a** (67)[c] |
| 4 | Ph | $FeSO_4/NH_3$ | C | 8 h | 53 | - |
| 5 | *c*-Hex | $FeSO_4/NH_3$ | C | 16 h | 55 | - |
| 6 | *i*-Pr | $FeSO_4/NH_3$ | C | 2 h | 61 | - |
| 7 | Ph | Fe/AcOH | D | 2 h | 77 | - |
| 8 | *c*-Hex | Fe/AcOH | D | 2 h | 51 | - |
| 9 | *i*-Pr | Fe/AcOH | D | 2 h | 63 | - |

[a]*Reaction conditions*: **A)** $H_2$, 10% Pd/C (10%, 0.1 eq.), EtOAc/EtOH 2:1 (0.03 M), 20 °C, 1 atm; **B)** 1,4-cyclohexadiene (1,4-CHDN, 6 eq.), Pd/C (10%, 0.05 eq.) MeOH (0.1 M), MW (120 °C); **C)** $FeSO_4 \cdot 7H_2O$ (10 eq.), $NH_4OH$, EtOH, reflux; **D)** Fe (20 eq.), AcOH (0.1 M), 70 °C; [b]Isolated yield after chromatographic purification; [c]Debenzylated nitro compound (22%) was also recovered.

### *3.1.3 Optimization of flow reaction conditions*

Thus, following our interest in exploiting modern synthetic technologies to improve classical organic reactions,[151] we considered the possibility to further study this reaction taking advantage of the continuous-flow technology. Usually flow-chemistry exhibits a number of potential advantages. Above all, it allows a tight control of the reaction variables, an increased safety, the possibility of run reactions at high temperature and pressure (process intensification), reduced manual handling and higher reproducibility, easier scale-up and many others.[152]

To perform our study, we made use of the hydrogenation reactor H-Cube Pro™ (Thales Nanotechnology Inc., Figure 3.2). This reactor allows the user to work in totally safe conditions, since the hydrogen is generated inside the instrument by the electrolysis of water and the catalysts are packaged in cartridges. Moreover, the fast and easy change of the catalyst cartridge and/or of various reaction parameters

(temperature, pressure and flow rate) consent the easy set-up of a wide range of experimental conditions.

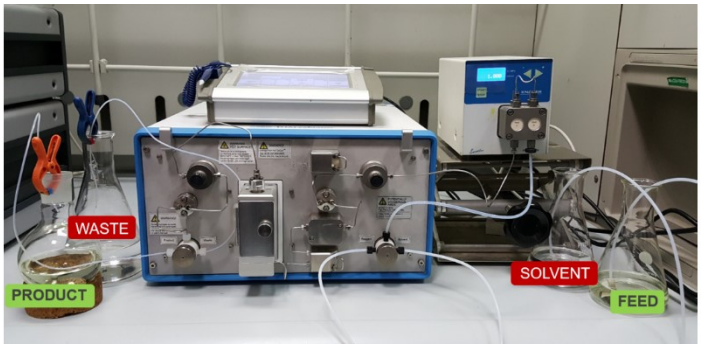


**Figure 3.2** H-Cube Pro™ (Thales Nanotechnology Inc.).

Hence, we performed a thorough screening of different catalysts and reaction conditions in order to identify the best ones for the reduction and concomitant cyclization of substrates **2**.

At first, the flow hydrogenation of 2-nitrobenzamide **2a** was optimized using a 0.03 M solution of substrate (0.30 mmol) in EtOAc/EtOH (10 mL), 1.0 mL/min as flow rate, 10 bar of pressure at 30 °C in full-$H_2$ mode. According to the results obtained under batch conditions, the hydrogenation of the 2-nitrobenzamide **2a** using Pd/C as catalyst yielded only the debenzylated anilino alcohol **14a** (Table 3.2, entry 1). The same result was observed using rhodium on carbon (5% Rh/C) as catalyst and 50 bar of pressure (Table 3.2, entry 2).

Instead, the use of platinum on carbon (5% Pt/C) had a more encouraging outcome, since it afforded the desired benzodiazepin-5-one **1a** even if in very low yield (12%, entry 3). The low yield was primarily due to ineffective cyclization step, as the main product of this reaction was the intermediate anthranylamide **16a** (Figure 3.1). Therefore, we decided to promote the cyclization by using a more appropriate solvent, THF (Table 3.2, entry 4), and raising the temperature to 80 °C (Table 3.2, entry 5). In this case, the partial conversion negatively affected the yields. Subsequently, the pressure was raised to increase conversion while the flow

rate was slowed down to promote ring closure (Table 3.2, entry 6). Nevertheless, in these conditions the desired product was obtained in moderate yield (52%). Moreover, the cyclization was still incomplete and the 1,2-dihydro-derivative **17a** (Figure 3.1) was also recovered as main byproduct.

Finally, we resolved to switch to ruthenium, an uncommon metal in heterogeneous catalysis, but reported to be selective for preferential hydrogenation of aromatic nitro groups.[153] To our pleasure, using the improved reaction conditions disclosed (THF as solvent, 0.3 mL/min as flow rate and 50 bar of pressure at 80 °C) the reaction gave exclusively the desired 3,4-dihydro-5*H*-benzo[*e*][1,4]diazepin-5-one **1a** in excellent 94% yield and without the need for further purification, as the yield did not significatively change after chromatographic purification (entry 7). Applying this the procedure also to the substrates **2b** and **2c**, the corresponding products **1b** and **1c** were obtained in comparable excellent yields (entries 8 and 9).

**Table 3.2** Reduction of 2-nitrobenzamides **2** under continuous-flow conditions.[a]

| Entry | R | Catalyst | T (°C) | Solvent | Flow rate (mL/min) | Pressure (bar) | Conversion[b] (%) | Yield 1[c] (%) | Main byproduct[c] (%) |
|---|---|---|---|---|---|---|---|---|---|
| 1 | Ph | 10% Pd/C | 30 | EtOAc/EtOH 2:1 | 1.0 | 10 | >99 | - | **14a** (>98) |
| 2 | Ph | 5% Rh/C | 30 | EtOAc/EtOH 2:1 | 1.0 | 50 | >99 | - | **14a** (>98) |
| 3 | Ph | 5% Pt/C | 30 | EtOAc/EtOH 2:1 | 1.0 | 10 | 94 | 12 | **16a** (82) |
| 4 | Ph | 5% Pt/C | 30 | THF | 1.0 | 10 | 54 | 21 | **16a** (33) |
| 5 | Ph | 5% Pt/C | 80 | THF | 1.0 | 10 | 60 | 50 | **16a** (10) |
| 6 | Ph | 5% Pt/C | 80 | THF | 0.3 | 50 | >99 | 52 | **16a** (18) + **17a** (25) |
| 7 | Ph | 5% Ru/C | 80 | THF | 0.3 | 50 | >99 | 94 (93)[c] | - |
| 8 | *i*-Pr | 5% Ru/C | 80 | THF | 0.3 | 50 | >99 | 94 (92)[c] | - |
| 9 | *c*-Hex | 5% Ru/C | 80 | THF | 0.3 | 50 | >99 | 92 (91)[c] | - |

[a]H-Cube Pro™, Full-$H_2$ mode, 30 mm × 4 mm i.d. catalyst cartridge, ~ 150 mg of catalyst; [b]Calculated as 100 − % of residual nitroderivative **2** as determined by HPLC; [c]Determined by HPLC; [d]Isolated yield after chromatographic purification.

In order to more accurately compare the results obtained with the continuous flow hydrogenation protocol to the traditional batch conditions, we took a step back and performed the catalytic hydrogenation of the derivative **2a** using ruthenium on carbon as catalyst in batch. As reported in Table 3.3 (entries 1 and 2), using the same molar substrate-to-catalyst *ratio* used in the continuous flow protocol, no reduction was observed at room temperature or even at higher temperature. The same result was obtained doubling the molar catalyst-to-substrate *ratio* (entry 3).

**Table 3.3** Reduction of 2-nitrobenzamide **2a** using ruthenium as catalyst in batch conditions.[a]

| Entry | R | Reducing agent | method[a] | time | Yield 1[b] (%) | Main product[b] (%) |
|---|---|---|---|---|---|---|
| 1 | Ph | $H_2$, Ru/C | E | 18 h | - | **2a** (98) |
| 2 | Ph | $H_2$, Ru/C | F | 10 h | - | **2a** (95) |
| 3 | Ph | $H_2$, Ru/C | G | 18 h | - | **2a** (98) |

[a]*Reaction conditions*: **E)** $H_2$, Ru/C (5%, 0.02 eq), THF (0.03 M), 20 °C, 1 atm; **F)** $H_2$, Ru/C (5%, 0.02 eq), THF (0.03 M), reflux, 1 atm; **G)** $H_2$, Ru/C (5%, 0.04 eq.), THF (0.03 M), 20 °C, 1 atm.

Finally, we evaluated the efficiency of this protocol on gram scale synthesis, by applying the same reaction conditions to obtain 1.3 g of compound **1a**. The amounts of substrate and solvent were proportionally scaled. Also in this case, the desired product was isolated with high purity and in excellent yield, without the need of multiple operator intervention. Of note, after a gram scale single run the conversion and the yield of the reaction were the same obtained with a new one, therefore proving the long-lasting efficiency of the cartridge.

### 3.2 Functionalization of the central core

Having obtained a robust and very efficient method for the preparation of the central core, we proceeded to its functionalization to obtain the designed compounds (Chapter 2). The synthetic strategy for the functionalization of the

central core is showed in Scheme 3.9. After the removal of the benzyl group from **1a** and **1b** by treatment with trifluoracetic acid, the resulting unprotected derivatives **18a** and **18b** were alkylated at the 8-hydroxy position with 1-chloro-3-iodopropane, affording the compounds **19a** and **19b**. Subsequently, the treatment of the derivatives **19** with triethyloxonium tetrafluoroborate yielded the corresponding 5-ethoxy analogues **20a** and **20b**. These derivatives were reacted with pyrrolidine in THF, in presence of sodium iodide and potassium carbonate, furnishing the compounds **21a** and **21b** in good yields. Finally, the target compounds **22a** (**EML693**) and **22b** (**EML741**) were obtained by reaction of derivatives **21a** and **21b** with 1-isopropylpiperidin-4-amine in *i*-PrOH, under microwave-assisted conditions.

The dihydro-analogues **26a** (**EML696**) and **26b** (**EML698**) were prepared by means of a slightly modified procedure (Scheme 3.9). The reduction of the imine group was achieved by treatment of compounds **18a** and **18b** with sodium borohydride, affording the reduced derivatives **15a** and **15b**, in high yields. Once again, the 8-hydroxy group was alkylated with 1-chloro-3-iodopropane, but unfortunately, any attempt to convert the chloropropoxy derivatives **23a** and **23b** into the corresponding 5-ethoxy-analogues with triethyloxonium tetrafluoroborate was unsuccessful, yielding the N-alkylated derivatives as main products. This issue was addressed converting compounds **23a** and **23b** into the corresponding thionated derivatives by treatment with Lawesson's reagent and subsequent *in situ* alkylation with iodoethane to afford the corresponding 5-ethylthio-derivatives **24a** and **24b**. The pyrrolidine moiety was then introduced as previously described (compounds **25a** and **25b**) and subsequently the 5-ethylthio group was substituted upon treatment with 1-isopropylpiperidin-4-amine, yielding the desired compounds **26a** (**EML696**) and **26b** (**EML698**).

Compared to the others, the yield of the last step is moderate (30-31%) and for the derivative **22b** (**EML741**) even unsatisfactory (<5%). For this derivative, an improvement was obtained by reacting **21b** with 1-isopropylpiperidin-4-amine in acetic acid, affording the desired product in a 30% yield (Scheme 3.9).

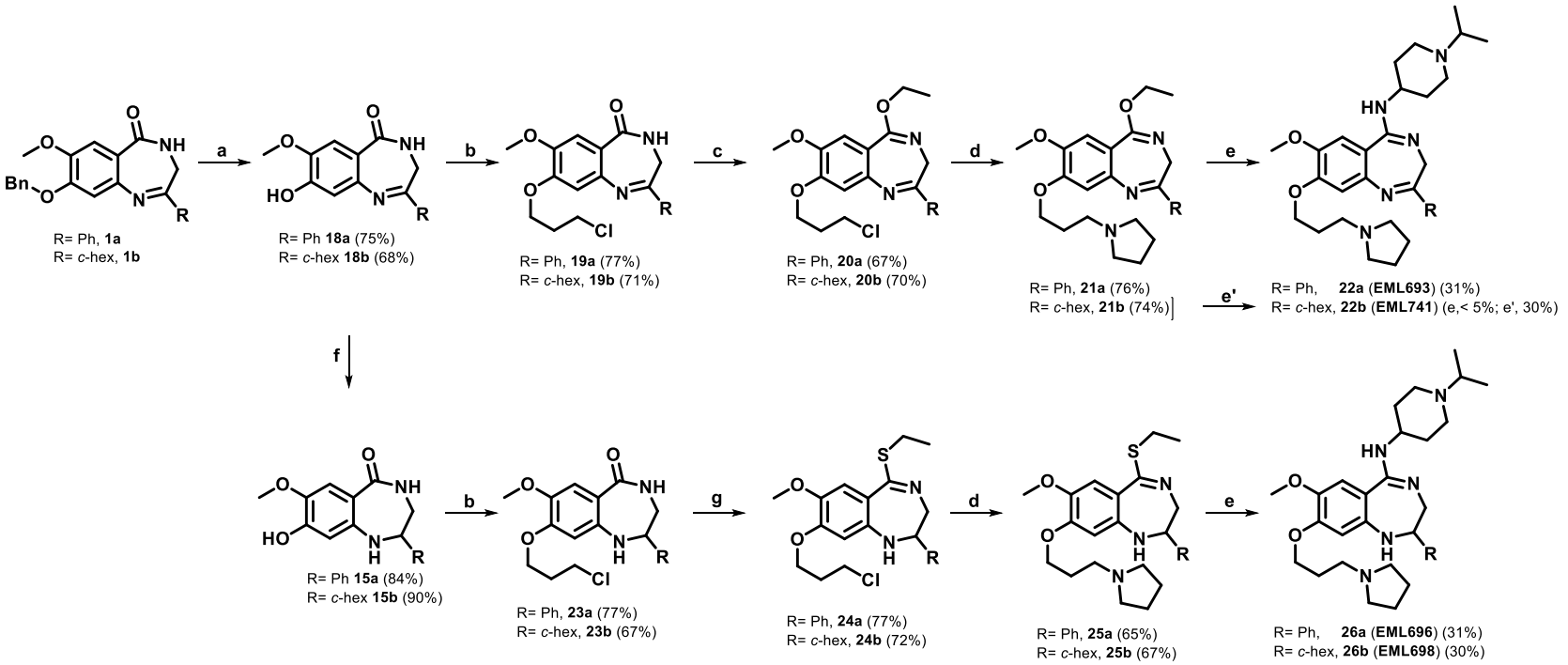


**Scheme 3.9** *Reagents and conditions*: **a)** DCM/TFA, 1:4, 50 °C, 4 h; **b)** 1-chloro-3-iodopropane, $K_2CO_3$, dry DMF, r.t., overnight; **c)** triethyloxonium tetrafluoroborate, $Na_2CO_3$, dry DCM, r.t., 15 min; **d)** pyrrolidine, NaI, $K_2CO_3$, dry THF, MW (80 °C, 90 min); **e)** 1-isopropylpiperidin-4-amine, *i*-PrOH, MW (200 °C, 2 h); **e')** 1-isopropylpiperidin-4-amine, AcOH, MW (120 °C, 1 h); **f)** $NaBH_4$, THF/MeOH, 0 °C; **g)** Lawesson's reagent, dry toluene, 85 °C, 1 h then $K_2CO_3$, iodoethane, 85 °C, 2 h.

## 3.3 Exploration of alternative strategies to obtain the 3*H*-1,4-benzodiazepine nucleus

The moderate yields of the last step of the presented synthetic route (Paragraph 3.2) prompted us to further explore the chemistry of the 3*H*-1,4-benzodiazepine (*3H*-1,4-BDZ) nucleus, and, in particular, to study a synthetic strategy to achieve the nucleus properly substituted in position 5.

In literature were reported few examples of the synthesis of 3*H*-1,4-BDZs by the photochemical ring expansion of 4-azidoquinolines. Sashida and co-workers describe the synthesis of fully unsaturated 1*H*- (**X**) and 3*H*-1,4-BDZs (**XI**) by photochemical ring-expansion of 4-azidoquinolines (**VIII**) in presence of different nucleophiles, *via* the azirine intermediate (**IX**), as shown in Scheme 3.10.[154-157] Of note, they frequently experience the poor stability of the 1*H*-1,4-BDZ nucleus and, consequently, the good result of the reaction often depends on the *in situ* isomerization to 3*H*- derivative, in presence of sodium methoxide.

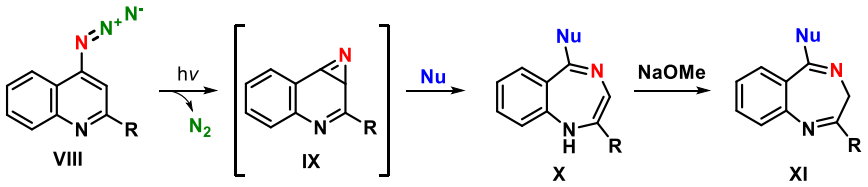


**Scheme 3.10** General schematic of 4-azidoquinolines photo-induced rearrangement.

### *3.3.1 Irradiation sources*

In the past decades, photochemical reactions were classically carried out using immersion well batch reactors. The light source was typically a mercury pressure lamp. Although these systems have found widespread use for many decades, they suffer from several drawbacks, such as:

- Intense heat generation, that require the use of cold-water cooled jackets to prevent thermal excitation of the substrate.
- Broad spectral output, that can result in an inefficient energy transfer, because, in most of the cases, only certain wavelength ranges are relevant.

- The lamps usually have short lifetimes, depending on the conditions of use (e.g. number of on-off cycles).

Recent progress in the manufacture of ultraviolet light emitting diodes (UV LEDs) has allowed the simple generation of very efficient energy systems for the near UV light, which is most suitable for photochemistry. LED systems are capable of outperforming traditional sources of high intensity UV light. Additionally, LED lamps do not generate big amounts of heat, have longer lifetimes and can be turned on and off as desired, which further increases their overall energy efficiency and practical lifetime.[158]

To study the ring expansion reaction, we made use of an immersion well batch reactor with a medium pressure mercury (HMP) lamp (Figure 3.3 A) and, in addition, we assembled an UV LED-based illuminator (365 nm) with Nichia chips, a system already successfully employed in photo-assisted organic chemistry (Figure 3.3 B).[159]

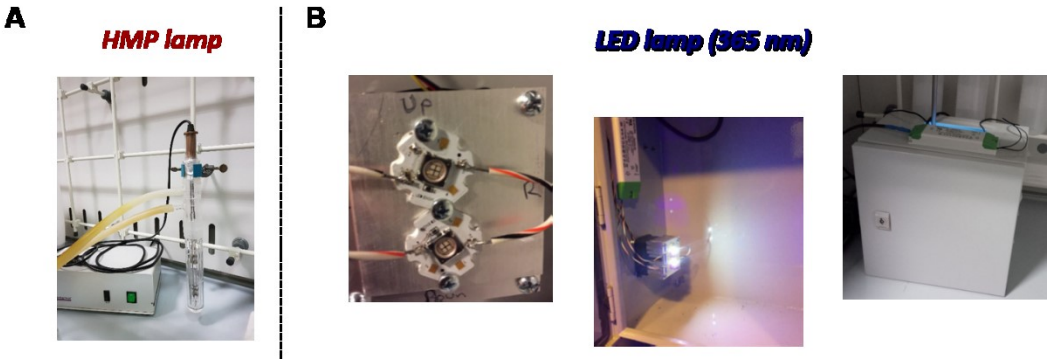


**Figure 3.3. A**, HMP immersion photoreactor; **B**, UV LED-based irradiator system.

To verify the suitability of this method for the preparation of our compounds, and in particular of **EML741**, we chose as model substrate the 4-azido-2-cyclohexylquinoline **27** that was irradiated with the two light sources disclosed in presence of isopropyl amine as nucleophile (Scheme 3.11).

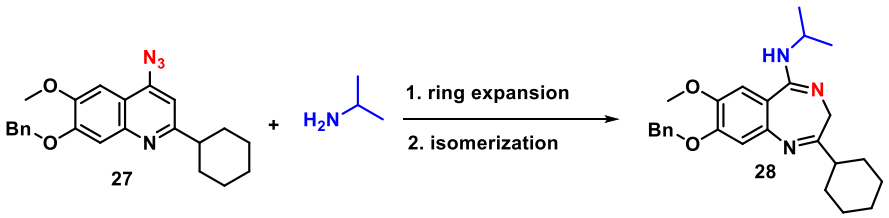


**Scheme 3.11** Model reaction of the photochemical ring expansion.

### *3.3.2 Synthesis of 4-azido-7-(benzyloxy)-2-cyclohexyl-6-methoxyquinoline (27)*

The synthesis of the 4-azidoquinoline derivative **27** is depicted in Scheme 3.12. The acetovanillone (**29**) was protected with a benzyl group and subsequently was nitrated with fuming nitric acid in acetic anhydride at 0 °C to afford the compound **31** in good yields. The nitro group was then reduced in presence of Fe/$NH_4Cl$ and the resulting aniline (**32**) was acylated with cyclohexanecarbonyl chloride to give N-(2-acetylphenyl)cyclohexanecarboxamide **33**. The derivative **33** was then cyclized with NaOH in 1,4-dioxane to obtain the corresponding 4-hydroxyquinoline **34**. Finally, the treatment of **34** with diphenyl phosphoryl azide and triethylamine in anhydrous DMF at 100 °C yielded the title compound **27**.

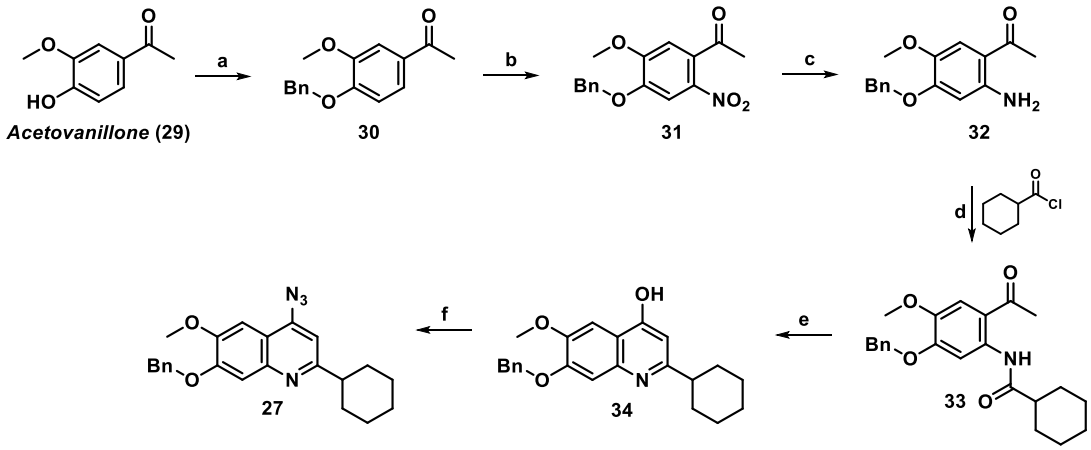


**Scheme 3.12** *Reagents and conditions*: **a)** benzyl bromide, $K_2CO_3$, acetone, reflux, 2 h (97%); **b)** $HNO_3$, $Ac_2O$, 0 °C, 15 min (83%); **c)** iron, $NH_4Cl$, EtOH/$H_2O$ 2:1, 30 min (87%); **d)** cyclohexanecarbonyl chloride, DIPEA, dry THF, 0 °C to r.t., 90 min (98%); **e)** NaOH, 1,4-dioxane, reflux, 24 h (80%); **f)** diphenyl phosphoryl azide, triethylamine, dry DMF, 100 °C, 1 h (73%).

### *3.3.3 Photochemical ring expansion of the 4-azidoquinoline 27*

Besides the irradiation sources, we tested several reaction conditions by changing temperature (0 °C and room temperature) or solvent (THF, 1,4-dioxane, methanol and ethyl acetate). Unfortunately, the desired product was never obtained (Scheme 3.13).

In fact, using the HMP lamp as light source, the conversion of the starting material into the 1*H*-1,4-BDZ intermediate (**35**) was detected by HPLC and MS analysis of the crude reaction. Nevertheless, it resulted too unstable to be isolated or isomerized to the corresponding 3*H*-1,4-BDZ (**28**). Besides unspecific degradation, we observed the formation of the ring-contracted derivative **36**, a side reaction already observed for this type of nucleus, in dependence on the reaction conditions.[160] On the other hand, when irradiated with the UV LED system, the reaction exclusively afforded the 4-aminoquinoline **37**, suggesting that the energetic input was not sufficient to enable the azirine intermediate formation.[161]

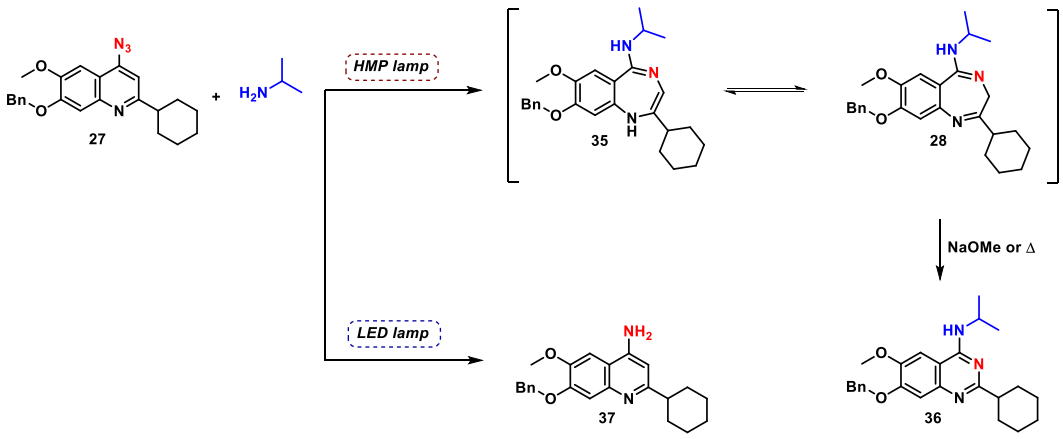


**Scheme 3.13** Schematic of the photochemical ring expansion of the 4-azidoquinoline **27**.

# CHAPTER 4

# RESULTS AND DISCUSSION

Preclinical drug research has placed an increased pressure on earlier stages of the discovery process, in particular on the generation of quality lead compounds, i.e. the molecular structures selected to undergo an optimization process to potentially become drug candidates.[162-164] A quality lead is expected to satisfy specific and demanding criteria, the main ones are summarized in Table 4.1.

**Table 4.1** Generic criteria for a quality lead compound.

| |
|---|
| - good activity *in vitro* |
| - robust and straightforward synthetic route |
| - facile substitutions and transformations of appendages |
| - logical structure-activity relationships (SARs) |
| - not a promiscuous inhibitor |
| - selectivity (counterscreen/secondary screen) |
| - stable under biological assays conditions |
| - favourable cell permeability profile |
| - good activity in cell-based assays |
| - high activity/toxicity *ratio* |
| - structure free of reactive/undesirable chemotypes |
| - structure reasonably drug-like |
| - favourable intellectual property (ip) position |

Having thoroughly explored the synthetic strategy to obtain **EML741** and its analogues, we moved to the physico-chemical and biochemical evaluation of our putative G9a inhibitor to establish its worth as lead for therapeutic development.

### 4.1 Biochemical evaluation

The effects of the ring-expanded derivatives on the catalytic activity of the human recombinant G9a protein were determined by means of AlphaLISA® homogeneous proximity immunoassay. This type of assay allows to measure enzyme activity by detecting the methylation of a biotinylated histone H3 peptide using

streptavidin-coated donor beads and AlphaLISA® acceptor beads conjugated to an antibody directed against the modified substrate (for instance the dimethylated lysine 9 of histone H3 (H3K9me2)). A schematic of the assay principle is showed in Figure 4.1.

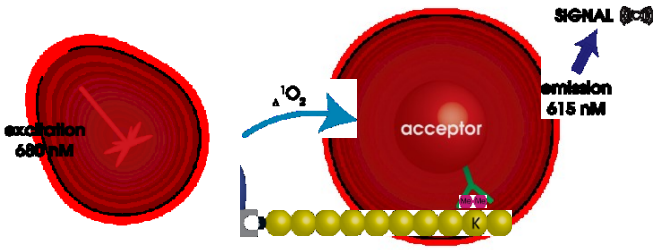


**Figure 4.1** AlphaLISA assay principle.

At first, the derivatives were preliminarily screened at the fixed dose of 50 μM. All the compounds showed an almost total inhibition at the tested dose (data not shown), therefore their activity was measured over a range of concentrations from which $IC_{50}$ values were determined (Table 4.2).

**Table 4.2** Compounds were tested in 10-dose $IC_{50}$ mode with two-fold serial dilutions. The results reported are the mean ± SD determined for at least two independent experiments.

| | **$IC_{50}$ (μM)** |
|---|---|
| **EML741** | 0.023 ± 0.008 |
| **EML693** | 1.090 ± 0.092 |
| **EML698** | 0.955 ± 0.087 |
| **EML696** | 2.091 ± 0.094 |
| **UNC0638** | 0.025 ± 0.006 |

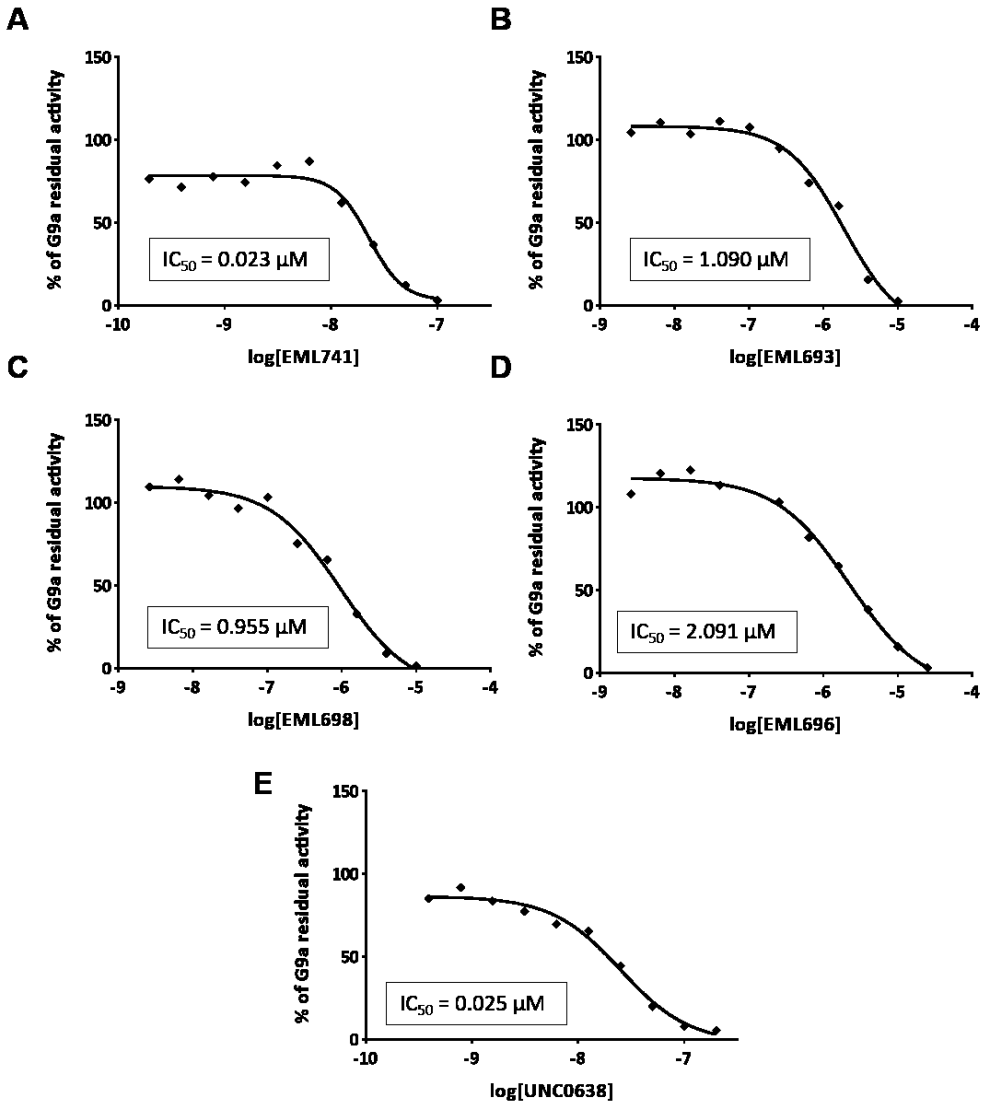


**Figure 4.2** $IC_{50}$ curves of compounds **EML741** (**A**), **EML693** (**B**), **EML698** (**C**), **EML696** (**D**), and UNC0638 (**E**). Data were analyzed using GraphPad Prism software (version 6.0) for curve fitting, using a sigmoidal concentration-response with a variable slope equation.

The ring-expanded 1,4-benzodiazepine derivative **EML741** showed the same activity of the parent compound UNC0638 ($IC_{50}$ = 0.023 ± 0.008 and 0.025 ± 0.006 µM, respectively), validating both the design strategy and the computational analysis. Comparing the $IC_{50}$ values of the different ring-expanded derivatives, it is also possible t establish preliminary structure-activity relationships (SARs). In particular, the substitution of cyclohexyl moiety with a phenyl ring (**EML693**) or the replacement of the 3*H*-benzo[1,4]diazepine core with the corresponding 2,3-

dihydro-analogue (**EML698**) caused an approximately 50-fold decrease in potency. In fact, according to the molecular modeling studies presented in Paragraph 2.1.1, the phenyl ring (**EML693**) could create unfavorable repulsive interactions with the Asp1074 and Asp1078 (anion-π). On the other hand, the reduction of the imino group, as in compound **EML698**, alters the geometry of the central core, thus possibly influencing the interactions established by the 1,4-benzodiazepine nucleus within the "peptide binding groove" and/or the position and therefore the interactions of the substituents. Moreover, these effects seemed to be additive, as the 2,3-dihydro-analogue bearing a phenyl group, **EML696**, resulted 100-fold less active than **EML741**.

### *4.1.1 Selectivity towards other epi-enzymes*

Once both potency and preliminary SARs were established, using the same technique **EML741** was profiled on a panel of selected in-house epigenetic enzymes. To have comparable data, UNC0638 was tested in the same conditions. **EML741** displayed a good selectivity profile towards the arginine methyltransferases PRMT1 and PRMT3. As regard the lysine methyltransferase SETD8, **EML741** was slightly more selective than the parent compound, giving an inhibition of less than 25% up to 25 μM. Finally, **EML741** did not markedly affect the activity of KDM4A, a member of the "eraser" class that specifically remove methyl marks on lysine-9 and lysine-36 residues of histone H3, and of the H3K9 acetyltransferase p300 (Figure 4.3).

The reason for the better selectivity of **EML741** towards SETD8 is currently unclear and could be elucidated by expanding the SARs with a larger collection of compounds. However, selectivity is essential for a chemical probe to unbiasedly investigate the biological role and disease links of the target enzyme. Moreover, in view of the development of a drug candidate, selectivity is an important parameter to optimize to avoid potential toxicities or any undesirable property due to off-target effects. Indeed, further experiments to evaluate **EML741** effect on the G9a closely related protein GLP and on other epigenetic enzymes are going to be carried out.

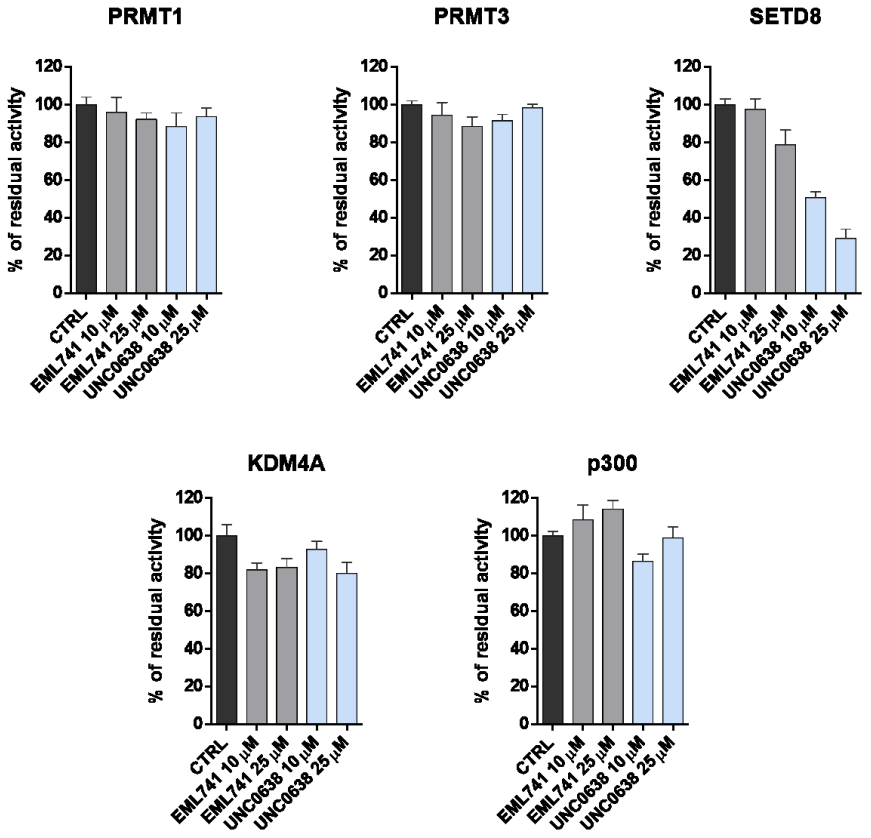


**Figure 4.3** Selectivity of **EML741**: effect on the activity of PRMT1 and -3, SETD8, KDM4A and p300. DMSO was used as control. UNC0638 was tested in the same conditions. The results are reported as mean ± SD of at least two separate experiments.

## 4.2 Kinetics Measurements and Mechanism of Inhibition

Although both molecular modeling studies and enzymatic assays results may indicate that our 1,4-benzodiazepine derivatives have the same inhibition mechanisms of the quinazoline inhibitors, we decided to better characterize the enzymatic activity of **EML741** by studying the kinetic mechanism of G9a inhibition, again by means of the AlphaLISA® technology.

Therefore, the inhibitory effect of **EML741** was explored by performing two sets of experiments, at three different concentrations (0, 7.25 and 14.5 nM). In one case, enzyme activity was measured by keeping constant the histone H3 peptide substrate concentration while varying the cofactor (SAM) concentration. In the

other set, the SAM concentration was constant while the H3 peptide concentration was varied.

The double-reciprocal plots obtained are showed in Figure 4.4. In particular, as it lowered the $V_{max}$ value, **EML741** showed non-competitive inhibition versus the cofactor ($K_i$ of 3.6 ± 0.6 nM, Figure 4.4 A). Conversely, **EML741** exhibited competitive inhibition for the histone H3 peptide substrate as it increased the $K_m$ while leaving unaffected the $V_{max}$, resulting in a $K_i$ value of 13.8 ± 1.7 nM (Figure 4.4 B). These results are in line with those reported by Vedadi *et al*. for UNC0638 ($K_i$ = 3.00 ± 0.05 nM).[120]

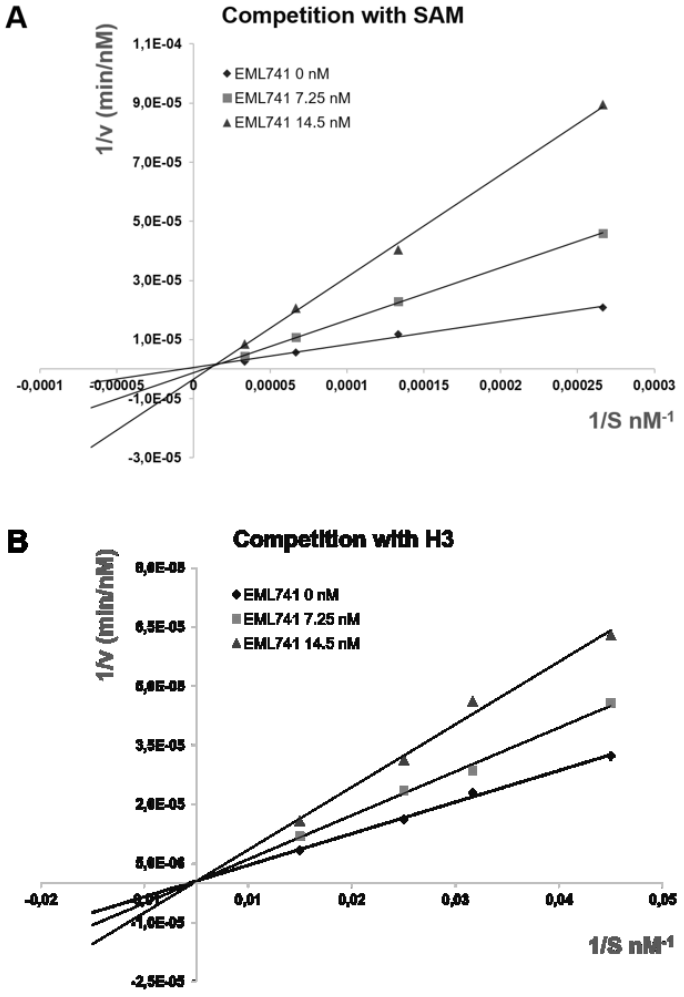


**Figure 4.4 A**, Plot of 1/v vs 1/[SAM] at a fixed H3 concentration (100 nM) and three different concentrations of **EML741** shows noncompetitive inhibition. **EML741** $K_i$ = 3.6 ± 0.6 nM, α $K_i$ = 1.1 ± 0.2 nM, SAM apparent $K_m$ = 164 ± 21 μM. **B**, Plot of 1/v vs 1/[H3] at a fixed SAM concentration (15 μM) and three

different concentrations of **EML741** shows competitive inhibition. **EML741** $K_i$ = 13.8 ± 1.7 nM, H3 apparent $K_m$ = 1.6 ± 0.3 μM.

### 4.3 Chemical stability assay

Small-molecules can be unstable in aqueous solutions and this can significantly limit their application as molecular probes.

In compound **EML741** we envisioned the imino group as a putative point of chemical instability, as it could be hydrolyzed in aqueous medium. Therefore, the compound was incubated with PBS solution, at room temperature. The presence of degradation products in the sample was assessed by HPLC analysis after 12, 24, 48 and 72 hours (Figure 4.5).

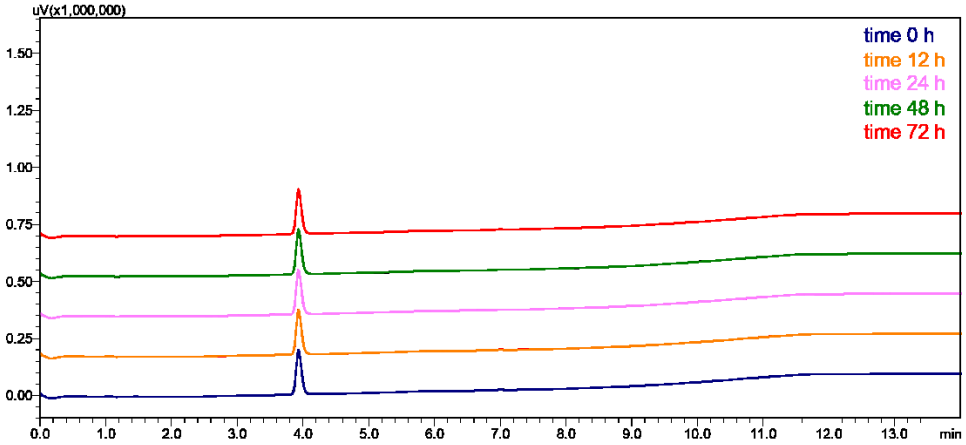


**Figure 4.5** HPLC chromatograms obtained for compound **EML741** injected immediately after the dissolution in PBS, after 12, 24, 48 and 72 h. Spectra were recorded at 220 nm.

Experimental results indicated that **EML741** is stable under the conditions routinely used in biochemical and biological assays, up to 72 hours.

### 4.4 Cell Permeability: Parallel artificial membrane permeability assay

Among the factors influencing the pharmacokinetic properties, a good permeability profile is widely recognized as an important characteristic of both chemical probes and drug candidates, as it strongly influences, for example,

gastrointestinal absorption, permeation of the blood–brain barrier (BBB) and, ultimately, whether a compound is able to reach the intracellular targets.[165]

Indeed, as discussed in Chapter 1, despite the good number of compounds with good potency and high selectivity for inhibiting G9a, a poor membrane permeability has frequently limited their use in cell-based assays and, therefore, the study of G9a involvement in both physiological and pathological pathways.

Parallel artificial membrane permeability assay (PAMPA) is a well-validated technique to estimate the ability of a compound to permeate model membranes.[166-167] In fact, due to its robustness, versatility and easy set-up, nowadays several PAMPA models have been developed, displaying a high degree of correlation with permeation across a variety of barriers (such as skin, gastrointestinal tract and blood–brain barrier).[167-170]

Therefore, we exploited this technique to evaluate the cell permeability of **EML741** using the highly permeable drug propranolol, the poorly permeable drug furosemide and the UNC0638 as references. Moreover, being interested in developing novel chemical probes for REST-expressing MBs models, we performed a PAMPA-BBB assay to estimate its ability to cross the blood–brain barrier. In this case, also the highly permeable drug chlorpromazine was used as reference (Table 4.3).

**Table 4.3** Permeability profile

| | **PAMPA $P_{app}$ cm/s** | **PAMPA-BBB $P_{app}$ cm/s** |
|---|---|---|
| **EML741** | $4.80 \times 10^{-7}$ | $2.30 \times 10^{-7}$ |
| **UNC0638** | $0.49 \times 10^{-7}$ | n.d.[b] |
| **Propranolol** | $54.0 \times 10^{-7}$ | $52.0 \times 10^{-7}$ |
| **Furosemide** | u.d.l.[a] | u.d.l.[a] |
| **Chlorpromazine** | n.d.[b] | $6.60 \times 10^{-7}$ |

[a] under detection limit; [b] not determined

**EML741** showed an interesting apparent permeability value ($P_{app}$) of 4.80 × $10^{-7}$ cm/s, higher than the UNC0638 ($P_{app}$ = 0.49 × $10^{-7}$ cm/s). Moreover, it showed a good $P_{app}$ value (2.30 × $10^{-7}$ cm/s) also using porcine brain lipid extract as membrane, mimicking the blood−brain barrier.

### 4.5 Cell-based assays: preliminary results

On the basis of these encouraging results, cell-based assays were planned and are now ongoing. In particular, we want to study the ability of **EML741** to reduce H3K9me2 levels in three tumor cell lines (MCF-7, MDA-MB-231, U343), detected by immunoblotting. Cell-cycle alteration will be also evaluated.

To date, preliminary data on the human breast cancer cell line MCF7 have already been collected. For comparative purposes, UNC0638 was assayed in the same conditions.

MCF-7 were treated with **EM741** with doses ranging from 0.05 to 50 μM. After 24, 48 and 72 hours of incubation, the percentage of viable cells in the treated samples, with respect to cells treated with an equal amount of DMSO (0.5% final concentration), was evaluated by means of methylthiazoletetrazolium (MTT) viability assay.

Interestingly, it was observed that **EM741** did not induce a strong reduction of the cell viability even at the higher dose and longer incubation time, while at the dose of 50 μM UNC0638 resulted cytotoxic even after 24 hours (Figure 4.6).

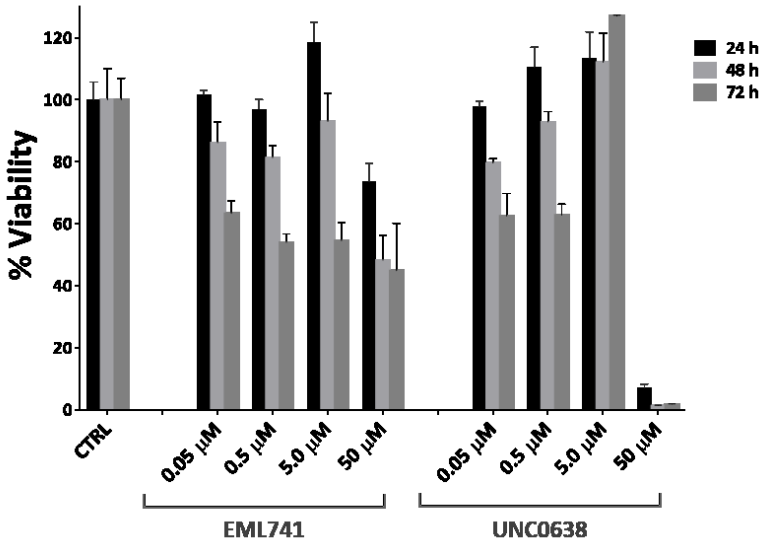


**Figure 4.6** Cytotoxic effect of **EML741** and UNC0638 on MCF7 cell line. Cells were seeded and allowed to adhere overnight, after which were treated with the indicated doses of both compounds and an equal amount of DMSO was used as control. Data were normalized with respect to control and the results are shown as the mean ± SD of four independent experiments.

Subsequently, we evaluated the effects on the cellular level of H3K9me2 after 48 and 72 hours incubation with 0.5 and 5.0 µM of **EML741**. After the treatment, the histone extracts were immunoblotted with an antibody specific for the abovementioned modification, using total histone H4 as loading control. An equal amount of DMSO was used to treat the control sample. As shown in Figure 4.7, **EML741** induced a significant dose and time dependent decrease in the H3K9me2 levels in bulk histones, in a comparable manner to 0.5 µM UNC0638, used as a reference.

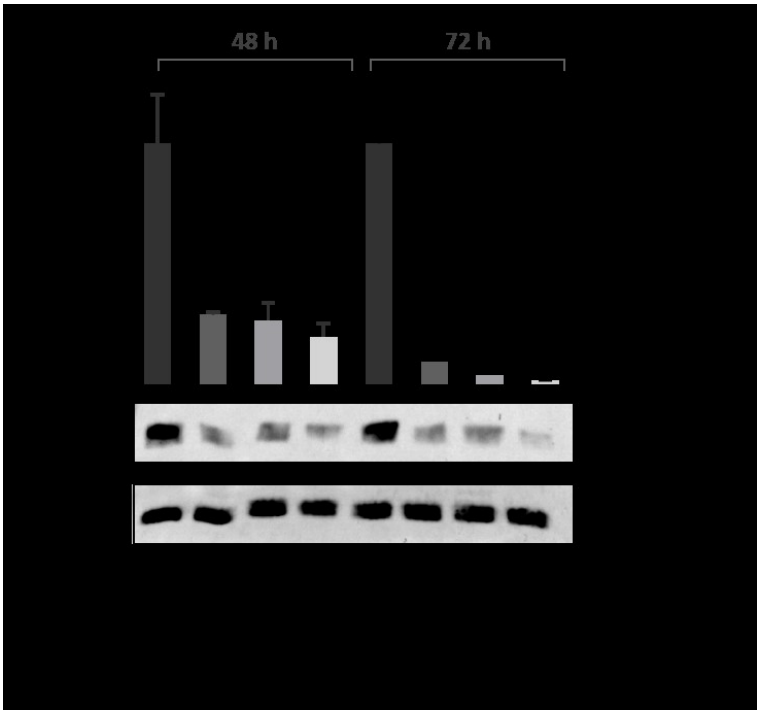


**Figure 4.7** Western blot analysis of H3K9me2 level after treatment of MCF7 cells with **EML741** and UNC0638. Cells were seeded and allowed to adhere overnight, after which were treated with the indicated doses of both compounds or DMSO. Signals were detected with the ImageQuant LAS 4000 digital imaging system and quantified by ImageQuantTL software (version 8.1); total histone H4 levels were used for normalization. The results are reported as the mean ± SD of three independent experiments.

Further studies on other tumor cell lines will deeply elucidate the role of **EML741** as novel valuable lead compound for cell-based assays of G9a activity.

# CHAPTER 5

# G9a REPORTER SYSTEM

Pursuing my efforts toward the identification of novel molecular entities that could serve as useful probes to elucidate both the physiological and the pathological role of G9a, I decided to spend 6 months of my PhD period in the group of Dr. Stefan Kubicek at CeMM (the Research Center of Molecular Medicine of the Austrian Academy of Science). The Kubicek laboratory hosts the PLACEBO (Platform Austria for Chemical Biology), which facilitates the access to chemical biology resources, including a vast compound library (comprising more than 90.000 small molecules) and HTS/HCS equipment, needed for the identification and characterization of small molecules to be used for the interrogation of biological processes as well as in drug discovery. Recently in the Kubicek group, S. Sdelci and co-workers published a Nature Chemical Biology article describing the generation of a fluorescent reporter cell line monitoring the inhibition of BRD4,[144] an epigenetic reader involved in transcription initiation and super enhancer formation. Inspired by that, I wanted to develop a cellular reporter system able to respond to epigenetic changes induced by G9a inhibition by enhancing the expression of a fluorescent protein.

As previously mentioned (Chapter 2), reporter gene technology is a valuable tool to monitor the cellular events associated with signal transduction and gene expression. The main advantages of this method are the high sensitivity and reliability, and suitability for large-scale measurements. The possibility of using a reporter gene t echnology in HTS makes cell-based assays an extremely attractive alternative to *in vitro* biochemical assays, as they better mimic physiological conditions.[142]

### 5.1 Generation of a reporter cell line for the inhibition of G9a

To generate a reporter cell line that specifically activate the expression of a fluorescent reporter phenocopying G9a inhibition, we used lentivirus particles encoding for a blue fluorescent protein (BFP). Lentiviral vectors are based on human immunodeficiency virus (HIV) and, to date, they are a validated research tool for gene knockdown, gene over expression efficient *in vivo* gene delivery (gene therapy). In fact, unlike other retroviruses, lentiviral vectors do not necessarily

require cell division for proviral integration and productive infection. Lentiviruses also transduce cells with high efficiency and stability of transgene expression.[171-172]

The BFP-lentiviral particles mentioned above were generated in 293T human kidney cells (HEK293T) by transient transfection of the vector of interest (pLV-BFP) together with the packaging (psPAX2) and the envelop plasmids (VSV-G). The virus-containing supernatant was collected after 30, 48 and 72 hours of transfection.

Aiming at performing chemical and genetic screenings with the developed reporter cell line, we chose as model the chronic myelogenous leukemia human cell line KBM7, which has a near-haploid karyotype and therefore allows unambiguous monoallelic genetic configurations.[173-174]

Before performing the BFP-lentiviral infection, we treated KBM7 cells with UNC0638, in order to induce chromatin remodeling in a G9a-inhibition specific manner. In this way, the integration of the fluorescent reporter can happen in a usually condensed locus of the genome which becomes open following G9a inhibition. To determine the activity-toxicity window of UNC0638 on these cells, wild type (wt) KBM7 cells were treated in five-point dose response for 24 and 48 hours. Western blot analysis in combination with CellTiter-Glo® Luminescent Cell Viability Assay (Promega) have shown that after 48 hours of incubation, UNC0638 2 μM was able to significantly reduce H3K9me2 levels, without drastically impairing cell viability (Figure 5.1).

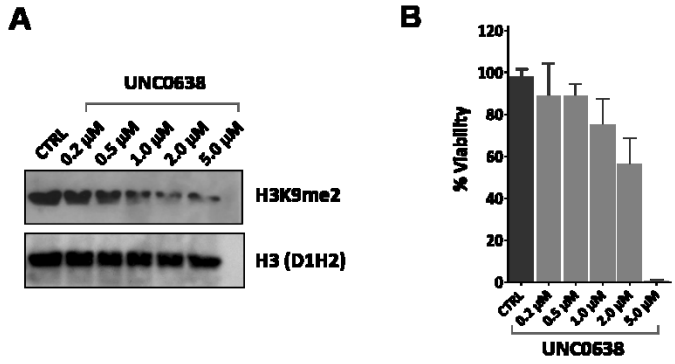


**Figure 5.1. A**, Western blot analysis of H3K9me2 methylation (H3 has been used as loading control) and **B**, Cell-Titer Glo® assay after treatment of wt KBM7 cells for 48 hours with the indicated amounts of UNC0638. Data were normalized with respect to control and the results are shown as the mean ± SD of three independent experiments.

Once chosen 2 μM as better UNC0638 performing concentration, we treated KBM7 in order to first induce chromatin remodeling. After 48 hours, treated cells were infected with BFP lentiviral particles, and 48 hours later sorted for their ability of expressing the BFP protein. The sorted population was plated in fresh media in absence of UNC0638, let recover in culture for additional 5 days, whereupon BFP-negative cells were sorted. With this double sorting strategy, we were able to select a population of cells that express BFP when G9a is inhibited and repress the fluorescent reporter after withdrawal of the compound (SWITCH-ON) (Figure 5.2).

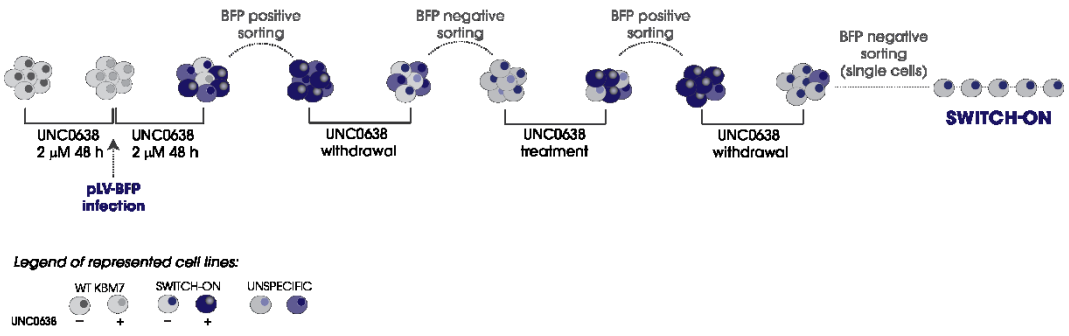


**Figure 5.2** Pipeline of the experimental approach.

Gates for BFP-positive/negative populations were done using wild type KBM7 as negative control. Exemplificative sorting analyses are reported in Figure 5.3.

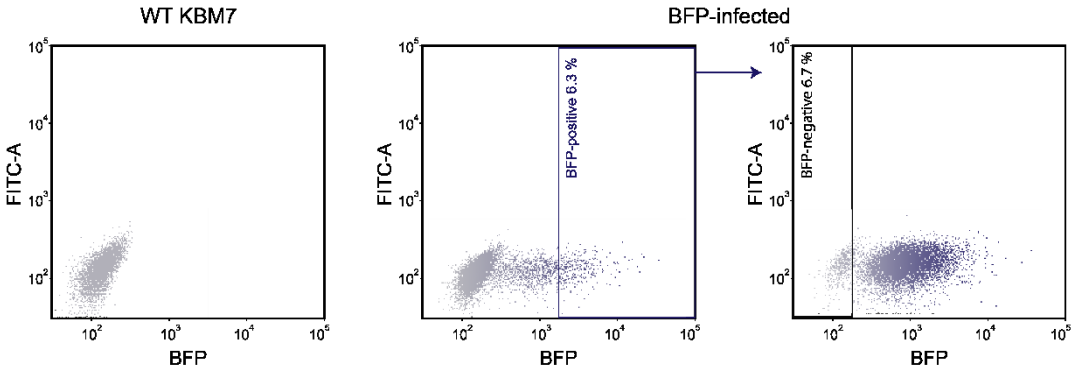


**Figure 5.3** Sorting analysis of wt KBM7 population (not infected; left panel), the infected and sorted population colored by increasing BFP intensity (from gray to blue). Cells were selected based on high BFP expression after infection (blue rectangle; middle panel) and BFP negativity after drug withdrawal (black rectangle, right panel).

Finally, to obtain a pure population, single cell sorting was performed, and outgrowing clones were further analyzed to select the best performing based on their ability of robustly express BFP in live-cell imaging (Figure 5.4). Briefly, all the reporter cell lines were first treated with a single concentration of UNC0638 (2 μM) to select SWITCH-ON positive clones which were further characterized in dose response assay (from 2.0 to 20 μM). Due to their strong BFP expression upon UNC0638 treatment, clones 1704001-A7 and 1704014-H3 were chosen for further studies.

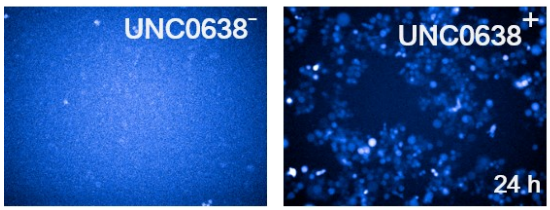


**Figure 5.4** Representative pictures of live cell imaging of a SWITCH-ON cell line.

## 5.2 Validation and preliminary results

To rule out the specificity of 1704001-A7 and 1704014-H3 detecting G9a inhibition, but also to identify new small molecules able to phenotypically mimic the effect of UNC0638, we performed a small molecule screening using a small library of 2000 compounds. Among the 90K compounds available at PLACEBO, these 2000 have an annotated target. In particular, 274 epigenetic inhibitors consent to thoroughly evaluate the ability of the cell line to detect G9a inhibition among other epigenetic perturbations. Moreover, other compounds resulting in an effective activation of BFP expression could represent a first pool of hits to validate or, having an annotated target, could give us a hint regarding G9a biology.

During the primary screening, 1704001-A7 and 1704014-H3 clones were treated in single dose of each compound, and 24 hours later live-cell imaging pictures were taken to assess their ability to induce BFP expression. UNC0638 10 and 20 μM were used as positive control, while DMSO was used as negative control. In order to select hit compounds, we used a software able to count BFP-positive cells; a given small molecule was selected as hit when the number of BFP positive cells exceeded the DMSO average plus 4× standard deviation (SD). Hits distribution from the preliminary screening on one clone is showed as dot plot in Figure 5.5.

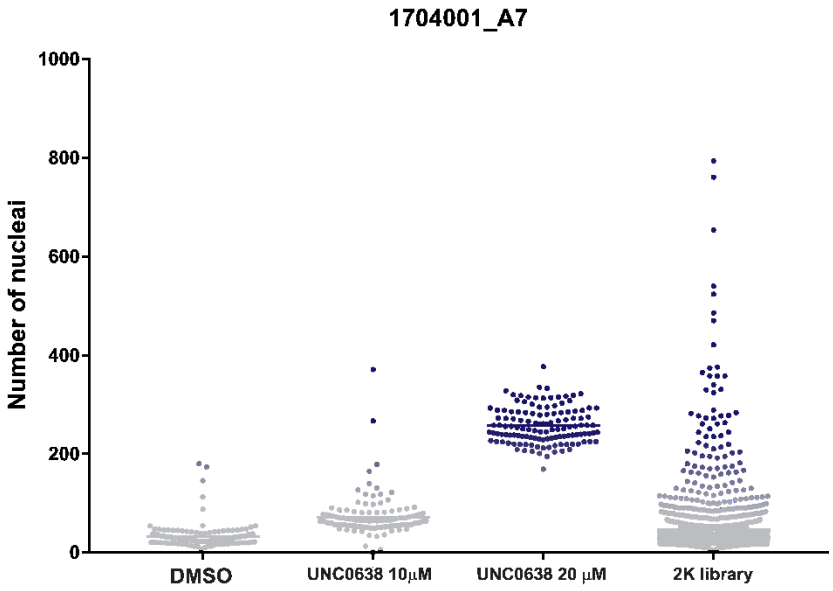


**Figure 5.5** Dot plot representing the hits distribution from the primary screening on 1704011-A7 cell line.

The small molecules selected as hits in the primary screening were used to treat wt KBM7 to exclude autofluorescent or toxic compounds. To this point, 18 small molecules were selected used to treat both reporter cell lines in parallel with wt KBM7 cells in eight-point dose in order to carefully select the best performing compounds (Figure 5.6 A). Finally, only 5 compounds confirmed as good hits (Figure 5.6 B) and for those the mechanism of action has to be clarified.

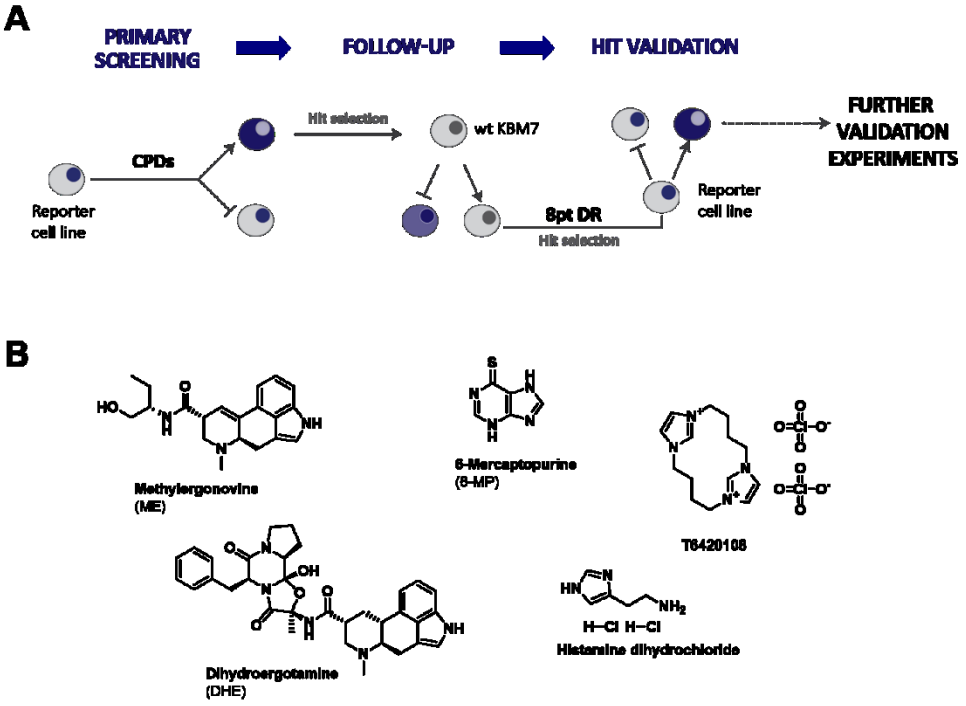


**Figure 5.6 A**, Pipeline for the selection of hits. DR: dose-response; **B**, selected hits from the performed screens.

To confirm the results using a different technology, we performed a real time PCR (RT-PCR) to detect the increase of BFP expression following the treatment with the selected compounds, at the transcriptional level. All the G9a inhibitors available at PLACEBO (BIX01294, UNC0224, UNC0642 and A366) were used as positive controls (Figure 5.7).

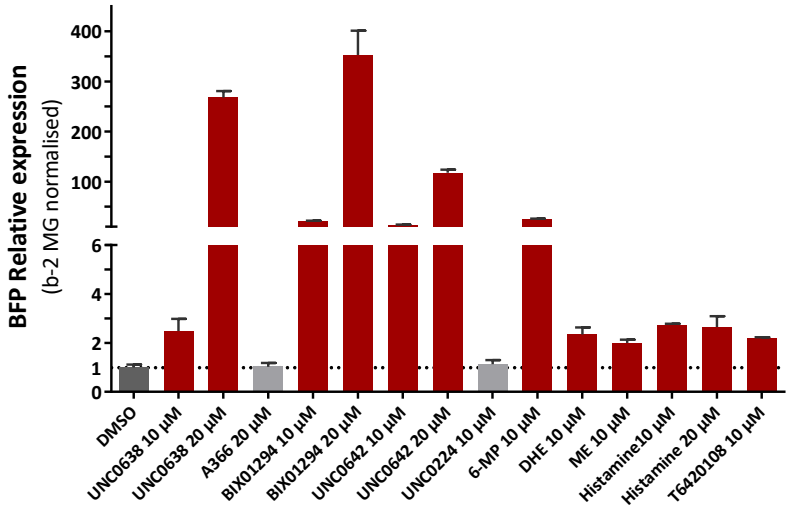


**Figure 5.7** BFP expression performed by RT-PCR in 1704001-A7 cells treated with indicated compounds and doses for 24 hours. An equal volume of DMSO was used as negative control. Two replicates were performed for each experimental condition (mean ± SD).

Among the G9a inhibitors, BIX01294 and UNC0642 increased the BFP expression in a manner comparable to UNC0638. On the other hand, neither UNC0224 nor A366 induced such increase. It is worth noting that, to the best of our knowledge, UNC0224 is reported as good G9a inhibitor *in vitro*, while its activity in cell-based assays was not investigated. Instead, as regards A366, few considerations have already been touched on in Chapter 1. Regarding the 2K screening hits, the RT-PCR data confirmed the increase of the BFP expression, in a comparable manner with respect to the lower dose of UNC0638. A deeper characterization of the molecular mechanism underlying the activation of the reporter is needed to elucidate their link to G9a biology.

Further validation experiments, such as G9a/GLP knock down and a genome-scale screening using a CRISPR/Cas9 Knockout Library (*Brunello*) are currently ongoing. Once the specificity is definitely confirmed, a 90Kcompound library available at the host lab (the PLACEBO screening platform) will be promptly screened.

# CHAPTER 6

# CONCLUSIONS

Because of its central role in many biological processes, and therefore, its involvement in several pathological conditions, the lysine methyltransferase G9a is considered a valuable drug target for the development of novel therapeutic strategies and, in particular, for cancer therapy (e.g. REST-expressing MBs). Therefore, in the past decades several research groups focused their efforts towards the development of potent and selective G9a inhibitors. However, since the chemical diversity of current available G9a inhibitors is very limited, the development of novel chemotypes is extremely desirable.

In this regard, my PhD project was aimed to the identification of novel chemotypes as G9a modulators by means of two different approaches. The first, basically relying on a medicinal chemistry perspective, considered the modification of the central core structure of the most used G9a chemical probe, UNC0638. The replacement of the quinazoline moiety of the UNC0638 with a "privileged" benzodiazepine nucleus led to the compound **EML741**. The central core of our ring-expanded derivative consist of a 3*H*-benzo[*e*][1,4]diazepine nucleus, whose synthesis was optimized by means of a continuous-flow protocol. **EML741** and a small set of analogues were synthesized and their ability of inhibiting G9a was assessed *in vitro*. **EML741** was able to inhibit G9a to the same extent as the parent compound UNC0638 ($IC_{50}$ = 0.023 μM and $IC_{50}$ = 0.025 μM, respectively), while it did not significantly affect the activity of a small panel of selected epigenetic enzymes, up to 25 μM. Furthermore, kinetic studies confirmed **EML741** as a substrate competitive and cofactor non-competitive inhibitor. These encouraging results, together with a promising membrane permeability profile (PAMPA and PAMPA-BBB), prompted us to better characterize the activity profile of **EML741** in tumor cell lines. These studies, currently ongoing, are aimed to assess its potential as new valuable lead for the development of a novel class of G9a modulators, to further validate G9a as drug target in cancer therapy, and in particular in REST-expressing MBs.

On the other hand, we considered to expand the chemical space of G9a modulators through a biological approach, generating a new cell-based screening platform. To this end, the human haploid cell line KBM7 was incubated with the G9a inhibitor UNC0638 to induce the reactivation of G9a-silenced regions, then

infected with a lentivirus encoding for a blue fluorescent protein. Applying multiple fluorescence-activated cell sorting (FACS) steps, we selected two population able to increase the expression of the reporter protein upon treatment with the G9a inhibitor. The specificity of these reporter cell lines to detect G9a inhibition was evaluated by excluding its expression in response to different epigenetic perturbations. A small library of about 2000 compounds was screened and 5 compounds were identified as hits. The molecular mechanism behind this activation has to be elucidated. Before moving on to large-scale screening, additional validation experiments are now ongoing. This approach laid the groundwork for a systematic search of novel chemical entities that interfere with G9a activity, as well as for the study of G9a biology.

# CHAPTER 7

# MATERIALS AND METHODS

## 7.1 Chemistry

General directions. All chemicals were purchased from Sigma Aldrich (Milan, Italy) or from Fluorochem Ltd (Hadfield, United Kingdom) and were of the highest purity. All solvents were reagent grade and, when necessary, were purified and dried by standard methods. All reactions requiring anhydrous conditions were conducted under a positive atmosphere of nitrogen in oven-dried glassware. Standard syringe techniques were used for anhydrous addition of liquids. Reactions were routinely monitored by TLC performed on aluminum-backed silica gel plates (Merck DC, Alufolien Kieselgel 60 F254) with spots visualized by UV light (λ = 254, 365 nm) or using a $KMnO_4$ alkaline solution. Solvents were removed using a rotary evaporator operating at a reduced pressure of ~10 Torr. Organic solutions were dried over anhydrous $Na_2SO_4$. Chromatographic purification was done on an automated flash chromatography system (IsoleraOne™, Biotage) using cartridges packed with KP-SIL, 60 Å (40−63 μm particle size). High performance liquid chromatography (HPLC) was performed on a Shimadzu SPD 20A UV/vis detector (λ = 220 nm) using C-18 column Phenomenex Synergi Fusion RP 80A (75mm × 4.60 mm; 4 μm) at 25 °C using a mobile phase A (water + 0.1% TFA) and B (ACN + 0.1% TFA) at a flow rate of 1 mL/min. Preparative HPLC was performed using an Shimadzu Prominence LC-20AP with the UV detector set to 220 nm and 254 nm. Samples were injected onto a Phenomenex Synergi Fusion – RP 80A (150× 21 mm; 4 μm) C18 column at room temperature. Mobile phases of A (water + 0.1% TFA) and B (ACN + 0.1% TFA) were used with a flow rate of 20 mL/min. A general gradient of 0–3 minutes at 15% B, 3–30 minutes increasing from 15 to 40% B, and 30–33 minutes increasing from 40 to 90% B was used, followed by a 90% B flush for another 2 minutes. Small variations in this purification method were made as needed to achieve ideal separation for each compound.$^1$H NMR spectra were recorded at 300 MHz on a Bruker Avance 300 spectrometer or at 400 MHz on a Bruker Avance 400 III HD. $^{13}$C NMR spectra were recorded at 100 MHz on a Bruker Avance 400 III HD. Chemical shifts are reported in $\delta$ (ppm) relative to the internal reference tetramethylsilane (TMS). Mass spectra were recorded on a Biotage Dalton 2000 (Uppsala, Sweden) mass spectrometer in atmospheric pressure chemical ionization, in positive and negative modes. High-resolution mass

spectrometry (HRMS) analysis was performed using Bruker SolariX XR 7T FT-ICR mass spectrometer in electrospray (ESI) positive ionization mode. Purity of tested compounds was ≥95%, established by HPLC analysis.

### *7.1.1 Preparation of 2-nitrobenzamides 2a-c*

#### *7.1.1.1 Procedures for the preparation of 4-(benzyloxy)-5-methoxy-2-nitrobenzoic acid (3)*

Synthesis of ethyl 4-hydroxy-3-methoxybenzoate (6)

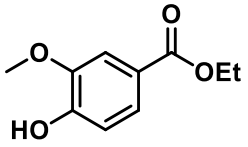


A mixture of vanillic acid (10 g, 59.5 mmol) and sulfuric acid (1.6 mL, 2.94 mmol) in anhydrous ethanol (50 mL) was heated under reflux for 8 h. The reaction mixture was concentrated under *vacuum*, taken up with $NaHCO_3$ saturated solution (75 mL) and extracted with EtOAc (3 × 100 mL). The combined organic layers were washed with brine, dried, filtered, and concentrated *in vacuo* affording the desired product as brown oil (11.5 g, 99%). $^1$H NMR (300 MHz, DMSO-$d_6$) δ 9.95 (br s, 1H exchangeable with $D_2O$), 7.72 – 7.24 (m, 2H), 6.86 (d, $J$ = 8.2 Hz, 1H), 4.25 (q, $J$ = 6.9 Hz, 2H), 3.81 (s, 3H), 1.29 (t, $J$ = 7.0 Hz, 3H); MS: *m/z* 195 [M – $H^-$].

Synthesis of ethyl 4-(benzyloxy)-3-methoxybenzoate (7)

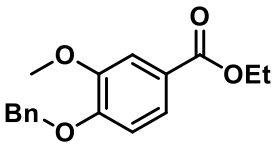


To a solution of ethyl 4-hydroxy-3-methoxybenzoate **6** (11.6 g, 59.1 mmol) in DMF (50 mL), potassium carbonate (12.3 g, 88.7 mmol) and benzyl bromide (11.1 g, 65.0 mmol) were added. The reaction mixture was stirred at room temperature overnight. Water was added to precipitate the product which was

filtered under vacuum, through a por.3 Gooch, and washed thoroughly with water. White solid (15.4 g, 90%); $^1$H NMR (300 MHz, DMSO-$d_6$) δ 7.57 (dd, $J$ = 8.5, 2.0 Hz, 1H), 7.51 – 7.30 (m, 6H), 7.17 (d, $J$ = 8.5 Hz, 1H), 5.17 (s, 2H), 4.28 (q, $J$ = 7.0 Hz, 2H), 3.82 (s, 3H), 1.30 (t, $J$ = 7.1 Hz, 3H); MS: *m/z* 287 [M + H$^+$].

Synthesis of ethyl 4-(benzyloxy)-5-methoxy-2-nitrobenzoate (8)

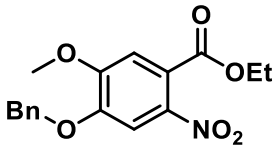


To an ice-cooled solution of ethyl 4-(benzyloxy)-3-methoxybenzoate **7** (15.3 g, 53.3 mmol) in acetic anhydride (175 mL) was added fuming nitric acid (13.7 mL, 309 mmol) dropwise. The reaction mixture was allowed to slowly warm to room temperature and stirred overnight. The mixture was poured into ice-water and the resulting precipitate was filtered through a por.3 Gooch, washed with water, and dried to provide ethyl 4-(benzyloxy)-5-methoxy-2-nitrobenzoate (16.3 g, 92%). Yellow solid. $^1$H NMR (400 MHz, DMSO-$d_6$) δ 7.76 (s, 1H), 7.49 – 7.34 (m, 5H), 7.32 (s, 1H), 5.26 (s, 2H), 4.29 (q, $J$ = 7.1 Hz, 2H), 3.92 (s, 3H), 1.27 (t, $J$ = 7.1 Hz, 3H); MS: *m/z* 332 [M + H$^+$].

Synthesis of 4-(benzyloxy)-5-methoxy-2-nitrobenzoic acid (3)

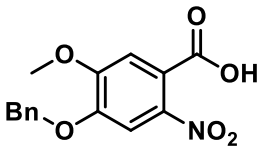


Ethyl 4-(benzyloxy)-5-methoxy-2-nitrobenzoate **8** (13.4 g, 40.5 mmol) was dissolved in THF (191 mL) and 2 N NaOH solution (61 mL) was added. The reaction mixture was stirred at room temperature for 24 h, then concentrated *in vacuo*. The residue was diluted with 1 N NaOH aqueous solution (50 mL) and washed with ether (3 × 50 mL). The aqueous phase was acidified with 6 N HCl aqueous solution till pH 1 and extracted with EtOAc (3 × 75 mL). The combined organic layers were washed with brine, dried, filtered, and concentrated under

reduced pressure to afford the desired product **3** as yellow solid (12.1 g, 98%); $^1$H NMR (300 MHz, DMSO-$d_6$) δ 13.61 (br s, 1H exchangeable with $D_2O$), 7.69 (s, 1H), 7.53 – 7.33 (m, 5H), 7.30 (s, 1H), 5.24 (s, 2H), 3.91 (s, 3H); MS: *m/z* 302 [M – $H^-$].

*7.1.1.2 Procedures for the preparation of α-aminoketones (4a-c)*

Synthesis of 2-azido-1-phenylethan-1-one (10)

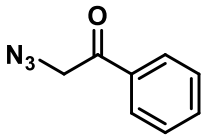


To an ice-cooled solution of 2-bromoacetophenone (5.0 g, 25.1 mmol) in DMF (60 mL) was added sodium azide (4.9 g, 75.4 mmol). The reaction mixture was stirred at 0 °C for 30 min, then diluted with water (40 mL) and EtOAc (40 mL). The phases were separated and the aqueous layer was extracted twice with EtOAc (2 × 40 mL). The combined organic layers were then washed with $NaHCO_3$ saturated solution (3 × 30 mL) and brine (50 mL), dried over $Na_2SO_4$, filtered, and concentrated *in vacuo*, affording the desired product (**10**) as yellow oil (4.0 g, 98%). *Known compound*. NMR data are consistent with those reported. $^1$H NMR (400 MHz, Chloroform-*d*) δ 7.92 – 7.89 (m, 2H), 7.63 – 7.59 (m, 1H), 7.52 – 7.50 (m, 2H), 4.56 (s, 2H);[175] MS: *m/z* 162 [M + $H^+$].

Synthesis of 2-amino-1-phenylethan-1-one hydrochloride (4a)

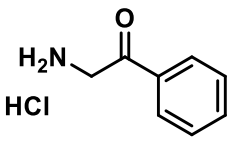


The 2-azido-1-phenylethan-1-one **10** (4.0 g, 24.8 mmol) was dissolved in MeOH (50 mL) and the solution was cooled at 0 °C. Then, 12 N HCl aqueous solution (3.0 mL) and triphenylphosphine (7.2 g, 27.3 mmol) were added. The reaction mixture was allowed to warm to room temperature and stirred overnight. The reaction mixture was diluted with 6 N HCl aqueous solution (15 mL) and

evaporated under reduced pressure to provide the 2-amino-1-phenylethan-1-one hydrochloride, which was directly in the next step, without further purification, considering a quantitative conversion of limiting reagent.

Synthesis of tert-butyl (2-(methoxy(methyl)amino)-2-oxoethyl)carbamate (12)

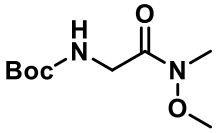


A solution of N-(Boc)glycine (5.0 g, 28.5 mmol) in anhydrous THF (40 mL) was cooled to 0 °C and 1,1-carbonyldiimidazole (CDI; 5.6 g, 34.3 mmol) was added portion-wise. The mixture was stirred at 0 °C for 15 minutes, then at room temperature for 1 h. *N,O*-dimethylhydroxylamine hydrochloride (3.3 g, 37.1 mmol) and triethylamine (5.2 mL, 37.1 mmol) were added in this order and the resulting suspension was stirred at room temperature overnight. After this time, the mixture was filtered and the filtrate evaporated to dryness. The residue was taken up with EtOAc (150 mL) and washed with 1 N HCl aqueous solution (3 × 50 mL), $NaHCO_3$ saturated solution (3 × 50 mL), brine (50 mL), dried over $Na_2SO_4$, filtered, and concentrated *in vacuo*, affording the desired product (**12**) as white solid (5.0 g, 80%). *Known compound*. NMR data are consistent with those reported. $^1$H NMR (400 MHz, Chloroform-*d*) δ 5.28 (s, 1H), 4.10 (d, *J* = 4.8 Hz, 2H), 3.74 (s, 3H), 3.23 (s, 3H), 1.48 (s, 9H);[176] MS: *m/z* 219 [M + $H^+$].

Synthesis of tert-butyl (2-cyclohexyl-2-oxoethyl)carbamate (13b)

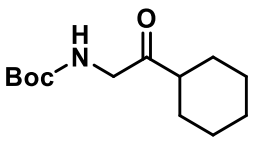


Tert-butyl (2-(methoxy(methyl)amino)-2-oxoethyl)carbamate **12** (4.40 g, 20.2 mmol) was dissolved in anhydrous THF (50 mL) and cooled to -15 °C. Then, cyclohexylmagnesium chloride (2.0 M solution in $Et_2O$, 21.1 mL) was added slowly, via syringe, and the resulting mixture was stirred at -15 °C for 1 h, and then

gently warmed to room temperature and stirred at the same temperature for 1 h. The reaction was quenched with $NH_4Cl$ satured solution and extracted with diethyl ether (3 × 100 mL). The organic phase was washed with brine, dried, filtered and concentrated under reduced pressure. The residue was purified by silica gel chromatography (*n*-Hex/EtOAc) to give the title compound as colorless oil (2.48 g, 50%); $^1$H NMR (300 MHz, DMSO-$d_6$) δ 6.94 (t, $J$ = 5.2 Hz, 1H exchangeable with $D_2O$), 3.80 (d, $J$ = 5.8 Hz, 2H), 2.46 – 2.31 (m, 1H), 1.81 – 1.53 (m, 5H), 1.37 (s, 9H), 1.28 – 1.08 (m, 5H); MS: *m/z* 242 [M + $H^+$].

Synthesis of tert-butyl (3-methyl-2-oxobutyl)carbamate (13c)

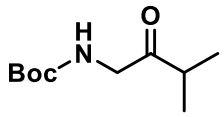


Synthesized in 45% yield using isopropylmagnesium chloride solution 2.0 M in THF, following the procedure described for **13b**. Colorless oil; $^1$H NMR (300 MHz, DMSO-$d_6$) δ 6.96 (t, $J$ = 5.2 Hz, 1H exchangeable with $D_2O$), 3.82 (d, $J$ = 5.9 Hz, 2H), 2.80 – 2.60 (m, 1H), 1.37 (s, 9H), 1.00 (d, $J$ = 6.9 Hz, 6H); MS: *m/z* 202 [M + $H^+$].

Synthesis of 2-amino-1-cyclohexylethan-1-one (4b)

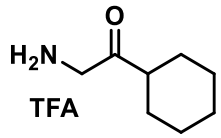


Tert-butyl (2-cyclohexyl-2-oxoethyl)carbamate **13b** (3.20 g, 13.3 mmol) was dissolved in 1:1 $CH_2Cl_2$/TFA (6 mL) and the solution was stirred at room temperature for 2 h. The reaction mixture was then diluted with toluene and evaporated under reduced pressure. The crude product was directly used in the next step without further purification, considering quantitative conversion of limiting reagent.

Synthesis of 1-amino-3-methylbutan-2-one (4c)

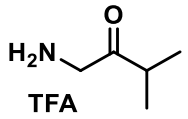


Synthesized starting from compound **13c** following the procedure described for **4b**. The crude product was directly used in the next step without further purification, considering quantitative conversion of limiting reagent.

*7.1.1.3 Procedures for the synthesis of 2-nitrobenzamides (2a-c)*

Synthesis of 4-(benzyloxy)-5-methoxy-2-nitro-N-(2-oxo-2-phenylethyl) benzamide (2a)

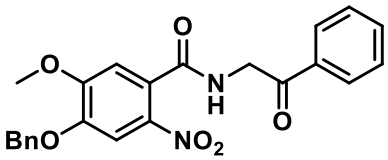


To an ice cooled suspension of 4-(benzyloxy)-5-methoxy-2-nitrobenzoic acid **3** (1.30 g, 4.29 mmol), HOBt·$H_2O$ (1.58 g, 10.3 mmol), HBTU (3.91 g, 10.3 mmol) in a mixture THF/DMF (100 mL; 4:1 ratio), N,N-diisopropylethylamine (DIPEA) (3.59 mL, 20.6 mmol) was added. The reaction mixture was stirred at room temperature for 15 min and then 2-amino-1-phenylethan-1-one hydrochloride (**4a**, 0.88 g, 5.15 mmol) was added. The mixture was stirred at room temperature for 12 h and then it was concentrated *in vacuo* and EtOAc (60 mL) was added. The organic layer was washed with $NaHCO_3$ saturated solution (3 × 20 mL), dried, and concentrated. Recrystallization from ethanol provided the title compound (1.52 g, 84 %) in high purity grade. $^1$H NMR (300 MHz, DMSO-$d_6$) $\delta$ 8.95 (t, J = 5.5 Hz, 1H exchangeable with $D_2O$), 8.06 – 8.04 (m, 2H), 7.73 – 7.67 (m, 2H), 7.60 – 7.55 (m, 2H), 7.49 – 7.31 (m, 5H), 7.15 (s, 1H), 5.26 (s, 2H), 4.79 (d, J = 5.5 Hz, 2H), 3.94 (s, 3H); MS: *m/z* 421 [M + $H^+$].

Synthesis of 4-(benzyloxy)-*N*-(2-cyclohexyl-2-oxoethyl)-5-methoxy-2-nitrobenzamide (2b)

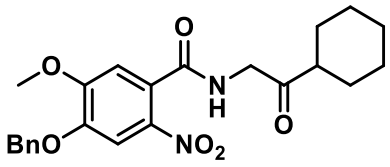


Synthesized in 70% yield starting from compounds **3** and **4b** following the procedure described for **2a**. White solid. $^1$H NMR (300 MHz, DMSO-$d_6$) $\delta$ 8.80 (t, J = 5.6 Hz, 1H exchangeable with $D_2O$), 7.72 (s, 1H), 7.49 – 7.35 (m, 5H), 7.13 (s, 1H), 5.25 (s, 2H), 4.15 (d, J = 5.6 Hz, 2H), 3.93 (s, 3H), 2.62 – 2.56 (m, 1H), 1.84 – 1.61 (m, 5H), 1.36 – 1.13 (m, 5H); MS: *m/z* 427 [M + H$^+$].

Synthesis of 4-(benzyloxy)-5-methoxy-N-(3-methyl-2-oxobutyl)-2-nitrobenzamide (2c)

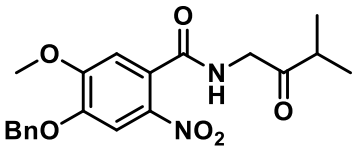


Synthesized in 85% yield starting from compounds **3** and **4c** following the procedure described for **2a**. White solid. $^1$H NMR (300 MHz, DMSO-$d_6$) $\delta$ 8.80 (t, J = 5.5 Hz, 1H exchangeable with $D_2O$), 7.72 (s, 1H), 7.48 – 7.34 (m, 5H), 7.12 (s, 1H), 5.25 (s, 2H), 4.18 (d, J = 5.5 Hz, 2H), 3.92 (s, 3H), 2.89 – 2.73 (m, 1H), 1.05 (d, J = 7.0 Hz, 6H); MS: *m/z* 387 [M + H$^+$].

### *7.1.2 General procedures for the reduction of 2-nitrobenzamides 2a-c*

**Methods A, E, F and G.** The proper catalyst was added to a solution of the appropriate 2-nitrobenzamide (0.60 mmol) in a mixture EtOAc/EtOH (20 mL; 2:1 ratio) and the reaction was stirred under $H_2$ (1 atm, balloon) at room temperature. The reaction mixture was filtered, concentrated and the residue was purified by silica gel chromatography ($CH_2Cl_2$/MeOH).

**Method B.** A 10 mL CEM microwave process vial with a stir bar was charged with the appropriate 2-nitrobenzamide **2** (0.10 mmol), 10 wt. % Pd/C (0.05 eq), and methanol (1 mL). 1,4-cyclohexadiene (57 µL, 0.60 mmol) was added. The vessel was capped and heated under microwave conditions at 120 °C for 10 min. The reaction was filtered through Celite, concentrated and the residue was purified by silica gel chromatography ($CH_2Cl_2$/MeOH).

**Method C.** A boiling solution of the appropriate 2-nitrobenzamide **2** (0.60 mmol) in ethanol (3 mL) was added to a suspension of iron (II) sulfate heptahydrate (1.67 g, 6.00 mmol) in water (3 mL) and 32% ammonium hydroxide solution (0.30 mL). The reaction mixture was heated under reflux until the disappearance of the starting material (TLC analysis) while 32% ammonium hydroxide was dropped (3 mL). The hot mixture was then filtered, concentrated and $CHCl_3$ (50 mL) was added. The organic layer was washed with $H_2O$ (3 × 20 mL) and brine (1 × 50 mL), dried, and concentrated in vacuo. The residue was purified by silica gel chromatography ($CH_2Cl_2$/MeOH).

**Method D.** Iron powder (0.67 g, 60.0 mg-atom) was added to a solution of the appropriate 2-nitrobenzamide **2** (0.60 mmol) in acetic acid (6 mL). The reaction mixture was heated at 70 °C until the disappearance of the starting material (TLC analysis). The mixture was diluted with water (20 mL) and $CHCl_3$ (20 mL) and filtered through a small pad of Celite. After separation of the two phases, the aqueous layer was extracted with $CHCl_3$ (2 × 20 mL). The organic phase was then washed with $H_2O$ (3 × 20 mL), $NaHCO_3$ saturated solution (1 × 20 mL) and brine (1 × 20 mL), dried and concentrated in vacuo. The residue was purified by silica gel chromatography ($CH_2Cl_2$/MeOH).

**Method H (Continuous flow processing H-Cube Pro™ hydrogenator)** A 10 mL stock solution of the appropriate 2-nitrobenzamide **2** with a 0.03 M concentration in THF was prepared in a glass vial. The reaction parameters (Full-$H_2$ mode, 80 °C, 50 bar and 0.3 mL/min flow rate) were selected on the H-Cube-Pro™ hydrogenator. The instrument was fitted with a 30 mm 5% Ru/C CatCart and the processing was started, whereby initially only pure solvent was pumped through the system until the instrument had achieved the desired reaction parameters and

stable processing. At that point, the sample inlet line was switched to the vial containing the substrate. A total reaction volume of 15 mL was collected, and the cartridge subsequently washed with pure solvent for 5 min to remove any substrate/product still adsorbed on the catalyst. Evaporation of the solvent afforded the desired 3,4-dihydro-5H-benzo[e][1,4]diazepin-5-ones 1a–c (99% crude yield), which were purified by flash chromatography to provide pure compounds (91-93%).

8-(benzyloxy)-7-methoxy-2-phenyl-3,4-dihydro-5H-benzo[e][1,4]diazepin-5-one (1a)

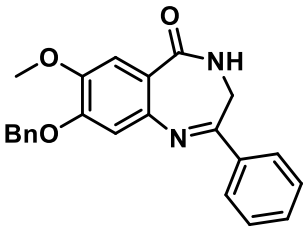


White solid; $^1$H NMR (300 MHz, DMSO-$d_6$): $\delta$ 8.41 (t, $J$ = 5.8 Hz, 1H exchangeable with $D_2O$), 8.06 – 8.03 (m, 2H), 7.55 – 7.33 (m, 9H), 7.02 (s, 1H), 5.21 (s, 2H), 3.94 (d, $J$ = 5.8 Hz, 2H), 3.85 (s, 3H). MS: *m/z* 373 [M + H$^+$].

8-(benzyloxy)-2-cyclohexyl-7-methoxy-3,4-dihydro-5H-benzo[e][1,4]diazepin-5-one (1b)

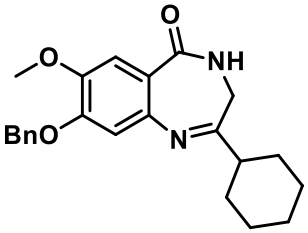


White solid; $^1$H NMR (300 MHz, DMSO-$d_6$): $\delta$ 8.26 (t, $J$ = 5.6 Hz, 1H exchangeable with $D_2O$), 7.47 – 7.34 (m, 5H), 7.29 (s, 1H), 6.82 (s, 1H), 5.15 (s, 2H), 3.81 (s, 3H), 3.40 (d, $J$ = 5.6 Hz, 2H), 2.45 – 2.36 (m, 1H), 1.93 – 1.65 (m, 5H), 1.42 – 1.17 (m, 5H); MS: *m/z* 379 [M + H$^+$].

8-(benzyloxy)-2-isopropyl-7-methoxy-3,4-dihydro-5*H*-benzo[*e*][1,4]diazepin-5-one (1c)

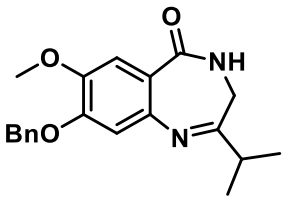


White solid; $^1$H NMR (300 MHz, DMSO-$d_6$): $\delta$ 8.31 (t, $J$ = 5.6 Hz, 1H exchangeable with $D_2O$), 7.48 – 7.35 (m, 5H), 7.31 (s, 1H), 6.85 (s, 1H), 5.17 (s, 2H), 3.82 (s, 3H), 3.41 (d, $J$ = 5.6 Hz, 2H), 2.83 – 2.70 (m, 1H), 1.18 (d, $J$ = 6.8 Hz, 6H); MS: *m/z* 339 [M + H$^+$].

2-amino-4-hydroxy-*N*-(2-hydroxy-2-phenylethyl)-5-methoxybenzamide (14a)

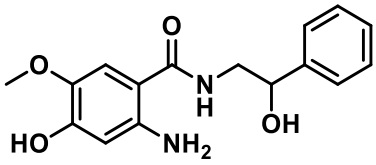


Yellow oil. $^1$H NMR (300 MHz, DMSO-$d_6$) $\delta$ 9.28 (br s, 1H exchangeable with $D_2O$), 8.02 (t, J = 5.7 Hz, 1H exchangeable with $D_2O$), 7.38 – 7.22 (m, 5H), 7.05 (s, 1H), 6.14 – 6.13 (m, 3H, 2H exchangeable with $D_2O$), 5.50 (d, J = 4.2 Hz, 1H exchangeable with $D_2O$), 4.77 – 4.71 (m, 1H), 3.67 (s, 3H), 3.25 – 3.17 (m, 2H); MS: *m/z* 303 [M + H$^+$].

8-hydroxy-7-methoxy-2-phenyl-1,2,3,4-tetrahydro-5*H*-benzo[*e*][1,4]diazepin-5-one (15a)

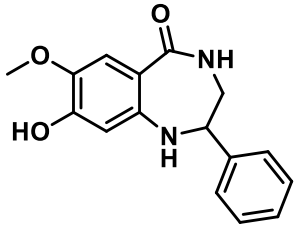


White solid; $^1$H NMR (300 MHz, DMSO-$d_6$) $\delta$ 9.37 (br s, 1H exchangeable with $D_2O$), 7.66 (t, J = 5.7 Hz, 1H exchangeable with $D_2O$), 7.37 – 7.26 (m, 5H),

7.15 (s, 1H), 6.35 (s, 1H), 5.75 (s, 1H exchangeable with $D_2O$), 4.66 (t, J = 5.7 Hz, 1H), 3.69 (s, 3H), 3.37 – 3.33 (m, 2H); MS: *m/z* 285 [M + $H^+$].

2-cyclohexyl-8-hydroxy-7-methoxy-1,2,3,4-tetrahydro-5*H*-benzo[*e*][1,4]diazepin-5-one (15b)

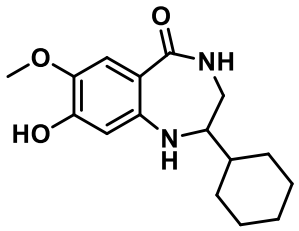


White solid; $^1H$ NMR (300 MHz, DMSO-$d_6$) $\delta$ 9.23 (br s, 1H exchangeable with $D_2O$), 7.68 (t, J = 5.8 Hz, 1H exchangeable with $D_2O$), 7.16 (s, 1H), 6.21 (s, 1H), 5.86 (d, J = 4.5 Hz, 1H exchangeable with $D_2O$), 3.64 (s, 3H), 3.21 – 3.10 (m, 2H), 3.03 – 3.00 (m, 1H), 1.77 – 1.62 (m, 5H), 1.45 – 1.36 (m, 1H), 1.23 – 0.87 (m, 5H); MS: *m/z* 291 [M + $H^+$].

2-amino-4-(benzyloxy)-5-methoxy-N-(2-oxo-2-phenylethyl)benzamide (16a)

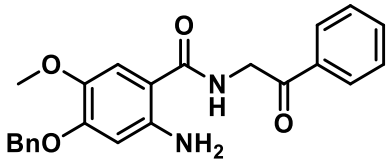


Yellow oil. $^1H$ NMR (300 MHz, DMSO-$d_6$) $\delta$ 8.40 (t, J = 5.8 Hz, 1H exchangeable with $D_2O$), 8.06 – 8.03 (m, 2H) 7.55 – 7.33 (m, 11H, 2H exchangeable with $D_2O$), 7.02 (s, 1H), 5.21 (s, 2H), 3.95 (d, J = 5.8 Hz, 2H), 3.85 (s, 3H); MS: *m/z* 391 [M + $H^+$].

8-(benzyloxy)-7-methoxy-2-phenyl-1,2,3,4-tetrahydro-5*H*-benzo[*e*][1,4]diazepin-5-one (17a)

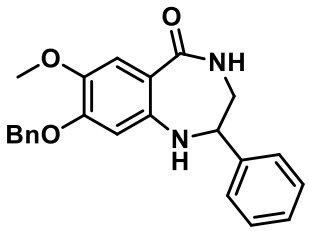


White solid; $^1$H NMR (300 MHz, DMSO-$d_6$) $\delta$ 7.73 (t, J = 5.5 Hz, 1H, exchangeable with $D_2O$), 7.48 – 7.26 (m, 10H), 7.20 (s, 1H), 6.61 (s, 1H), 6.22 (d, J = 3.6 Hz, 1H, exchangeable with $D_2O$), 5.04 (s, 2H), 4.69 – 4.67 (m, 1H), 3.69 (s, 3H); MS: *m/z* 375 [M + $H^+$].

### *7.1.3 General procedures for the functionalization of the 1,4-benzodiazepine nucleus*

Synthesis of 8-hydroxy-7-methoxy-2-phenyl-3,4-dihydro-5*H*-benzo[*e*][1,4]diazepin-5-one (18a)

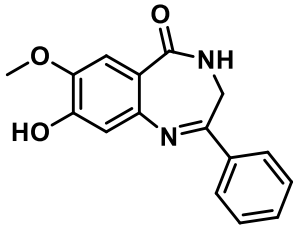


Compound **1a** (240 mg, 0.64 mmol) was dissolved in a mixture $CH_2Cl_2$/TFA (25 mL; 1:4 ratio). After stirring at 50 °C for 4 h, the reaction mixture was concentrated under reduced pressure. The residue was dissolved in EtOAc (20 mL), washed with $NaHCO_3$ saturated solution (3 × 10 mL) and brine (20 mL). The organic phase was dried over sodium sulfate, filtered and evaporated to give the title compound (137 mg) in 75% yield as pale yellow solid. $^1$H NMR (400 MHz, DMSO-$d_6$) δ 9.89 (br s, 1H exchangeable with $D_2O$), 8.31 (t, *J* = 5.9 Hz, 1H exchangeable with $D_2O$), 8.05 – 7.99 (m, 2H), 7.55 – 7.51 (m, 3H), 7.32 (s, 1H), 6.76 (s, 1H), 3.92 (d, *J* = 5.9 Hz, 2H), 3.84 (s, 3H); MS: *m/z* 283 [M + $H^+$].

Synthesis of 2-cyclohexyl-8-hydroxy-7-methoxy-3,4-dihydro-5H-benzo[e][1,4]diazepin-5-one (18b)

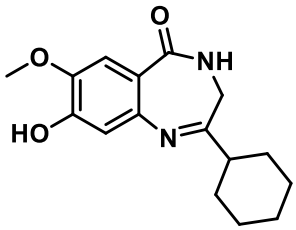


Synthesized in 68% yield starting from compound **1b** following the procedure described for **18a**. White solid; $^1$H NMR (400 MHz, DMSO-$d_6$) δ 9.76 (br s, 1H exchangeable with $D_2O$), 8.14 (t, $J$ = 5.5 Hz, 1H exchangeable with $D_2O$), 7.24 (s, 1H), 6.58 (s, 1H), 3.79 (s, 3H), 3.37 (d, $J$ = 5.6 Hz, 2H), 2.46 – 2.35 (m, 1H), 1.95 – 1.61 (m, 5H), 1.43 – 1.10 (m, 5H); MS: *m/z* 289 [M + H$^+$].

Synthesis of 8-(3-chloropropoxy)-7-methoxy-2-phenyl-3,4-dihydro-5H-benzo[e][1,4]diazepin-5-one (19a)

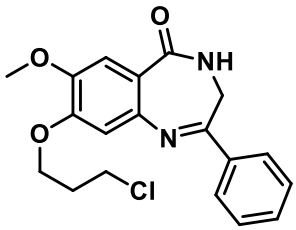


To a suspension of compound **18a** (50 mg, 0.18 mmol) and potassium carbonate (108 mg, 0.78 mmol) in anhydrous DMF (1 mL), 1-chloro-3-iodopropane (159 mg, 0.78 mmol) was added. The reaction mixture was stirred, under nitrogen atmosphere, at room temperature overnight. The mixture was then diluted with EtOAc (60 mL) and washed with $NaHCO_3$ saturated solution (3 × 20 mL) and brine (30 mL), dried over sodium sulfate, filtered and concentrated *in vacuo*. The crude was purified by silica gel chromatography ($CH_2Cl_2$/EtOAc), giving the desired product (49 mg) in 77% yield as a yellow solid. $^1$H NMR (400 MHz, DMSO-$d_6$) δ 8.40 (t, $J$ = 5.8 Hz, 1H exchangeable with $D_2O$), 8.08 – 8.01 (m, 2H), 7.57 – 7.51 (m, 3H), 7.35 (s, 1H), 6.94 (s, 1H), 4.20 (t, $J$ = 6.1 Hz, 2H), 3.95 (d, $J$ = 5.9 Hz,

2H), 3.85 (s, 3H), 3.80 (t, *J* = 6.5 Hz, 2H), 2.28 – 2.16 (m, 2H); MS: *m/z* (%) 359 (100) [M + $H^+$]; 361 (32) [M + H + $2^+$].

Synthesis of 8-(3-chloropropoxy)-2-cyclohexyl-7-methoxy-3,4-dihydro-5H-benzo[e][1,4]diazepin-5-one (19b)

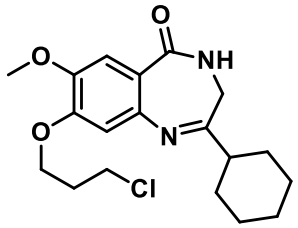


Synthesized in 71% yield starting from compound **18b** following the procedure described for **19a**. White solid; $^1$H NMR (400 MHz, DMSO-$d_6$) δ 8.25 (t, J = 5.7 Hz, 1H exchangeable with $D_2O$), 7.27 (s, 1H), 6.73 (s,1H), 4.14 (t, J = 6.1 Hz, 2H), 3.82 – 3.75 (m, 5H), 3.40 (d, J = 5.7 Hz, 2H), 2.47 – 2.41 (m, 1H), 2.25 – 2.14 (m, 2H), 1.96 – 1.61 (m, 5H), 1.45 – 1.14 (m, 5H); MS: *m/z* (%) 365 (100) [M + $H^+$]; 367 (32) [M + H + $2^+$].

Synthesis of 8-(3-chloropropoxy)-5-ethoxy-7-methoxy-2-phenyl-3H-benzo[e][1,4]diazepine (20a)

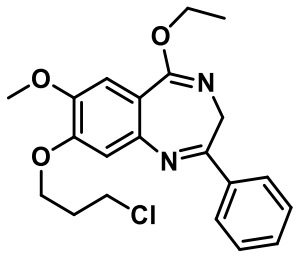


To an ice-cooled suspension of **19a** (200 mg, 0.56 mmol) and sodium carbonate (59 mg, 0.56 mmol) in anhydrous $CH_2CH_2$ (4.2 mL), triethyloxonium tetrafluoroborate (212 mg, 1.12 mmol) was added. The reaction mixture was allowed to warm to room temperature and stirred for 15 minutes. The mixture was diluted with $CH_2CH_2$ (10 mL) and the organic phase was washed twice with brine (2 × 5 mL), dried over sodium sulfate, filtered and concentrated *in vacuo*. The

residue was purified by silica gel chromatography (*n*-Hex/EtOAc) to give the title compound (145 mg) in 67% yield as a yellow oil; $^1$H NMR (400 MHz, DMSO-$d_6$) δ 8.12 – 8.02 (m, 2H), 7.56 – 7.48 (m, 3H), 7.24 (s, 1H), 7.00 (s, 1H), 4.26 – 4.10 (m, 4H), 4.04 (br s, 2H), 3.85 (s, 3H), 3.81 (t, $J$ = 6.5 Hz, 2H), 2.29 – 2.16 (m, 2H), 1.27 (t, $J$ = 7.0 Hz, 3H); MS: *m/z* (%) 387 (100) [M + H$^+$]; 389 (32) [M + H + 2$^+$].

Synthesis of 8-(3-chloropropoxy)-2-cyclohexyl-5-ethoxy-7-methoxy-3H-benzo[e][1,4]diazepine (20b)

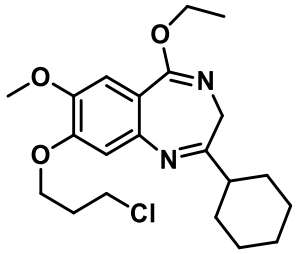


Synthesized in 70% yield starting from compound **19b** following the procedure described for **20a**. Pale yellow oil; $^1$H NMR (400 MHz, DMSO- $d_6$) δ 7.16 (s, 1H), 6.80 (s, 1H), 4.21 – 4.06 (m, 4H), 3.85 – 3.75 (m, 5H), 3.51 (br s, 2H), 2.47 – 2.40 (m, 1H), 2.28 – 2.11 (m, 2H), 2.01 – 1.58 (m, 5H), 1.45 – 1.14 (m, 8H); MS: *m/z* (%) 393 (100) [M + H$^+$]; 395 (32) [M + H + 2$^+$].

Synthesis of 5-ethoxy-7-methoxy-2-phenyl-8-(3-(pyrrolidin-1-yl)propoxy)-3H-benzo[e][1,4]diazepine (21a)

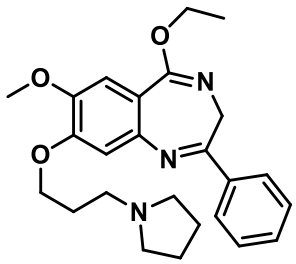


A 10 mL CEM pressure vessel equipped with a stirrer bar was charged with compound **20a** (87 mg, 0.23 mmol), sodium iodide (34 mg, 0.22 mmol), potassium

carbonate (47 mg, 0.34 mmol), pyrrolidine (189 μL) and anhydrous THF (2.3 mL). The microwave vial was sealed and heated in a CEM Discover microwave synthesizer to 80 °C (measured by the vertically focused IR temperature sensor) for 90 min. After cooling to room temperature, the reaction mixture was diluted with water (5 mL) and extracted with EtOAc (3 × 5 mL). The combined organic layers were washed with brine, dried, filtered, and concentrated *in vacuo*. The crude was purified by silica gel chromatography ($CH_2Cl_2$/MeOH/$NH_3$) to afford the title compound (72 mg) in 76% yield as a brownish oil. $^1$H NMR (400 MHz, DMSO-$d_6$) δ 8.13 – 8.05 (m, 2H), 7.58 – 7.48 (m, 3H), 7.24 (s, 1H), 6.98 (s, 1H), 4.21 – 4.10 (m, 4H), 4.03 (br s, 1H), 3.86 (s, 3H), 2.80 – 2.57 (m, 6H), 2.05 – 1.92 (m, 2H), 1.83 – 1.67 (m, 4H), 1.28 (t, $J$ = 7.0 Hz, 4H); MS: *m/z* 422 [M + $H^+$].

Synthesis of 2-cyclohexyl-5-ethoxy-7-methoxy-8-(3-(pyrrolidin-1-yl)propoxy)-3H-benzo[e][1,4]diazepine (21b)

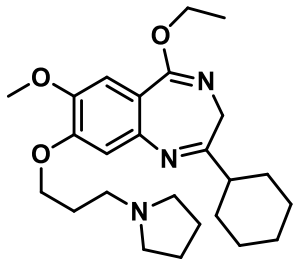

Synthesized in 74% yield starting from compound **20b** following the procedure described for **21a**. Brownish oil. $^1$H NMR (400 MHz, DMSO-$d_6$) δ 7.13 (s, 1H), 6.76 (s, 1H), 4.13 (q, $J$ = 7.0 Hz, 2H), 4.07 (t, $J$ = 6.5 Hz, 2H), 3.80 (s, 3H), 3.47 (br s, 2H), 2.46 – 2.31 (m, 5H), 1.98 – 1.61 (m, 11H), 1.44 – 1.15 (m, 8H); MS: *m/z* 428 [M + $H^+$].

Synthesis of N-(1-isopropylpiperidin-4-yl)-7-methoxy-2-phenyl-8-(3-(pyrrolidin-1-yl)propoxy)-3H-benzo[e][1,4]diazepin-5-amine 22a (EML693)

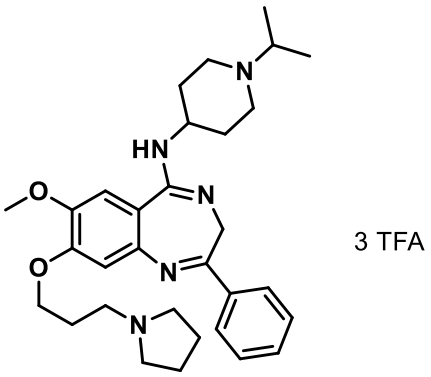


A 10 mL CEM pressure vessel equipped with a stirrer bar was charged with compound **21a** (71 mg, 0.168 mmol), 4-amino-1-isopropyl piperidine (266 µL) and *i*-PrOH (600 µL). The microwave vial was sealed and heated in a CEM Discover microwave synthesizer to 200 °C (measured by the vertically focused IR temperature sensor) for 2 h. The crude material is diluted with a mixture ACN/$H_2O$ in 2:8 ratio and purified by reverse phase high-performance liquid chromatography (RP-HPLC) to afford the 3 × TFA salt of **22a** as a yellow solid (45 mg, 31%). $^1$H NMR (400 MHz, $D_2O$) δ 7.75 – 7.69 (m, 5H), 7.51 (s, 1H), 7.26 (s, 1H), 4.43 – 4.27 (m, 3H), 4.09 (s, 3H), 3.86 – 3.74 (m, 2H), 3.67 – 3.54 (m, 3H), 3.49 (t, *J* = 7.5 Hz, 2H), 3.29 – 3.09 (m, 4H), 2.48 – 2.32 (m, 4H), 2.31 – 2.13 (m, 4H), 2.12 – 1.98 (m, 4H), 1.37 (d, *J* = 6.7 Hz, 6H); $^{13}$C NMR (100 MHz, $D_2O$ the signal of TFA was not included) δ 152.24, 149.67, 145.60, 140.71, 132.33, 131.31, 130.17, 129.60, 129.08, 115.89, 101.53, 100.13, 66.77, 58.42, 56.25, 54.35, 52.71, 50.26, 47.78, 30.59, 24.96, 22.64, 16.10; HRMS (ESI): *m/z* calculated for $C_{31}H_{43}N_5O_2 + H^+$ [M + $H^+$]: 518.3490. Found: 518.3518.

.

Synthesis of 2-cyclohexyl-N-(1-isopropylpiperidin-4-yl)-7-methoxy-8-(3-(pyrrolidin-1-yl)propoxy)-3H-benzo[e][1,4]diazepin-5-amine 22b (EML741)

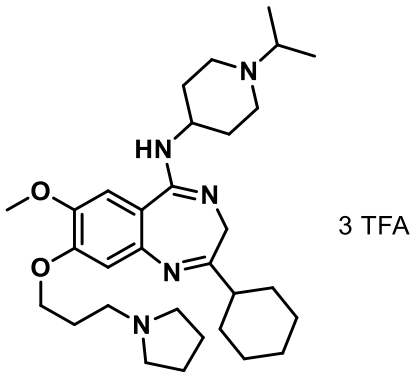


**Method A.** Compound **22b** was obtained as a yellow solid (<5%) from derivative **21b** according to the procedure described for **22a**.

**Method B.** A 10 mL CEM pressure vessel equipped with a stirrer bar was charged with compound **21b** (60 mg, 0.140 mmol), 4-amino-1-isopropyl piperidine (222 µL) and acetic acid (161 µL). The microwave vial was sealed and heated in a CEM Discover microwave synthesizer to 120 °C (measured by the vertically focused IR temperature sensor) for 60 min. The crude material is diluted with a mixture ACN/$H_2O$ in 2:8 ratio and purified by reverse phase high–performance liquid chromatography (RP-HPLC) to afford the 3 × TFA salt of **22b** (37 mg, 30%). $^1$H NMR (400 MHz, $D_2O$) δ 7.44 (s, 2H), 4.37 (t, *J* = 5.7 Hz, 2H), 4.20 – 4.11 (m, 1H), 4.05 (s, 3H), 3.85 – 3.74 (m, 2H), 3.64 – 3.54 (m, 3H), 3.50 (t, *J* = 7.5 Hz, 2H), 3.28 – 3.09 (m, 5H), 2.43 – 2.30 (m, 4H), 2.27 – 2.17 (m, 2H), 2.13 – 1.93 (m, 8H), 1.89 – 1.65 (m, 4H), 1.61 – 1.38 (m, 4H), 1.39 – 1.32 (m, 6H); $^{13}$C NMR (100 MHz, $D_2O$ the signal of TFA was not included) δ 151.80, 149.34, 147.90, 145.65, 132.11, 115.57, 101.58, 100.23, 66.70, 58.40, 56.18, 54.35, 52.71, 50.59, 47.77, 38.52, 30.54, 29.85, 25.75, 25.04, 24.95, 22.64, 16.08; HRMS (ESI): *m/z* calculated for $C_{31}H_{49}N_5O_2 + H^+$ [M + $H^+$]: 524.3959. Found: 524.3972.

Synthesis of 8-hydroxy-7-methoxy-2-phenyl-1,2,3,4-tetrahydro-5H-benzo[e][1,4]diazepin-5-one (15a)

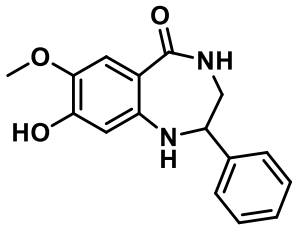


To a solution of **18a** (600 mg, 2.13 mmol) in THF/MeOH (60 mL; 1:1 ratio) cooled at 0 °C, $NaBH_4$ was added portion-wise until disappearance of the starting material (TLC silica gel). The reaction mixture was evaporated, taken up with water (40 mL), and extracted with $CHCl_3$ (3 × 30 mL). The organic phase was dried and the solvent evaporated to give pure **15a** (510 mg, 84%). Characterization, see Paragraph 7.1.2.

Synthesis of 2-cyclohexyl-8-hydroxy-7-methoxy-1,2,3,4-tetrahydro-5H-benzo[e][1,4]diazepin-5-one (15b)

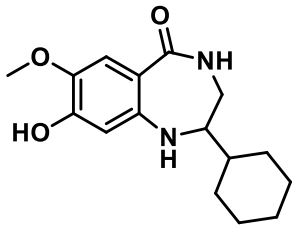


Synthesized in 90% yield starting from compound **18b** following the procedure described for **15a**. Characterization, see Paragraph 7.1.2.

Synthesis of 8-(3-chloropropoxy)-7-methoxy-2-phenyl-1,2,3,4-tetrahydro-5*H*-benzo[*e*][1,4]diazepin-5-one (23a)

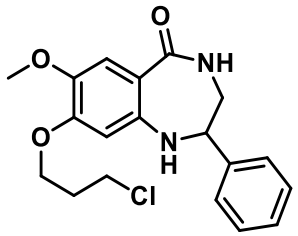


Compound **23a** was obtained as a pale yellow solid (77%) from derivative **15a** according to the procedure described for **19a**. $^1$H NMR (400 MHz, DMSO-$d_6$) δ 7.71 (t, $J$ = 5.8 Hz, 1H exchangeable with $D_2O$), 7.39 – 7.23 (m, 5H), 7.19 (s, 1H), 6.53 (s, 1H), 6.23 (d, $J$ = 3.8 Hz, 1H, exchangeable with $D_2O$), 4.73 – 4.60 (m, 1H), 4.09 – 3.99 (m, 2H), 3.79 (t, $J$ = 6.4 Hz, 2H), 3.68 (s, 3H), 3.43 – 3.34 (m, 2H), 2.24 – 2.13 (m, 2H); MS: *m/z* (%) 361 (100) [M + H$^+$]; 363 (32) [M + H + 2$^+$].

Synthesis of 8-(3-chloropropoxy)-2-cyclohexyl-7-methoxy-1,2,3,4-tetrahydro-5H-benzo[e][1,4]diazepin-5-one (23b)

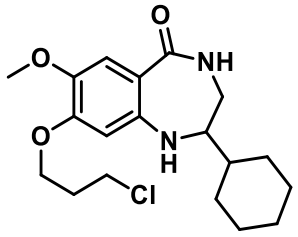


Compound **23b** was obtained as a white solid (67%) from derivative **15b** according to the procedure described for **19a**. $^1$H NMR (400 MHz, DMSO-$d_6$) δ 7.76 (t, $J$ = 5.3 Hz, 1H exchangeable with $D_2O$), 7.19 (s, 1H), 6.44 (s, 1H), 6.00 (d, $J$ = 4.5 Hz, 1H exchangeable with $D_2O$), 4.01 (t, $J$ = 6.2 Hz, 2H), 3.78 (t, $J$ = 6.4 Hz, 2H), 3.64 (s, 3H), 3.27 – 3.11 (m, 2H), 3.10 – 3.02 (m, 1H), 2.25 – 2.13 (m, 2H), 1.89 – 1.55 (m, 5H), 1.50 – 1.36 (m, 1H), 1.27 – 0.83 (m, 5H); MS: *m/z* (%) 367 (100) [M + H$^+$]; 369 (32) [M + H + 2$^+$].

Synthesis of 8-(3-chloropropoxy)-5-(ethylthio)-7-methoxy-2-phenyl-2,3-dihydro-1*H*-benzo[e][1,4]diazepine (24a)

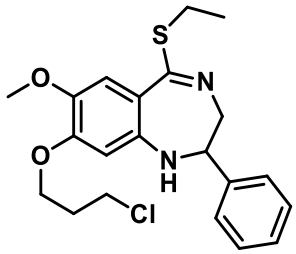


To a suspension of compound **23a** (100 mg, 0.28 mmol) in anhydrous toluene (5 mL), Lawesson's reagent (168 mg, 0.42 mmol) was added. The reaction mixture was heated at 85 °C for 1 h. After cooling at room temperature, potassium carbonate (69 mg, 0.50 mmol) and iodoethane (446 µL) were added and the reaction mixture was heated again to 85 °C for 2 h. The solvent was evaporated and the residue was was partitioned between $H_2O$ (5 mL) and EtOAc (10 mL). The organic layer was washed with water (2 × 5 mL), 10% $Na_2S_2O_3$ solution (3 × 5 mL) and brine (10 mL), dried over sodium sulfate, filtered and concentrated *in vacuo*. The residue was purified by silica gel chromatography ($CH_2Cl_2$/MeOH) to give the desired product **24a** (86 mg) in 77% yield as yellow solid. $^1$H NMR (400 MHz, DMSO-$d_6$) δ 7.43 – 7.18 (m, 5H), 7.00 (s, 1H), 6.64 (s, 1H), 6.02 (br s, 1H exchangeable with $D_2O$), 5.01 – 4.88 (m, 1H), 4.13 – 3.99 (m, 2H), 3.92 – 3.59 (m, 7H), 2.99 – 2.79 (m, 2H), 2.30 – 2.11 (m, 2H), 1.15 (t, $J$ = 7.3 Hz, 3H). MS: *m/z* (%) 405 (100) [M + H$^+$]; 407 (32) [M + H + 2$^+$].

Synthesis of 8-(3-chloropropoxy)-2-cyclohexyl-5-(ethylthio)-7-methoxy-2,3-dihydro-1H-benzo[e][1,4]diazepine (24b)

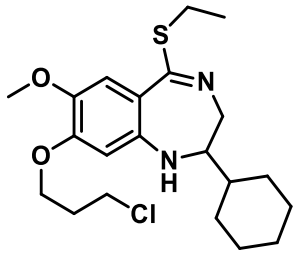


Compound **24b** was obtained as yellow solid (72%) from derivative **23b** according to the procedure described for **24a**. $^1$H NMR (400 MHz, DMSO-$d_6$) δ 6.97 (s, 1H), 6.55 (s, 1H), 5.84 (br s, 1H exchangeable with $D_2O$), 4.02 (t, $J$ = 6.1 Hz, 2H), 3.78 (t, $J$ = 6.3 Hz, 2H), 3.69 – 3.55 (m, 5H), 3.05 – 2.79 (m, 2H), 2.30 – 2.11 (m, 2H), 1.98 – 1.52 (m, 5H), 1.44 – 0.91 (m, 9H); MS: *m/z* (%) 411 (100) [M + $H^+$]; 413 (32) [M + H + $2^+$].

Synthesis of 5-(ethylthio)-7-methoxy-2-phenyl-8-(3-(pyrrolidin-1-yl)propoxy)-2,3-dihydro-1H-benzo[e][1,4]diazepine (25a)

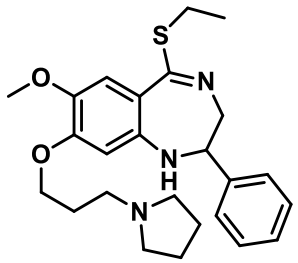


Synthesized in 65% yield starting from compound **24a** following the procedure described for **25a**. Yellow oil. $^1$H NMR (400 MHz, DMSO-$d_6$) δ 7.43 – 7.18 (m, 5H), 6.98 (s, 1H), 6.60 (s, 1H), 5.87 (d, J = 2.6 Hz, 1H exchangeable with $D_2O$), 4.93 – 4.85 (m, 1H), 4.08 – 3.89 (m, 2H), 3.86 – 3.72 (m, 4H), 3.69 (s, 3H), 2.97 – 2.78 (m, 2H), 2.46 – 2.38 (m, 4H), 1.98 – 1.83 (m, 2H), 1.71 – 1.64 (m, 4H), 1.14 (t, J = 7.3 Hz, 3H); MS: *m/z* 440 [M + $H^+$].

Synthesis of 2-cyclohexyl-5-(ethylthio)-7-methoxy-8-(3-(pyrrolidin-1-yl)propoxy)-2,3-dihydro-1H-benzo[e][1,4]diazepine (25b)

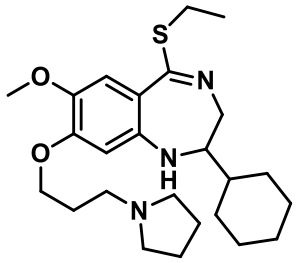

Synthesized in 67% yield starting from compound **24b** following the procedure described for **25a**. Yellow oil. $^1$H NMR (400 MHz, DMSO-$d_6$) δ 6.94 (s, 1H), 6.51 (s, 1H), 5.67 (d, $J$ = 3.3 Hz, 1H exchangeable with $D_2O$), 3.93 (t, $J$ = 6.7 Hz, 2H), 3.78 – 3.53 (m, 5H), 3.42 – 3.35 (m, 2H), 3.27 – 3.19 (m, 1H), 3.02 – 2.77 (m, 2H), 2.45 – 2.34 (m, 4H), 2.05 – 1.56 (m, 11H), 1.40 – 0.81 (m, 9H). MS: *m/z* 446 [M + H$^+$].

Synthesis of N-(1-isopropylpiperidin-4-yl)-7-methoxy-2-phenyl-8-(3-(pyrrolidin-1-yl)propoxy)-2,3-dihydro-1*H*-benzo[*e*][1,4]diazepin-5-amine 26a (EML696)

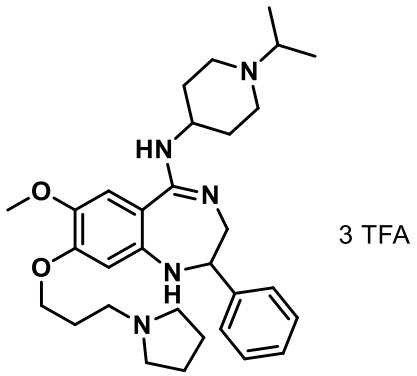


Compound **26a** (3 × TFA salt) was obtained as a yellow solid (31%) from derivative **25a** according to the procedure described for **22a**. $^1$H NMR (400 MHz, $D_2O$) δ 7.50 – 7.33 (m, 5H), 7.10 (s, 1H), 6.64 (s, 1H), 5.14 – 5.06 (m, 1H), 4.23 (t, $J$ = 5.0 Hz, 2H), 3.92 – 3.87 (m, 3H), 3.83 – 3.73 (m, 5H), 3.67 – 3.51 (m, 3H), 3.46 (t, $J$ = 7.6 Hz, 2H), 3.22 – 2.99 (m, 4H), 2.47 – 2.38 (m, 1H), 2.31 (h, $J$ = 5.9 Hz, 2H), 2.26 – 2.12 (m, 2H), 2.13 – 1.96 (m, 4H), 1.93 – 1.76 (m, 1H), 1.35 (d, $J$ = 6.7

Hz, 6H); 13C NMR (100 MHz, $D_2O$ the signal of TFA was not included) δ 163.44, 153.50, 143.35, 142.78, 141.32, 128.96, 128.26, 126.52, 112.82, 105.89, 104.74, 66.29, 66.11, 58.59, 56.42, 54.34, 52.68, 47.40, 47.36, 47.12, 46.69, 28.11, 28.01, 25.04, 22.63, 16.07; HRMS (ESI): *m/z* calculated for $C_{31}H_{45}N_5O_2 + H^+$ [M + $H^+$]: 520.3646. Found: 520.3647.

Synthesis of 2-cyclohexyl-N-(1-isopropylpiperidin-4-yl)-7-methoxy-8-(3-(pyrrolidin-1-yl)propoxy)-2,3-dihydro-1H-benzo[e][1,4]diazepin-5-amine 26b (EML698)

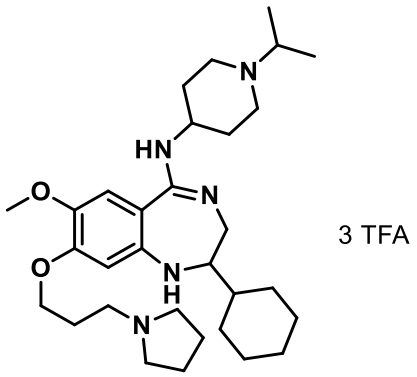


Compound **26b** (3 × TFA salt) was obtained as a yellow solid (30%) from derivative **25b** according to the procedure described for **22a**; $^1$H NMR (400 MHz, $D_2O$) δ 7.21 (s, 1H), 7.00 (s, 1H), 4.26 (t, *J* = 5.2 Hz, 2H), 4.06 – 3.95 (m, 1H), 3.91 (s, 3H), 3.85 – 3.70 (m, 3H), 3.69 – 3.50 (m, 5H), 3.44 (t, *J* = 7.6 Hz, 2H), 3.28 – 3.06 (m, 4H), 2.45 (t, *J* = 12.3 Hz, 2H), 2.30 (q, *J* = 6.6, 6.1 Hz, 2H), 2.18 (q, *J* = 7.5, 7.0 Hz, 2H), 2.09 – 1.92 (m, 4H), 1.91 – 1.61 (m, 6H), 1.41 – 1.35 (m, 6H), 1.31 – 1.01 (m, 5H); $^{13}$C NMR (100 MHz, $D_2O$ the signal of TFA was not included) δ 162.53, 152.90, 146.47, 134.88, 112.72, 111.43, 107.29, 70.38, 66.67, 58.65, 56.39, 54.32, 52.62, 47.81, 47.27, 47.22, 41.92, 39.38, 28.87, 28.49, 28.10, 28.04, 25.53, 25.37, 25.01, 22.62, 16.06; HRMS (ESI): *m/z* calculated for $C_{31}H_{51}N_5O_2$ + $H^+$ [M + $H^+$]: 526.4116. Found: 526.41115.

### *7.1.4 Procedures for the preparation of 4-azidoquinoline 27*

Synthesis of 1-(4-(benzyloxy)-3-methoxyphenyl)ethan-1-one (30)

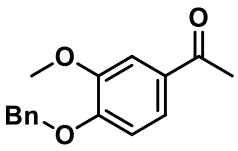


To a solution of acetovanillone (5.0 g, 30.1 mmol) in acetone (90 mL) $K_2CO_3$ (6.2 g, 45.1 mmol) and benzyl bromide (5.7 g, 33.1 mmol) were added. The reaction mixture was refluxed for 2 h, then cooled to room temperature and concentrated *in vacuo*. The residue was taken up with EtOAc (150 mL) and washed with water (3 × 50 mL) and brine (75 mL), dried over $Na_2SO_4$, filtered, and concentrated to afford the desired product (**30**) as white solid (7.5 g, 97%); *Known compound*. NMR data are consistent with those reported.[1]H NMR (400 MHz, Chloroform-*d*) δ 7.53 – 7.29 (m, 7H), 6.87 (d, *J* = 8.4 Hz, 1H), 5.20 (s, 2H), 3.91 (s, 3H), 2.52 (s, 3H);[177] MS: *m/z* 257 [M + $H^+$].

Synthesis of 1-(4-(benzyloxy)-5-methoxy-2-nitrophenyl)ethan-1-one (31)

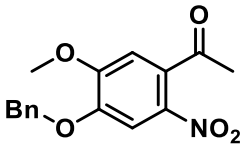


To an ice-cooled solution of compound **30** (3.00 g,11.7 mmol) in acetic anhydride (60 mL), fuming nitric acid (1.6 mL, 35.1 mmol) was added. The reaction mixture was stirred at 0 °C for 15 min, then it was poured into ice-water and extracted with $CH_2CH_2$ (3 × 50 mL). The combined organic layers were washed with $NaHCO_3$ saturated solution (3 × 50 mL) and brine, dried, and concentrated *in vacuo*. The product was recovered as yellow solid (2.94 g, 83%). [1]H NMR (400 MHz, DMSO-$d_6$) δ 7.76 (s, 1H), 7.50 – 7.33 (m, 5H), 7.25 (s, 1H), 5.25 (s, 2H), 3.93 (s, 3H), 2.52 (s, 3H). MS: *m/z* 302 [M + $H^+$].

Synthesis of 1-(2-amino-4-(benzyloxy)-5-methoxyphenyl)ethan-1-one (32)

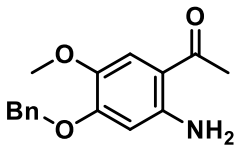


1-(4-(benzyloxy)-5-methoxy-2-nitrophenyl)ethan-1-one **31** (0.51 g, 1.69 mmol), iron powder (0.47 g, 8.46 mmol) and ammonium chloride (0.05 g, 0.85 mmol) were added to a mixture EtOH/$H_2O$ (12 mL; 2:1 ratio). The mixture was stirred at reflux for 30 min, then cooled and filtered through a pad of Celite. The solvents were removed under reduced pressure and the residue was taken up with EtOAc (30 mL) and washed with $H_2O$ (2 × 15 mL) and brine, dried over $Na_2SO_4$, filtered and evaporated to give a residue that was purified by flash chromatography (*n*-Hex/EtOAc) to yield the desired compound as a yellow solid (4.00 g, 87%). *Known compound*. NMR data are consistent with those reported. $^1$H NMR (400 MHz, DMSO-$d_6$) δ 7.50 – 7.29 (m, 5H), 7.15 (s, 1H), 7.07 (br s, 2H exchangeable with $D_2O$), 6.41 (s, 1H), 5.07 (s, 2H), 3.71 (s, 3H), 2.43 (s, 3H);[178] MS: *m/z* 272 [M + $H^+$].

Synthesis of N-(2-acetyl-5-(benzyloxy)-4-methoxyphenyl) cyclohexanecarboxamide (33)

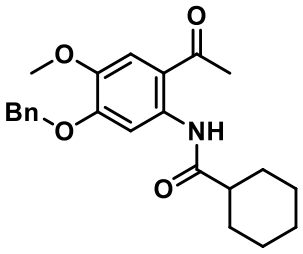


A solution of compound **32** (1.11 g, 4.09 mmol) and DIPEA (1.43 mL, 8.18 mL) in anhydrous THF (30 mL) was cooled in ice bath, then cyclohexanecarbonyl chloride (0.66 g, 4.50 mmol) was added. The reaction mixture was allowed to warm to room temperature and was stirred for 90 min. The solvent was removed under reduced pressure and the residue was taken up with EtOAc (50 mL) and washed with $H_2O$ (2 × 20 mL) and brine, dried over $Na_2SO_4$, filtered and evaporated,

affording the title compound as yellow solid (1.53 g, 98%); $^1$H NMR (400 MHz, DMSO-$d_6$) δ 11.79 (s, 1H exchangeable with $D_2O$), 8.47 (s, 1H), 7.54 – 7.28 (m, 6H), 5.14 (s, 2H), 3.83 (s, 3H), 2.63 (s, 3H), 2.37 – 2.22 (m, 1H), 2.05 – 1.55 (m, 5H), 1.51 – 1.12 (m, 5H). MS: *m/z* 382 [M + $H^+$].

Synthesis of 7-(benzyloxy)-2-cyclohexyl-6-methoxyquinolin-4-ol (34)

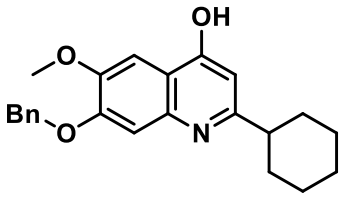


A mixture of derivative **33** (1.69 g, 4.43 mmol) and NaOH (1.77 g, 44.30 mmol) in 1,4-dioxane (150 mL) was refluxed for 24 h. The reaction mixture was concentrated *in vacuo* then ice-water was added and the precipitate was collected *via* filtration over a Büchner funnel. Yellow solid (1.12 g, 80%); $^1$H NMR (400 MHz, DMSO-$d_6$) δ 11.18 (br s, 1H exchangeable with $D_2O$), 7.56 – 7.30 (m, 6H), 7.10 (s, 1H), 5.82 (s, 1H), 5.18 (s, 2H), 3.82 (s, 3H), 2.47 – 2.41 (m, 1H), 1.94 – 1.63 (m, 5H), 1.55 – 1.13 (m, 5H); MS: *m/z* 364 [M + $H^+$].

Synthesis of 4-azido-7-(benzyloxy)-2-cyclohexyl-6-methoxyquinoline (27)

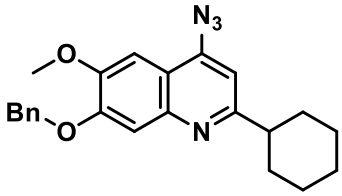


7-(benzyloxy)-2-cyclohexyl-6-methoxyquinolin-4-ol **34** (1.00 g, 2.75 mmol) was suspended in anhydrous DMF (15 mL), then triethylamine (0.50 mL, 3.58 mmol) and diphenyl phosphoryl azide (0.65 mL, 3.03 mmol) were added. The mixture was heated to 100 °C and stirred for 1 h, then it was cooled to room temperature, diluted with $H_2O$ (60 mL) and extracted with EtOAc (3 × 60 mL). The combined organic extracts were washed with $NaHCO_3$ saturated solution (3 × 50

mL) and brine, dried, and concentrated *in vacuo*. The residue was purified by silica gel chromatography (*n*-Hex/EtOAc) to give the title compound (0.73 g) in 73% yield as pale yellow solid. $^1$H NMR (400 MHz, DMSO-$d_6$) δ 7.52 – 7.47 (m, 2H), 7.46 – 7.33 (m, 4H), 7.22 – 7.15 (m, 2H), 5.28 (s, 2H), 3.89 (s, 3H), 2.80 (t, $J$ = 11.9 Hz, 1H), 2.00 – 1.14 (m, 10H); MS: *m/z* 389 [M + H$^+$].

## 7.2 AlphaLISA assays protocols

General directions. All the assays were performed in white Optiplate-384 (PerkinElmer, # 6007299) at room temperature in a final volume of 25 µL. Signals were read in Alpha mode with the EnSight Multimode Plate Reader (PerkinElmer). All incubation steps with AlphaLISA beads were performed at room temperature under subdued lighting condition.

***G9a***

The assays were performed using the following Assay Buffer: 50 mM Tris-HCl, pH 9.0, 50 mM NaCl, 1 mM DTT, 0.01% Tween-20. Human recombinant G9a (BPS Bioscience, # 51001) (0.1 nM, final concentration) was diluted in Assay Buffer, then and proper inhibitor (0.1% DMSO, final concentration) was added. After a pre-incubation time of 15 minutes, Histone H3 (1-21) peptide, biotinylated (AnaSpec, # 61702) (100 nM, final concentration) and SAM (Sigma, # A7007) (15 µM, final concentration) were added. The reaction was incubated for 30 min, afterwards the Anti-methyl-Histone H3 Lysine 9 (H3K9me2) AlphaLISA Acceptor Beads (PerkinElmer, # AL117) in Epigenetic Buffer 1X were added in each well (20 µg/mL, final concentration). After an incubation of 1 h, Streptavidin Donor beads (PerkinElmer, # 6760002) were diluted in Epigenetic Buffer 1X and added in each well (20 µg/mL, final concentration). The Alpha signal was read after 30 minutes of incubation.

To determine the inhibition pattern of **EML741**, were performed two different set of experiments. In the first set, SAM concentration was varied from 3.75 to 30 µM, while holding H3 biotinylated peptide constant (100 nM). In the

second one, using fixed SAM concentration (15 μM), the concentration of the H3 biotinylated peptide was varied from 25 to 100 nM.

***PRMT1***

The assays were performed using the following Assay Buffer: 30 mM Tris-HCl, pH 8.0, 1 mM DTT, 0.01% BSA, 0.01% Tween-20. Human recombinant PRMT1 (BPS BioScience, # 51041) (0.87 nM, final concentration) was diluted in Assay Buffer, then and proper inhibitor (0.1% DMSO, final concentration) was added. After a pre-incubation time of 15 minutes, Histone H4 (1-21) peptide, biotinylated (AnaSpec, # 62555) (100 nM, final concentration) and SAM (Sigma # A7007) (2 μM, final concentration) were added. The reaction was incubated for 1 h, afterwards the Anti-methyl-Histone H4 Arginine 3 (H4R3me) AlphaLISA Acceptor Beads (PerkinElmer, # AL150) in Epigenetic Buffer 1X were added in each well, to reach a final concentration of 20 μg/mL. After an incubation of 1 h, Streptavidin Donor beads (PerkinElmer, # 6760002) were diluted in Epigenetic Buffer 1X and added in each well (20 μg/mL, final concentration). The Alpha signal was read after 30 minutes of incubation.

***PRMT3***

The assays were performed using the following Assay Buffer: 30 mM Tris-HCl, pH 8.0, 1 mM DTT, 0.01% BSA, 0.01% Tween-20. Human recombinant PRMT3 (BPS BioScience, # 51043) (2 ng/ μL, final concentration) was diluted in Assay Buffer, then and proper inhibitor (0.1% DMSO, final concentration) was added. After a pre-incubation time of 15 minutes, Histone H4 (1-21) peptide, biotinylated (AnaSpec, # 62555) (50 nM, final concentration) and SAM (Sigma, # A7007) (10 μM, final concentration) were added. The reaction was incubated for 1 h, afterwards the Anti-methyl-Histone H4 Arginine 3 (H4R3me) AlphaLISA Acceptor Beads (PerkinElmer, # AL150) in Epigenetic Buffer 1X were added in each well, to reach a final concentration of 20 μg/mL. After an incubation of 1 h, Streptavidin Donor beads (PerkinElmer, # 6760002) were diluted in Epigenetic

Buffer 1X and added in each well to reach a final concentration of 20 µg/mL. The Alpha signal was read after 30 minutes of incubation.

***SETD8***

The assays were performed using the following Assay Buffer: TrisHCl 50 mM pH 8.5, NaCl 50 mM, MgCl2 5 mM, DTT 1 mM, BSA 0.01%. GST-SETD8 (expressed in house) (1 µM, final concentration) was diluted in Assay Buffer, then and proper inhibitor (0.1% DMSO, final concentration) was added. After a pre-incubation time of 15 minutes, Histone H4 (Active Motif, # 31223), (150 nM, final concentration) and SAM (Sigma, # A7007) (200 µM, final concentration) were added. The reaction was incubated for 1 h, afterwards it was stopped by adding 5 µL of High Salt Buffer (50 mM Tris-HCl pH 7.4, 0.1% Tween-20, 1 M NaCl, 0.3% poly-L-lysine). After an incubation of 15 min, a mixture of anti-Histone H4K20me1 Acceptor beads (PerkinElmer, # AL145) and biotinylated anti-H4 antibody (PerkinElmer, # AL146) was prepared in Epigenetic Buffer 1X and added in each well, to reach a final concentration of 20 µg/mL and 1 nM respectively. After an incubation of 1 h, Streptavidin Donor beads (PerkinElmer, # 6760002) were diluted in Epigenetic Buffer 1X and added in each well (20 µg/mL, final concentration). The Alpha signal was read after 30 minutes of incubation.

***KDM4A***

The assays were performed using the following Assay Buffer: 50 mM Hepes pH 7.5, 0.01% Tween-20, 0.1% BSA. *h*KDM4A (BPS BioScience, # 50103) (100 nM, final concentration) was diluted in Assay Buffer, then a mixture of Fe(II) (Sigma # 215406) (5 µM, final concentration), ascorbate (Sigma, # 11140) (100 µM, final concentration) and proper inhibitor (0.1% DMSO, final concentration) was added. After a pre-incubation time of 15 minutes, Histone H3 (1 - 21) lysine 9 tri-methylated peptide, biotinylated (H3K9me3) (AnaSpec, # 64360) (200 nM, final concentration) and 2OG (Sigma, # K2000) (5 µM, final concentration) were added. The reaction was incubated for 1 h, afterwards the Anti-methyl-Histone H3 Lysine

9 (H3K9me2) AlphaLISA Acceptor beads (PerkinElmer, # AL117) in Epigenetic Buffer 1X were added in each well, to reach a final concentration of 20 μg/mL. After an incubation of 1 h, Streptavidin Donor beads (PerkinElmer, # 6760002) were diluted in Epigenetic Buffer 1X and added in each well to reach a final concentration of 20 μg/mL. The Alpha signal was read after 30 minutes of incubation.

***p300***

The assays were performed using the following Assay Buffer: 50 mM Tris-HCl, pH 8.0, 0.1 mM EDTA, 1 mM DTT, 0.01% Tween-20, 0.01% BSA, 330 nM TSA. Human recombinant p300 (Enzo LifeScience, # BML-SE451) (5 nM, final concentration) was diluted in Assay Buffer, then and proper inhibitor (0.1% DMSO, final concentration) was added. After a pre-incubation time of 15 minutes, Histone H3 (1-21) peptide, biotinylated (Anaspec # 61702) (50 nM, final concentration) and Acetyl CoA (Sigma, # A2056) (3 μM, final concentration) were added. After an incubation of 30 min, reactions were stopped by adding garcinol (Sigma, # G5173) (61.6 μM, final concentration) and Anti-acetyl histone H3 lysine 9 (H3K9Ac) acceptor beads (PerkinElmer, # AL114) in Epigenetic Buffer 1X was added in each well, to reach a final concentration of 20 μg/mL. After an incubation of 1 h, Streptavidin Donor beads (PerkinElmer, # 6760002) were diluted in Epigenetic Buffer 1X and added in each well (20 μg/mL, final concentration). The Alpha signal was read after 30 minutes of incubation.

### 7.3 EML741 Stability assay

Compound **EML741** was dissolved in PBS to reach a final concentration of 100 μM. 5 μL aliquots of the prepared solution were analyzed by HPLC at time 0 (soon after the preparation) and after 12, 24, 48 and 72 h. Spectra were recorded on a Shimadzu SPD 20A UV/vis detector (λ = 220 nm) using C-18 column Phenomenex Synergi Fusion RP 80A (75mm × 4.60 mm; 4 μm) at 25 °C using a

mobile phase A (water + 0.1% TFA) and B (ACN + 0.1% TFA) at a flow rate of 1 mL/min.

### 7.4 PAMPA, general protocol

Test compounds were dissolved in DMSO and for each sample, donor solution (500 μM) was prepared by diluting 1 mM DMSO stock solution using phosphate buffer (pH 7.4, 0.01 M). In the donor plate (96-well polycarbonate-based filter plate), filters were covered with 5 μL of a 1% (w/v) dodecane solution of L-α-phosphatidylcholine for PAMPA or 2% (w/v) of BBB-specific lipid solution (Avanti Lipids Polar, 141101P) for PAMPA-BBB. Donor solution (150 μL) was added to each well. The acceptor plate wells were filled with 300 μL of solution (50% DMSO in phosphate buffer). The sandwich was incubated for 24 h at room temperature under gentle shaking. Then, the sandwich plates were separated and 250 μL of the acceptor plate were transferred to a UV quartz microtiter plate and measured by UV spectroscopy, using a Multiskan GO microplate spectrophotometer (Thermo Scientific) at 250-500 nm (steps of 5 nm). Reference solutions (250 μL) were prepared diluting the sample stock solutions to the same concentration as that with no membrane barrier. The apparent permeability value $P_{app}$ is determined from the ratio *r* of the absorbance of compound found in the acceptor chamber divided by the theoretical equilibrium absorbance (determined independently) applying the Faller modification of Sugano equation:

$$Papp = -\left(\frac{VD * VR}{(VD + VR) * At}\right) * \ln(1 - r)$$

In this equation, VR is the volume of the acceptor compartment (0.3 $cm^3$), VD is the donor volume (0.15 $cm^3$), A is the accessible filter area (0.24 $cm^2$), and *t* is the incubation time in seconds. All the compounds were tested in triplicate.

### 7.5 Cell culture and transfection

The human chronic myelogenous leukemia cell line KBM7 was cultured in Iscove's modified Dulbecco's medium (IMDM, Gibco), supplemented with 10% fetal bovine serum (FBS; Gibco) and 100 units/ml streptomycin and penicillin (both from Gibco). The human embryonic kidney HEK293T and breast cancer MCF7 cell lines were cultured in Dulbecco's modified Eagle's medium (DMEM, Gibco) supplemented with 10% of fetal bovine serum (FBS, Gibco) and 100 units/mL streptomycin and penicillin. All cell lines were incubated in a 5% $CO_2$ atmosphere at 37 °C.

HEK293T cells were transfected with Lipofectamine 2000 (Invitrogen) according to the manufacturer's instructions. The plasmids used (pLV-Azurite (Addgene, #36086), psPAX2 (Addgene, #12259) and pCMV-VSV-G (Addgene, #8454)) were purified from cultured transformed bacteria using a Plasmid Maxiprep Purification Kit (Qiagen) following to the manufacturer's protocol.

### 7.6 Western blot

KBM7 (8 mL, $2.5 \times 10^5$ cells/mL) were seeded and incubated with UNC0638 at different concentrations for the specified time and conditions. MCF7 (10 mL, $3.5 \times 10^4$ cells/mL) were seeded, allowed to attach overnight and subsequently treated with the indicated compounds for the specified time and concentrations. An equal amount of DMSO (0.5 %) was used to treat the control samples. After the treatment, the cells were harvested and washed three times with 1X PBS (Phosphate Buffered Saline, Gibco) and then resuspended in Tryton extraction buffer (PBS containing 0.5% Triton × 100 (v/v), 2mM phenylmethylsulfonyl fluoride (PMSF), 0.02% (w/v) $NaN_3$) supplemented with a protease inhibitor cocktail Sigma-Aldrich # 11873580001). All subsequent manipulations were performed at 4 °C. After incubation for 30 min on a rotator, nuclei were collected by centrifugation for 10 min at 500 rcf. The nuclear pellets were suspended in 0.2 N HCl solution and incubated overnight on a rotator. After centrifugation for 10 min at 500 rcf, histones containing supernatant was collected. Protein concentrations were determined

using the Bradford assay. For each sample, equal amounts of proteins were separated on 15% polyacrylamide gels with SDS running buffer (50 mM Tris, 380 mM glycine and 7 mM SDS) and transferred to nitrocellulose blotting membranes. All membranes were blocked with blocking buffer (5% (w/v) milk powder (BioRad) in TBST (Tris-buffered saline with Tween: 50 mM Tris (tris (hydroxymethyl)aminomethane), 150 mM NaCl, 0.05% (v/v) Tween 20, adjusted to pH 7.6)). Proteins were probed using the following antibodies: anti-H3K9me2 (1:1000, Cell Signaling Technology, #4658), anti-histone H3 (1:1000, Cell Signaling Technology, #4499), anti-histone H4 (1:1000, Abcam, #ab7311) detected by HRP (horseradish peroxidase) conjugated donkey anti-rabbit IgG antibody (1:10000, Abcam, #ab16284) or donkey anti-mouse IgG antibody (Pierce) and visualized with the Pierce ECL Western Blotting substrate (Amersham), according to the provided protocol.

### 7.7 Cell viability

MTT Assay

MCF7 (0.2 mL, $3.5 \times 10^4$ cells/mL) were seeded in 96-well microtiter plates (Corning), allowed to attach overnight and subsequently treated with the indicated compounds for the specified conditions. Control samples were treated with an equal amount of DMSO (0.5 %). After the specified incubation time, 10 µL of 3-(4,5-dimethylthiazol-2-yl)-2,5-diphenyltetrazolium bromide (MTT; Sigma-Aldrich # M2128) solution (5.0 mg/mL) was added to each well, and incubation continued for an additional 2 hours. Formed blue formazan crystals were dissolved by adding 100 µL of DMSO. The absorbance was read in a Multiskan GO microplate spectrophotometer (Thermo Scientific) at 550 nm, using a 620 nm filter as reference.

CellTiter-Glo® Assay

KBM7 (0.1 mL, $2.5 \times 10^5$ cells/mL) were seeded in 96-well microtiter plates (Corning) and incubated with UNC0638 at different concentrations, an equal

amount of DMSO was used as control (0.5% final). After 24 or 48 h CellTiter-Glo® Reagent (Promega) was added and the plates were incubated in the dark for 30 minutes. The luminescent signal was read with EnVision 2105 Multimode Plate Reader (PerkinElmer).

### 7.8 Cell sorting

Cell sorting was performed using the FACSAria (BD Biosciences) sorter. Briefly, BFP-infected cells were sorted in presence of 2 μM UNC0638, 48 h after the infection. Wild type KMB7 as negative control. BFP-positive cells (6.3%, very positive) were seeded in fresh medium, without UNC0638. After five days from the first sorting, cells were sorted again, in absence of UNC0638, selecting the negative population (6.7%, very negative). These steps were repeated two times. Clones were isolated by single cell sorting in the last passage.

### 7.9 Screening

KBM7 were seeded on clear flat-bottom 384-well plates (Corning) and treated with the compounds in single dose (primary screening) or dose response (hit validation). DMSO was used as negative control. After 24 h, live-cell imaging pictures were taken with the Operetta High Content Screening System (PerkinElmer), 20x objective and nonconfocal mode and analyzed using the Harmony software (PerkinElmer) for nuclei detection and analysis, adapted for the nucleus diameter range of KBM7 (13 μM).

### 7.10 Quantitative PCR (qPCR)

1704001-A7 cells ($4.0 \times 10^5$ cells/mL) were seeded and incubated with the indicated compounds for 24 h. the cells were harvested and washed three times with ice cold-1X PBS (Gibco). RNA was extracted with RNeasy Mini Kit (Quiagen), following the recommended protocol. RNA was quantified and evaluated for purity (NanoDrop, Thermo Fisher Scientific).

1 µg of each sample was converted to cDNA with High Capacity cDNA Reverse Transcription (RT) Kit (Applied Biosystems) following the standard protocol. RT was performed in a thermal cycler (SimpliAmp Thermal Cycler, Thermo Fisher Scientific) programmed for 25 °C (10 min), 37 °C (120 min), 85 °C (5 min), then 4 °C (∞).

qPCR was performed using the Power SYBR Green Master mix (Invitrogen) as described in the manufacture's protocol. qPCR was conducted at 95 °C for 10 min, followed by 40 cycles of 95 °C for 15 s and 60 °C for 1 min (ramp rate: 4.8 °C/s; LightCycler 480 II, Roche). RT-PCR primers used: *Azurite* BFP (Sigma; forward 5′- CCTGAAGTTCATCTGCACCA, reverse 5′- GGTCTTGTAGTTGCCGTCGT); *beta-2-microglobulin* B2MG (Sigma; forward 5′- GAGGCTATCCAGCGTACTC, reverse 5′- CCAGACACATAGCAATTCAGG).

Real-time amplification results were normalized to the endogenous housekeeping gene beta-2-microglobulin. The relative quantities were calculated using the comparative cycle threshold (ΔΔCT) method.

### 7.11 NMR Data

$^{1}$H-NMR **EML693**, 3 × TFA salt

$^{13}$C-NMR **EML693**, 3 × TFA salt

$^{1}$H-NMR **EML741**, 3 × TFA salt

$^{13}$C-NMR **EML741**, 3 × TFA salt

$^{1}$H-NMR **EML696**, 3 × TFA salt

$^{13}$C-NMR **EML696**, 3 × TFA salt

$^{1}$H-NMR **EML698**, 3 × TFA salt

$^{13}$C-NMR **EML698**, 3 × TFA salt

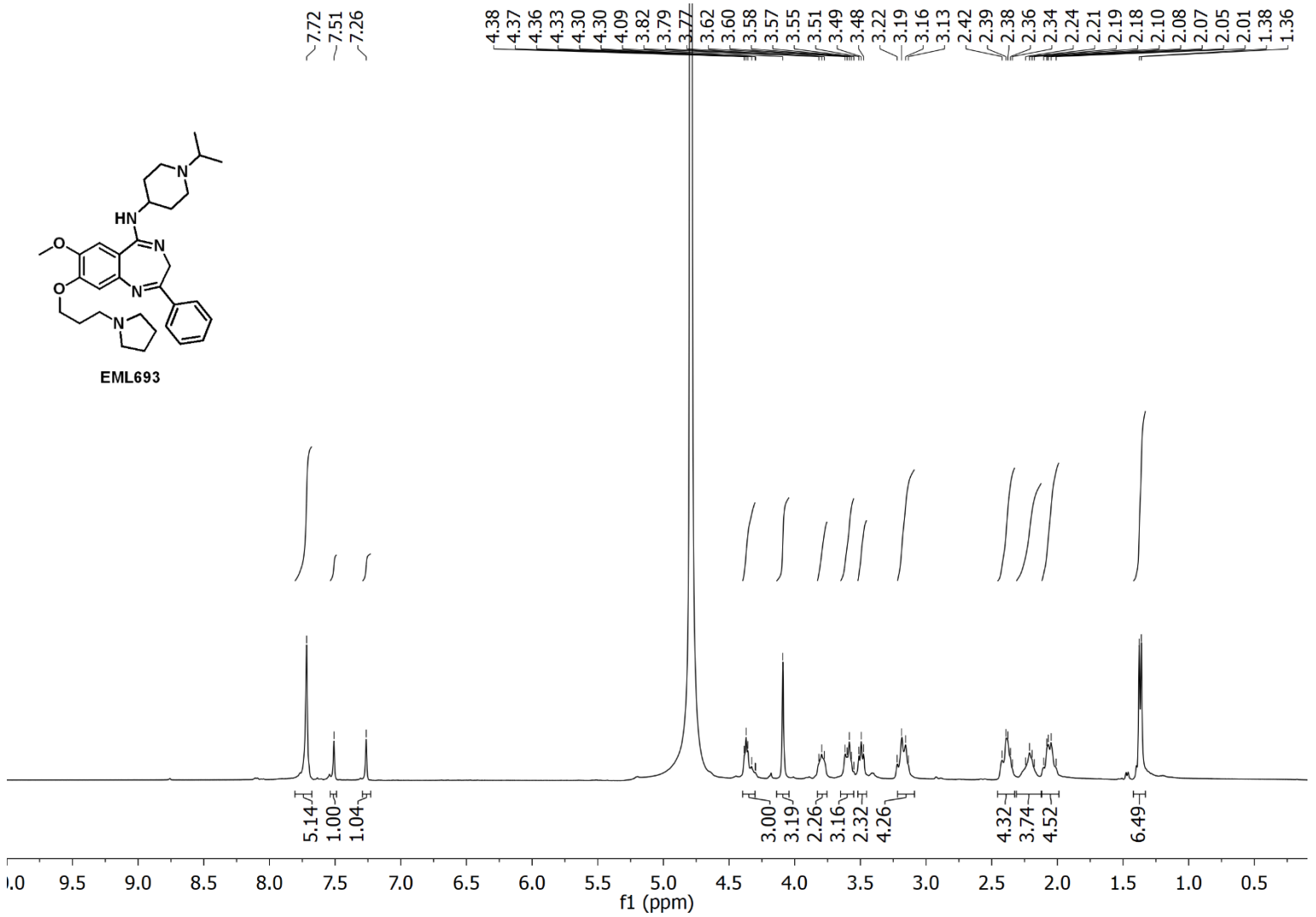
7.72
7.51
7.26
4.38
4.37
4.36
4.33
4.30
4.30
4.09
3.82
3.79
3.77
3.62
3.60
3.58
3.57
3.55
3.51
3.49
3.48
3.22
3.19
3.16
3.13
2.42
2.39
2.38
2.36
2.34
2.24
2.21
2.19
2.18
2.10
2.08
2.07
2.05
2.01
1.38
1.36
HN
O
O
N
N
N
N
EML693
5.14
1.00
1.04
3.00
3.19
2.26
3.16
2.32
4.26
4.32
3.74
4.52
6.49
f1 (ppm)

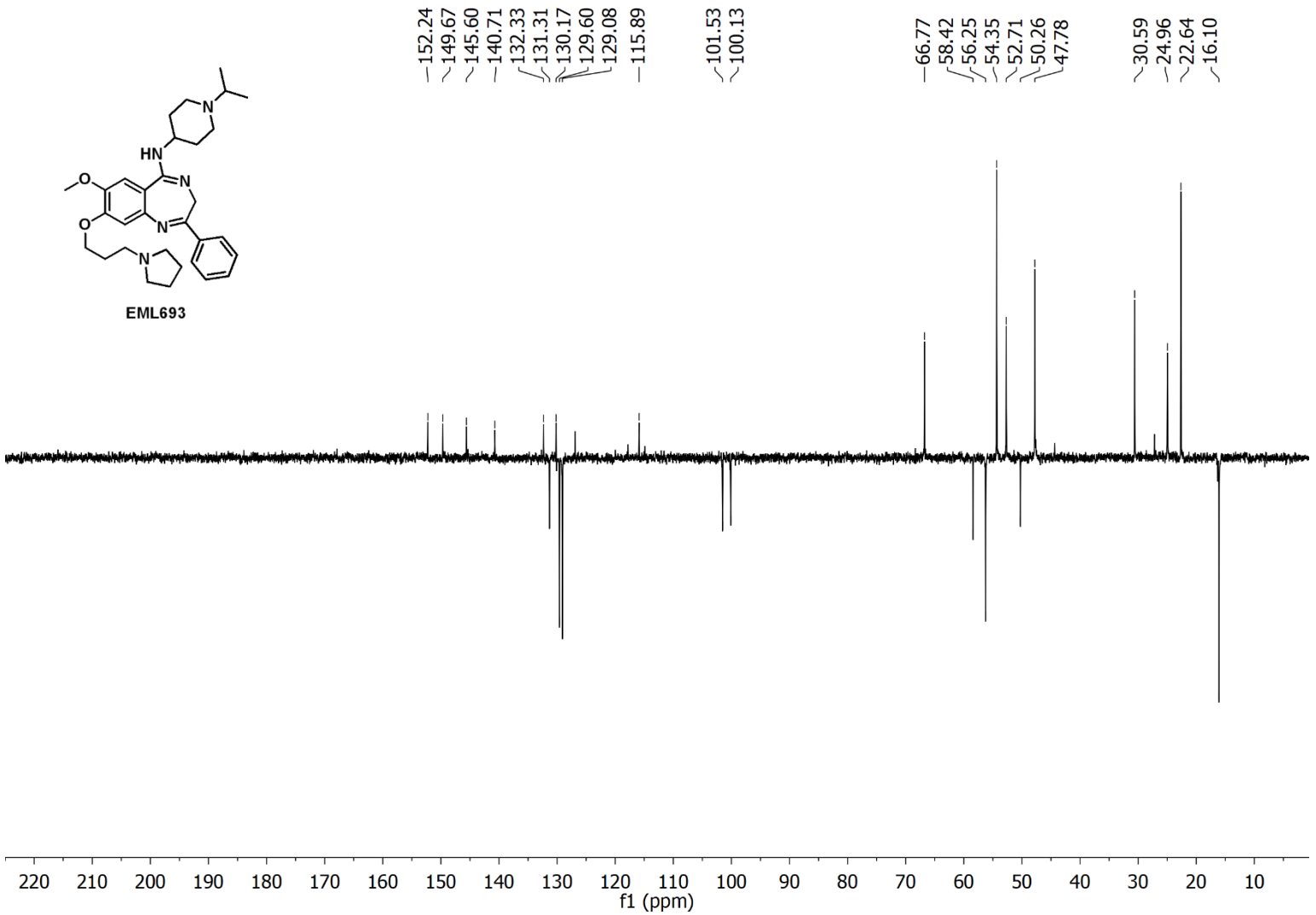
152.24
149.67
145.60
140.71
132.33
131.31
130.17
129.60
129.08
115.89
101.53
100.13
66.77
58.42
56.25
54.35
52.71
50.26
47.78
30.59
24.96
22.64
16.10
EML693
220 210 200 190 180 170 160 150 140 130 120 110 100 90 80 70 60 50 40 30 20 10
f1 (ppm)

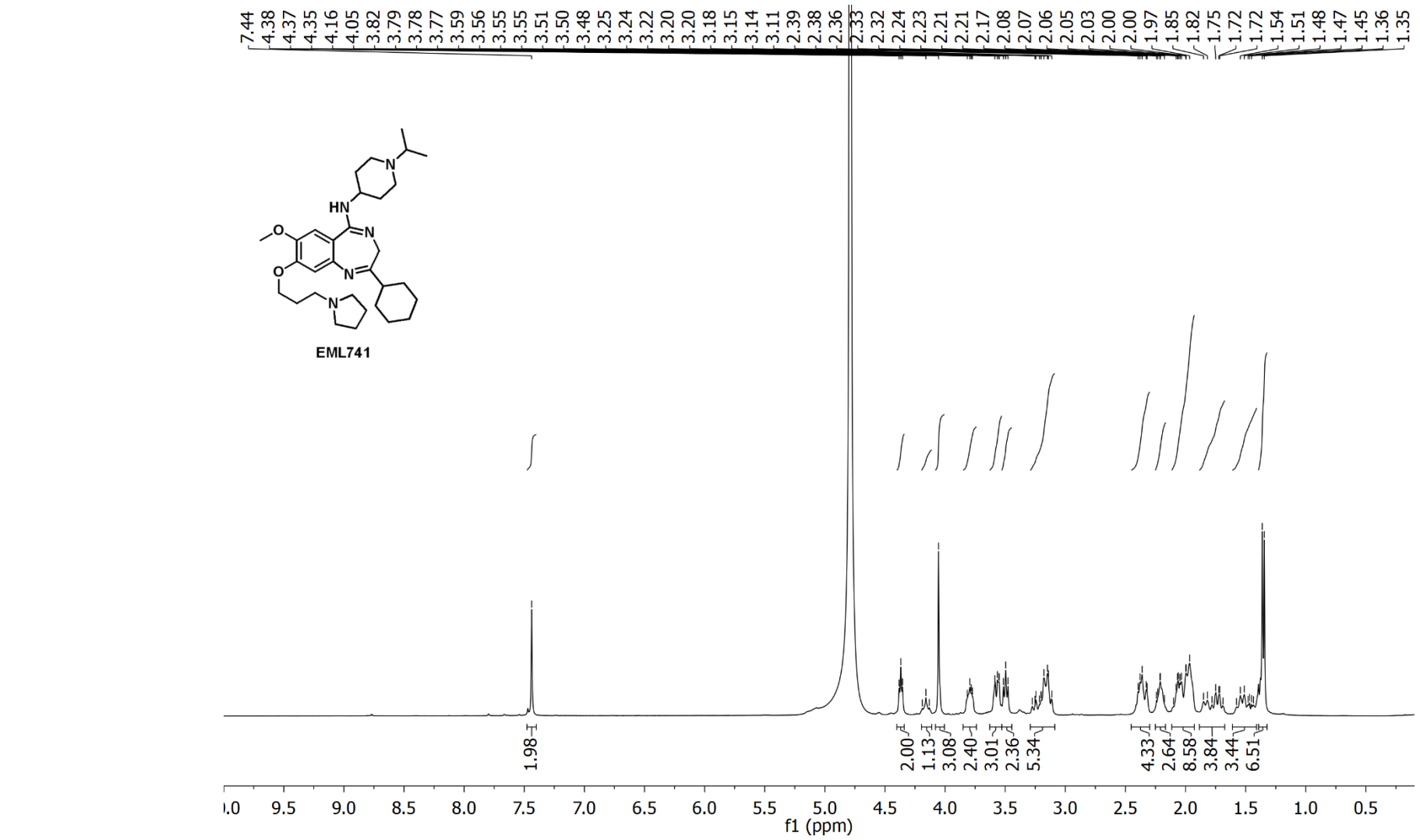
7.44
4.38
4.37
4.35
4.16
4.05
3.82
3.79
3.78
3.77
3.59
3.56
3.55
3.55
3.51
3.50
3.48
3.25
3.24
3.22
3.20
3.20
3.18
3.15
3.14
3.11
2.39
2.38
2.36
2.33
2.32
2.24
2.23
2.21
2.21
2.17
2.08
2.07
2.06
2.05
2.03
2.00
2.00
1.97
1.85
1.82
1.75
1.72
1.72
1.54
1.51
1.48
1.47
1.45
1.36
1.35
HN
O
N
O
N
N
EML741
1.98
2.00
1.13
3.08
2.40
3.01
2.36
5.34
4.33
2.64
8.58
3.84
3.44
6.51
f1 (ppm)

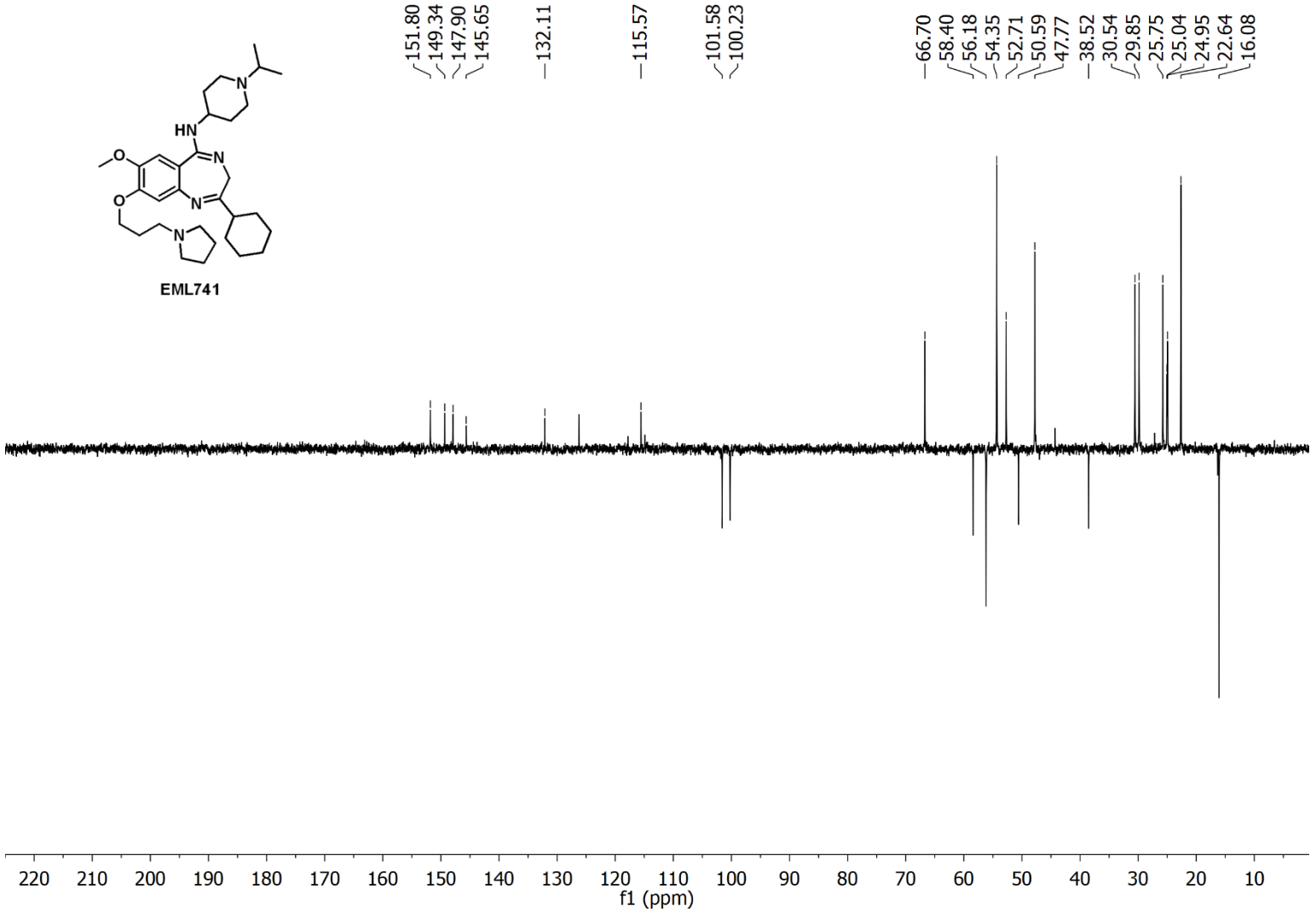
151.80
149.34
147.90
145.65
132.11
115.57
101.58
100.23
66.70
58.40
56.18
54.35
52.71
50.59
47.77
38.52
30.54
29.85
25.75
25.04
24.95
22.64
16.08
HN
O
O
N
N
N
N
EML741
220 210 200 190 180 170 160 150 140 130 120 110 100 90 80 70 60 50 40 30 20 10
f1 (ppm)

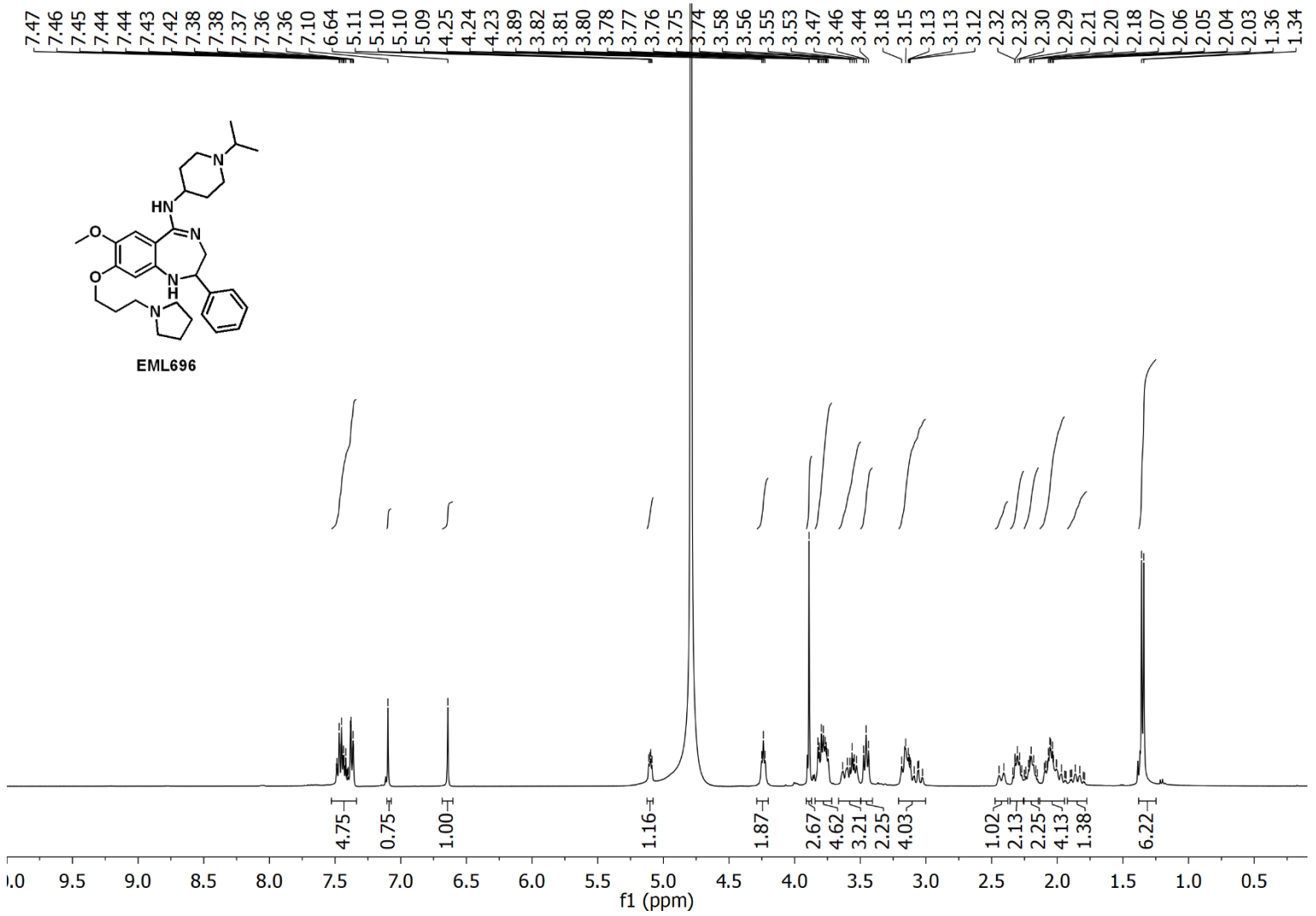
7.47
7.46
7.45
7.44
7.44
7.43
7.42
7.38
7.38
7.37
7.36
7.36
7.10
6.64
5.11
5.10
5.10
5.09
4.25
4.24
4.23
3.89
3.82
3.81
3.80
3.78
3.77
3.76
3.75
3.74
3.58
3.56
3.55
3.53
3.47
3.46
3.44
3.18
3.15
3.13
3.13
3.12
2.32
2.32
2.30
2.29
2.21
2.20
2.18
2.07
2.06
2.05
2.04
2.03
1.36
1.34
EML696
4.75
0.75
1.00
1.16
1.87
2.67
4.62
3.21
2.25
4.03
1.02
2.13
2.25
4.13
1.38
6.22
f1 (ppm)

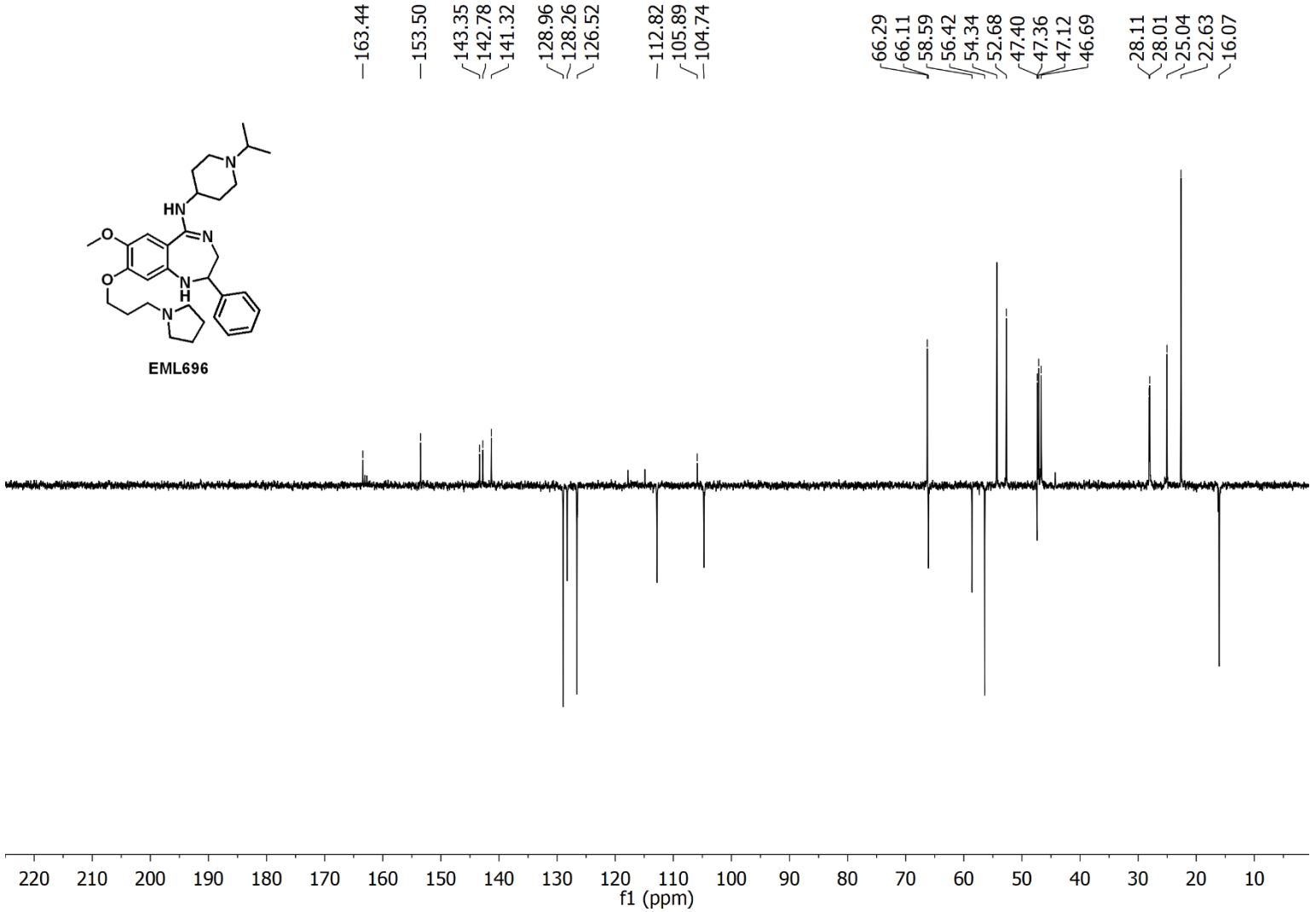
163.44
153.50
143.35
142.78
141.32
128.96
128.26
126.52
112.82
105.89
104.74
66.29
66.11
58.59
56.42
54.34
52.68
47.40
47.36
47.12
46.69
28.11
28.01
25.04
22.63
16.07
EML696
220 210 200 190 180 170 160 150 140 130 120 110 100 90 80 70 60 50 40 30 20 10
f1 (ppm)

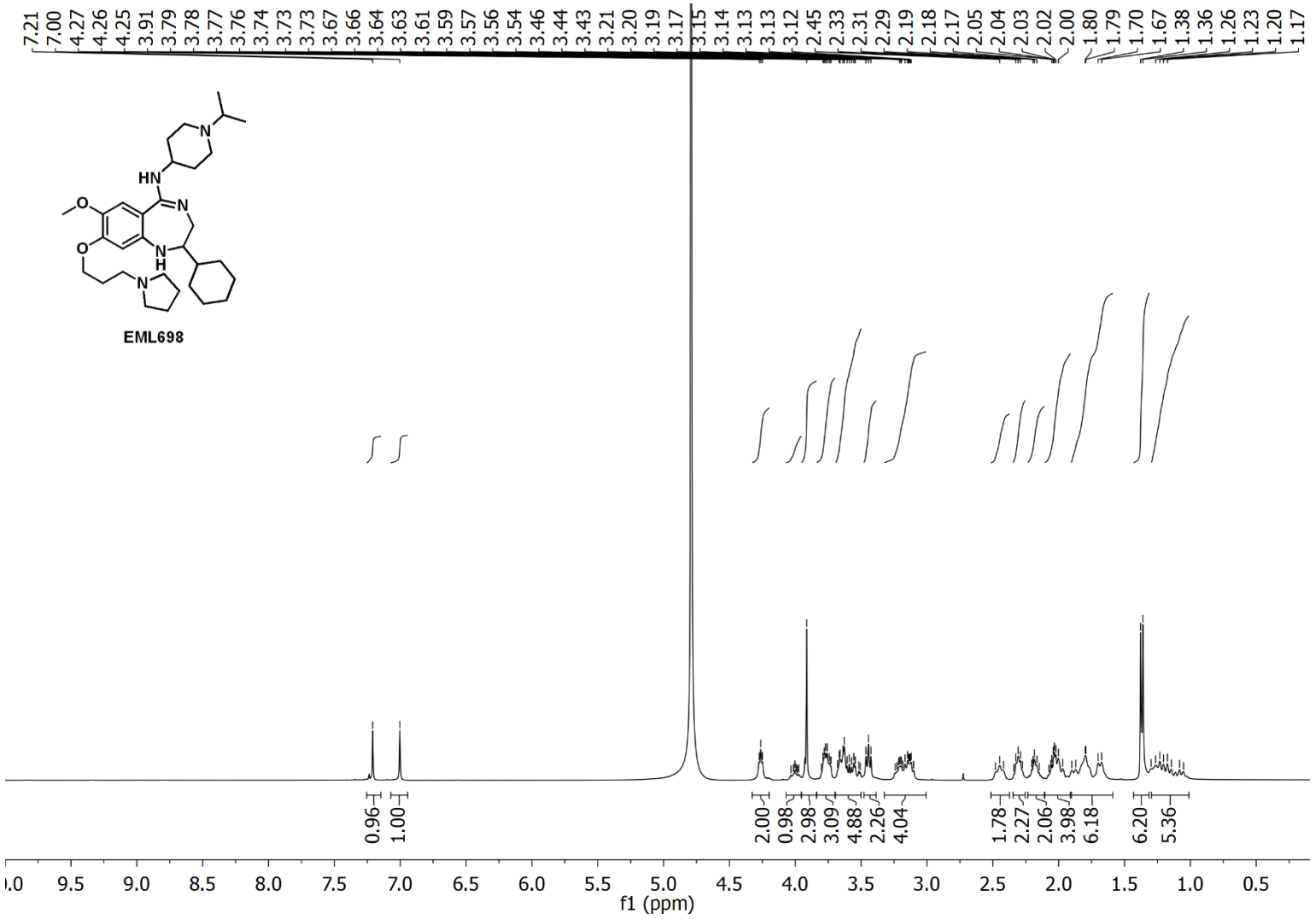
7.21
7.00
4.27
4.26
4.25
3.91
3.79
3.78
3.77
3.76
3.74
3.73
3.73
3.67
3.66
3.64
3.63
3.61
3.59
3.57
3.56
3.54
3.46
3.44
3.43
3.21
3.20
3.19
3.17
3.15
3.14
3.13
3.13
3.12
2.45
2.33
2.31
2.29
2.19
2.18
2.17
2.05
2.04
2.03
2.02
2.00
1.80
1.79
1.70
1.67
1.38
1.36
1.26
1.23
1.20
1.17
HN
N
O
N
O
N
H
N
EML698
0.96
1.00
2.00
0.98
2.98
3.09
4.88
2.26
4.04
1.78
2.27
2.06
3.98
6.18
6.20
5.36
f1 (ppm)

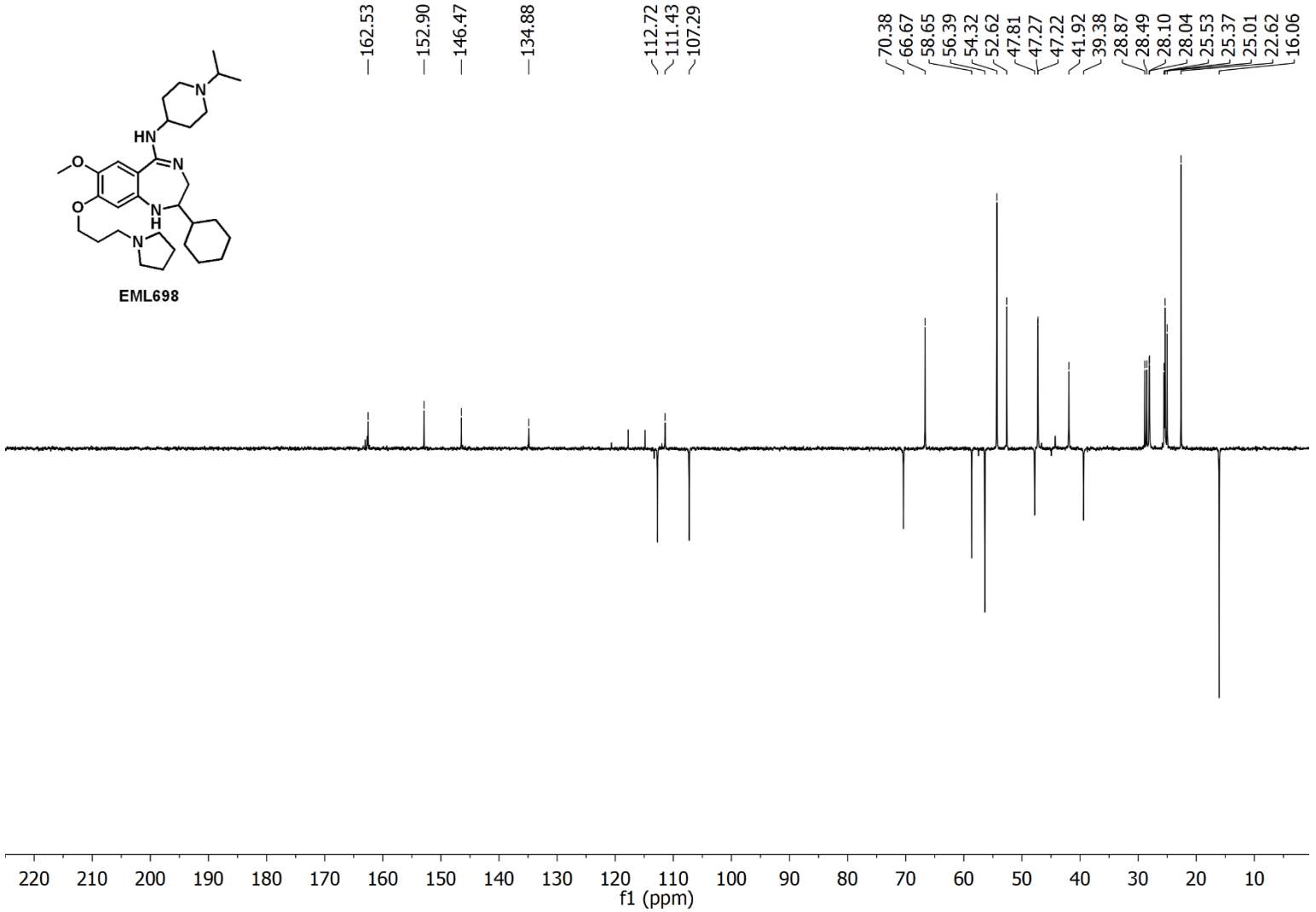
162.53
152.90
146.47
134.88
112.72
111.43
107.29
70.38
66.67
58.65
56.39
54.32
52.62
47.81
47.27
47.22
41.92
39.38
28.87
28.49
28.10
28.04
25.53
25.37
25.01
22.62
16.06
EML698
220 210 200 190 180 170 160 150 140 130 120 110 100 90 80 70 60 50 40 30 20 10
f1 (ppm)

# ACKNOWLEDGEMENTS

First of all, I would like to deeply and sincerely thank my advisor, Prof. Sabrina Castellano, for the continuous support and guidance, for her advices, for the constant encouragement to overcome my limits and improve myself as scientist. Profound gratitude goes to Prof. Gianluca Sbardella for his patience, the strong motivation and enthusiasm, and for his numerous, illuminating ideas for the realization of this project.

A special thank goes to Dr. Stefan Kubicek for welcoming me in his group, for his help and guidance and for showing me a new point of view.

Since I started as undergraduate, I am grate to Dr. Ciro Milite and also to Dr. Monica Viviano and Dr. Alessandra Feoli for the unconditional support, the time and the help they gave me every day during these years but also for the time spent together outside the laboratory, becoming good friends. Words can not express how grateful I am to you.

Thanks to Dr. Sara Sdelci for introducing me to the complex world of biology, for her endless kindness, for being always ready to answer my questions and for being, above all, a friend.

I would like to thank all my Italian and Austrian labmates. Thanks for making enjoyable all the time (a lot!) we spent together working, laughing, and then working and discussing.

I am infinitely indebted with my family for their immense love, for the encouragement and for having endured my bad moods.

Last, but not least, thanks to Luca for being always by my side, for the continuous encouragement to believe in myself, for helping me to see the bright side even in the darkest moments.

# REFERENCES


1. Waddington, C. H., The epigenotype. 1942. *Int. J. Epidemiol.* **2012,** *41* (1), 10-13.

2. Deans, C.; Maggert, K. A., What do you mean, "Epigenetic"? *Genetics* **2015,** *199* (4), 887-896.

3. Allis, C. D.; Jenuwein, T., The molecular hallmarks of epigenetic control. *Nat. Rev. Genet.* **2016,** *17* (8), 487-500.

4. Wright, J., Epigenetics: Reversible tags. *Nature* **2013,** *498*, S10.

5. Reik, W., Stability and flexibility of epigenetic gene regulation in mammalian development. *Nature* **2007,** *447* (7143), 425-432.

6. Setiaputra, D. T.; Yip, C. K., Characterizing the molecular architectures of chromatin-modifying complexes. *Biochim. Biophys. Acta, Proteins Proteomics* **2017,** *1865* (11 Part B), 1613-1622.

7. Kouzarides, T., Chromatin modifications and their function. *Cell* **2007,** *128* (4), 693-705.

8. Yang, X.; Lay, F.; Han, H.; Jones, P. A., Targeting DNA methylation for epigenetic therapy. *Trends Pharmacol. Sci.* **2010,** *31* (11), 536-546.

9. Bannister, A. J.; Kouzarides, T., Regulation of chromatin by histone modifications. *Cell Res.* **2011,** *21* (3), 381-395.

10. Lawrence, M.; Daujat, S.; Schneider, R., Lateral Thinking: How Histone Modifications Regulate Gene Expression. *Trends Genet.* **2016,** *32* (1), 42-56.

11. Falkenberg, K. J.; Johnstone, R. W., Histone deacetylases and their inhibitors in cancer, neurological diseases and immune disorders. *Nat. Rev. Drug Discov.* **2014,** *13* (9), 673-691.

12. Copeland, R. A.; Solomon, M. E.; Richon, V. M., Protein methyltransferases as a target class for drug discovery. *Nat. Rev. Drug Discov.* **2009,** *8* (9), 724-732.

13. Luo, M., Current Chemical Biology Approaches to Interrogate Protein Methyltransferases. *ACS Chem. Biol.* **2012,** *7* (3), 443-463.

14. Copeland, R. A.; Moyer, M. P.; Richon, V. M., Targeting genetic alterations in protein methyltransferases for personalized cancer therapeutics. *Oncogene* **2013,** *32* (8), 939-946.

15. Arrowsmith, C. H.; Bountra, C.; Fish, P. V.; Lee, K.; Schapira, M., Epigenetic protein families: a new frontier for drug discovery. *Nat. Rev. Drug Discov.* **2012,** *11* (5), 384-400.

16. Martin, C.; Zhang, Y., The diverse functions of histone lysine methylation. *Nat. Rev. Mol. Cell Biol.* **2005,** *6* (11), 838-849.

17. Alam, H.; Gu, B.; Lee, M. G., Histone methylation modifiers in cellular signaling pathways. *Cell. Mol. Life Sci.* **2015,** *72* (23), 4577-4592.

18. Huang, B.; Yang, X.-D.; Lamb, A.; Chen, L.-F., Posttranslational modifications of NF-κB: Another layer of regulation for NF-κB signaling pathway. *Cell. Signal.* **2010,** *22* (9), 1282-1290.

19. Stark, G. R.; Wang, Y.; Lu, T., Lysine methylation of promoter-bound transcription factors and relevance to cancer. *Cell Res.* **2011,** *21* (3), 375-380.

20. Zhang, X.; Wen, H.; Shi, X., Lysine methylation: beyond histones. *Acta Biochim. Biophys. Sin.* **2012,** *44* (1), 14-27.

21. Black, Joshua C.; Van Rechem, C.; Whetstine, Johnathan R., Histone Lysine Methylation Dynamics: Establishment, Regulation, and Biological Impact. *Mol. Cell* **2012,** *48* (4), 491-507.

22. Tschiersch, B.; Hofmann, A.; Krauss, V.; Dorn, R.; Korge, G.; Reuter, G., The protein encoded by the Drosophila position-effect variegation suppressor gene Su(var)3-9 combines domains of antagonistic regulators of homeotic gene complexes. *EMBO J.* **1994,** *13* (16), 3822-3831.

23. Jones, R. S.; Gelbart, W. M., The Drosophila polycomb-group gene Enhancer of zeste contains a region with sequence similarity to trithorax. *Mol. Cell. Biol.* **1993,** *13* (10), 6357-6366.

24. Stassen, M. J.; Bailey, D.; Nelson, S.; Chinwalla, V.; Harte, P. J., The Drosophila trithorax proteins contain a novel variant of the nuclear receptor type DNA binding domain and an ancient conserved motif found in other chromosomal proteins. *Mech. Dev.* **1995,** *52* (2,3), 209-223.

25. Dillon, S. C.; Zhang, X.; Trievel, R. C.; Cheng, X., The SET-domain protein superfamily: protein lysine methyltransferases. *Genome Biol.* **2005,** *6* (8:227).

26. Qian, C.; Zhou, M. M., SET domain protein lysine methyltransferases: structure, specificity and catalysis. *Cell. Mol. Life Sci.* **2006,** *63* (23), 2755-2763.

27. Zhang, X.; Yang, Z.; Khan, S. I.; Horton, J. R.; Tamaru, H.; Selker, E. U.; Cheng, X., Structural basis for the product specificity of histone lysine methyltransferases. *Mol. Cell* **2003,** *12* (1), 177-185.

28. Herz, H.-M.; Garruss, A.; Shilatifard, A., SET for life: biochemical activities and biological functions of SET domain-containing proteins. *Trends Biochem. Sci.* **2013,** *38* (12), 621-639.

29. Hyun, K.; Jeon, J.; Park, K.; Kim, J., Writing, erasing and reading histone lysine methylations. *Exp. Mol. Med.* **2017,** *49*, e324.

30. Smith, A. E.; Chronis, C.; Christodoulakis, M.; Orr, S. J.; Lea, N. C.; Twine, N. A.; Bhinge, A.; Mufti, G. J.; Thomas, N. S. B., Epigenetics of human T cells during the G(0)→G(1) transition. *Genome Res.* **2009,** *19* (8), 1325-1337.

31. Schulze, J. M.; Jackson, J.; Nakanishi, S.; Gardner, J. M.; Hentrich, T.; Haug, J.; Johnston, M.; Jaspersen, S. L.; Kobor, M. S.; Shilatifard, A., Linking cell cycle to histone modifications: SBF and H2B monoubiquitination machinery and cell-cycle regulation of H3K79 dimethylation. *Mol. Cell* **2009,** *35* (5), 626-641.

32. Sims, R. J., 3rd; Nishioka, K.; Reinberg, D., Histone lysine methylation: a signature for chromatin function. *Trends Genet.* **2003,** *19* (11), 629-639.

33. Strahl, B. D.; Allis, C. D., The language of covalent histone modifications. *Nature* **2000,** *403* (6765), 41-45.

34. Keniry, A.; Gearing, L. J.; Jansz, N.; Liu, J.; Holik, A. Z.; Hickey, P. F.; Kinkel, S. A.; Moore, D. L.; Breslin, K.; Chen, K.; Liu, R.; Phillips, C.; Pakusch, M.; Biben, C.; Sheridan, J. M.; Kile, B. T.; Carmichael, C.; Ritchie, M. E.; Hilton, D. J.; Blewitt, M. E., Setdb1-mediated H3K9 methylation is enriched on the inactive X and plays a role in its epigenetic silencing. *Epigenetics Chromatin* **2016,** *9* (1:16).

35. Nishioka, K.; Rice, J. C.; Sarma, K.; Erdjument-Bromage, H.; Werner, J.; Wang, Y.; Chuikov, S.; Valenzuela, P.; Tempst, P.; Steward, R.; Lis, J. T.; Allis, C. D.; Reinberg, D., PR-Set7 is a nucleosome-specific methyltransferase that modifies

lysine 20 of histone H4 and is associated with silent Chromatin. *Mol. Cell* **2002,** *9* (6), 1201-1213.

36. Hall, I. M.; Shankaranarayana, G. D.; Noma, K.-i.; Ayoub, N.; Cohen, A.; Grewal, S. I. S., Establishment and maintenance of a heterochromatin domain. *Science* **2002,** *297* (5590), 2232-2237.

37. Krasnov, A. N.; Mazina, M. Y.; Nikolenko, J. V.; Vorobyeva, N. E., On the way of revealing coactivator complexes cross-talk during transcriptional activation. *Cell Biosci.* **2016,** *6* (1:15).

38. Rivera, C.; Gurard-Levin, Z. A.; Almouzni, G.; Loyola, A., Histone lysine methylation and chromatin replication. *Biochim. Biophys. Acta, Gene Regul. Mech.* **2014,** *1839* (12), 1433-1439.

39. Gong, F.; Miller, K. M., Histone methylation and the DNA damage response. *Mutat. Res. Rev. Mutat. Res.* **2017**, http://dx.doi.org/10.1016/j.mrrev.2017.09.003.

40. Wu, Z.; Connolly, J.; Biggar, K. K., Beyond histones - the expanding roles of protein lysine methylation. *FEBS J.* **2017,** *284* (17), 2732-2744.

41. Chi, P.; Allis, C. D.; Wang, G. G., Covalent histone modifications - miswritten, misinterpreted and mis-erased in human cancers. *Nat. Rev. Cancer* **2010,** *10* (7), 457-469.

42. Pollina, E. A.; Brunet, A., Epigenetic regulation of aging stem cells. *Oncogene* **2011,** *30* (28), 3105-3126.

43. Greer, E. L.; Shi, Y., Histone methylation: a dynamic mark in health, disease and inheritance. *Nat. Rev. Genet.* **2012,** *13* (5), 343-357.

44. Au, S. L.-K.; Wong, C. C.-L.; Lee, J. M.-F.; Wong, C.-M.; Ng, I. O.-L., EZH2-mediated H3K27me3 is involved in epigenetic repression of deleted in liver cancer 1 in human cancers. *PLoS One* **2013,** *8* (6), e68226.

45. Barlesi, F.; Giaccone, G.; Gallegos-Ruiz, M. I.; Loundou, A.; Span, S. W.; Lefesvre, P.; Kruyt, F. A. E.; Rodriguez, J. A., Global histone modifications predict prognosis of resected non small-cell lung cancer. *J. Clin. Oncol.* **2007,** *25* (28), 4358-4364.

46. Elsheikh, S. E.; Green, A. R.; Rakha, E. A.; Powe, D. G.; Ahmed, R. A.; Collins, H. M.; Soria, D.; Garibaldi, J. M.; Paish, C. E.; Ammar, A. A.; Grainge,

M. J.; Ball, G. R.; Abdelghany, M. K.; Martinez-Pomares, L.; Heery, D. M.; Ellis, I. O., Global histone modifications in breast cancer correlate with tumor phenotypes, prognostic factors, and patient outcome. *Cancer Res.* **2009,** *69* (9), 3802-3809.

47. Wei, Y.; Xia, W.; Zhang, Z.; Liu, J.; Wang, H.; Adsay, N. V.; Albarracin, C.; Yu, D.; Abbruzzese, J. L.; Mills, G. B.; Bast, R. C., Jr.; Hortobagyi, G. N.; Hung, M.-C., Loss of trimethylation at lysine 27 of histone H3 is a predictor of poor outcome in breast, ovarian, and pancreatic cancers. *Mol. Carcinog.* **2008,** *47* (9), 701-706.

48. Visser, H. P. J.; Gunster, M. J.; Kluin-Nelemans, H. C.; Manders, E. M. M.; Raaphorst, F. M.; Meijer, C. J. L. M.; Willemze, R.; Otte, A. P., The polycomb group protein EZH2 is upregulated in proliferating, cultured human mantle cell lymphoma. *Br. J. Haematol.* **2001,** *112* (4), 950-958.

49. Ernst, T.; Chase, A. J.; Score, J.; Hidalgo-Curtis, C. E.; Bryant, C.; Jones, A. V.; Waghorn, K.; Zoi, K.; Ross, F. M.; Reiter, A.; Hochhaus, A.; Drexler, H. G.; Duncombe, A.; Cervantes, F.; Oscier, D.; Boultwood, J.; Grand, F. H.; Cross, N. C. P., Inactivating mutations of the histone methyltransferase gene EZH2 in myeloid disorders. *Nat. Genet.* **2010,** *42* (8), 722-726.

50. Krivtsov, A. V.; Armstrong, S. A., MLL translocations, histone modifications and leukaemia stem-cell development. *Nat. Rev. Cancer* **2007,** *7* (11), 823-833.

51. Ryu, H.; Lee, J.; Hagerty, S. W.; Soh, B. Y.; McAlpin, S. E.; Cormier, K. A.; Smith, K. M.; Ferrante, R. J., ESET/SETDB1 gene expression and histone H3 (K9) trimethylation in Huntington's disease. *Proc. Natl. Acad. Sci. U. S. A.* **2006,** *103* (50), 19176-19181.

52. Vallianatos, C. N.; Iwase, S., Disrupted intricacy of histone H3K4 methylation in neurodevelopmental disorders. *Epigenomics* **2015,** *7* (3), 503-519.

53. Huang, H.-S.; Matevossian, A.; Whittle, C.; Kim, S. Y.; Schumacher, A.; Baker, S. P.; Akbarian, S., Prefrontal Dysfunction in Schizophrenia Involves Mixed-Lineage Leukemia 1-Regulated Histone Methylation at GABAergic Gene Promoters. *J. Neurosci.* **2007,** *27* (42), 11254-11262.

54. Iwase, S.; Shi, Y., Histone and DNA modifications in mental retardation. *Prog. Drug Res.* **2011,** *67* (Epigenetics and Disease), 147-173.

55. Yamashita, M.; Hirahara, K.; Shinnakasu, R.; Hosokawa, H.; Norikane, S.; Kimura, M. Y.; Hasegawa, A.; Nakayama, T., Crucial role of MLL for the maintenance of memory T helper type 2 cell responses. *Immunity* **2006,** *24* (5), 611-22.

56. Hu, N.; Qiu, X.; Luo, Y.; Yuan, J.; Li, Y.; Lei, W.; Zhang, G.; Zhou, Y.; Su, Y.; Lu, Q., Abnormal histone modification patterns in lupus CD4+ T cells. *J. Rheumatol.* **2008,** *35* (5), 804-810.

57. Yi, X.; Jiang, X.; Li, X.; Jiang, D. S., Histone lysine methylation and congenital heart disease: From bench to bedside (Review). *Int. J. Mol. Med.* **2017,** *40* (4), 953-964.

58. Lorenzen, J. M.; Martino, F.; Thum, T., Epigenetic modifications in cardiovascular disease. *Basic Res. Cardiol.* **2012,** *107* (2:245),

59. Sun, G.-d.; Cui, W.-p.; Guo, Q.-y.; Miao, L.-n., Histone lysine methylation in diabetic nephropathy. *J. Diabetes Res.* **2014**, 654148/1-654148/10.

60. Collins, R. E.; Northrop, J. P.; Horton, J. R.; Lee, D. Y.; Zhang, X.; Stallcup, M. R.; Cheng, X., The ankyrin repeats of G9a and GLP histone methyltransferases are mono- and dimethyllysine binding modules. *Nat. Struct. Mol. Biol.* **2008,** *15* (3), 245-250.

61. Kramer, J. M., Regulation of cell differentiation and function by the euchromatin histone methyltranserfases G9a and GLP. *Biochem. Cell Biol.* **2015,** *94* (1), 26-32.

62. Tachibana, M.; Ueda, J.; Fukuda, M.; Takeda, N.; Ohta, T.; Iwanari, H.; Sakihama, T.; Kodama, T.; Hamakubo, T.; Shinkai, Y., Histone methyltransferases G9a and GLP form heteromeric complexes and are both crucial for methylation of euchromatin at H3-K9. *Genes Dev.* **2005,** *19* (7), 815-826.

63. Liu, N.; Zhang, Z.; Wu, H.; Jiang, Y.; Meng, L.; Xiong, J.; Zhao, Z.; Zhou, X.; Li, J.; Li, H.; Zheng, Y.; Chen, S.; Cai, T.; Gao, S.; Zhu, B., Recognition of H3K9 methylation by GLP is required for efficient establishment of H3K9 methylation, rapid target gene repression, and mouse viability. *Genes Dev.* **2015,** *29* (4), 379-393.

64. Ohno, H.; Shinoda, K.; Ohyama, K.; Sharp, L. Z.; Kajimura, S., EHMT1 controls brown adipose cell fate and thermogenesis through the PRDM16 complex. *Nature* **2013,** *504* (7478), 163-167.

65. Battisti, V.; Pontis, J.; Boyarchuk, E.; Fritsch, L.; Robin, P.; Ait-Si-Ali, S.; Joliot, V., Unexpected Distinct Roles of the Related Histone H3 Lysine 9 Methyltransferases G9a and G9a-Like Protein in Myoblasts. *J. Mol. Biol.* **2016,** *428* (11), 2329-2343.

66. Shankar, S. R.; Bahirvani, A. G.; Rao, V. K.; Bharathy, N.; Ow, J. R.; Taneja, R., G9a, a multipotent regulator of gene expression. *Epigenetics* **2013,** *8* (1), 16-22.

67. Yu, Y.; Song, C.; Zhang, Q.; DiMaggio, P. A.; Garcia, B. A.; York, A.; Carey, M. F.; Grunstein, M., Histone H3 lysine 56 methylation regulates DNA replication through its interaction with PCNA. *Mol. Cell* **2012,** *46* (1), 7-17.

68. Tachibana, M.; Sugimoto, K.; Nozaki, M.; Ueda, J.; Ohta, T.; Ohki, M.; Fukuda, M.; Takeda, N.; Niida, H.; Kato, H.; Shinkai, Y., G9a histone methyltransferase plays a dominant role in euchromatic histone H3 lysine 9 methylation and is essential for early embryogenesis. *Genes Dev.* **2002,** *16* (14), 1779-1791.

69. Tachibana, M.; Nozaki, M.; Takeda, N.; Shinkai, Y., Functional dynamics of H3K9 methylation during meiotic prophase progression. *EMBO J.* **2007,** *26* (14), 3346-3359.

70. Lehnertz, B.; Northrop, J. P.; Antignano, F.; Burrows, K.; Hadidi, S.; Mullaly, S. C.; Rossi, F. M. V.; Zaph, C., Activating and inhibitory functions for the histone lysine methyltransferase G9a in T helper cell differentiation and function. *J. Exp. Med.* **2010,** *207* (5), 915-922.

71. Roopra, A.; Qazi, R.; Schoenike, B.; Daley, T. J.; Morrison, J. F., Localized domains of G9a-mediated histone methylation are required for silencing of neuronal genes. *Mol. Cell* **2004,** *14* (6), 727-738.

72. Ballas, N.; Grunseich, C.; Lu, D. D.; Speh, J. C.; Mandel, G., REST and Its Corepressors Mediate Plasticity of Neuronal Gene Chromatin throughout Neurogenesis. *Cell* **2005,** *121* (4), 645-657.

73. Győry, I.; Wu, J.; Fejér, G.; Seto, E.; Wright, K. L., PRDI-BF1 recruits the histone H3 methyltransferase G9a in transcriptional silencing. *Nat. Immunol.* **2004,** *5* (3), 299-308.

74. Tachibana, M.; Matsumura, Y.; Fukuda, M.; Kimura, H.; Shinkai, Y., G9a/GLP complexes independently mediate H3K9 and DNA methylation to silence transcription. *EMBO J.* **2008,** *27* (20), 2681-2690.

75. Wagschal, A.; Sutherland, H. G.; Woodfine, K.; Henckel, A.; Chebli, K.; Schulz, R.; Oakey, R. J.; Bickmore, W. A.; Feil, R., G9a histone methyltransferase contributes to imprinting in the mouse placenta. *Mol. Cell. Biol.* **2008,** *28* (3), 1104-1113.

76. Leung, D. C.; Dong, K. B.; Maksakova, I. A.; Goyal, P.; Appanah, R.; Lee, S.; Tachibana, M.; Shinkai, Y.; Lehnertz, B.; Mager, D. L.; Rossi, F.; Lorincz, M. C., Lysine methyltransferase G9a is required for de novo DNA methylation and the establishment, but not the maintenance, of proviral silencing. *Proc. Nat. Acad. Sci.* **2011,** *108* (14), 5718-5723.

77. Dong, K. B.; Maksakova, I. A.; Mohn, F.; Leung, D.; Appanah, R.; Lee, S.; Yang, H. W.; Lam, L. L.; Mager, D. L.; Schubeler, D.; Tachibana, M.; Shinkai, Y.; Lorincz, M. C., DNA methylation in ES cells requires the lysine methyltransferase G9a but not its catalytic activity. *EMBO J.* **2008,** *27* (20), 2691-2701.

78. Epsztejn-Litman, S.; Feldman, N.; Abu-Remaileh, M.; Shufaro, Y.; Gerson, A.; Ueda, J.; Deplus, R.; Fuks, F.; Shinkai, Y.; Cedar, H.; Bergman, Y., De novo DNA methylation promoted by G9a prevents reprogramming of embryonically silenced genes. *Nat. Struct. Mol. Biol.* **2008,** *15* (11), 1176-1183.

79. Rathert, P.; Dhayalan, A.; Murakami, M.; Zhang, X.; Tamas, R.; Jurkowska, R.; Komatsu, Y.; Shinkai, Y.; Cheng, X.; Jeltsch, A., Protein lysine methyltransferase G9a acts on non-histone targets. *Nat. Chem. Biol.* **2008,** *4* (6), 344-346.

80. Zhang, X.; Huang, Y.; Shi, X., Emerging roles of lysine methylation on non-histone proteins. *Cell. Mol. Life Sci.* **2015,** *72* (22), 4257-4272.

81. Sampath, S. C.; Marazzi, I.; Yap, K. L.; Sampath, S. C.; Krutchinsky, A. N.; Mecklenbrauker, I.; Viale, A.; Rudensky, E.; Zhou, M. M.; Chait, B. T.; Tarakhovsky, A., Methylation of a histone mimic within the histone

methyltransferase G9a regulates protein complex assembly. *Mol. Cell* **2007,** *27* (4), 596-608.

82. Pless, O.; Kowenz-Leutz, E.; Knoblich, M.; Lausen, J.; Beyermann, M.; Walsh, M. J.; Leutz, A., G9a-mediated lysine methylation alters the function of CCAAT/enhancer-binding protein-β. *J. Biol. Chem.* **2008,** *283* (39), 26357-26363.

83. Ling, B. M. T.; Bharathy, N.; Chung, T.-K.; Kok, W. K.; Li, S.; Tan, Y. H.; Rao, V. K.; Gopinadhan, S.; Sartorelli, V.; Walsh, M. J.; Taneja, R., Lysine methyltransferase G9a methylates the transcription factor MyoD and regulates skeletal muscle differentiation. *Proc. Nat. Acad. Sci.* **2012,** *109* (3), 841-846.

84. Huang, J.; Dorsey, J.; Chuikov, S.; Zhang, X.; Jenuwein, T.; Reinberg, D.; Berger, S. L., G9a and Glp Methylate Lysine 373 in the Tumor Suppressor p53. *J. Biol. Chem.* **2010,** *285* (13), 9636-9641.

85. Portela, A.; Esteller, M., Epigenetic modifications and human disease. *Nat. Biotechnol.* **2010,** *28* (10), 1057-1068.

86. Kim, K.-B.; Son, H.-J.; Choi, S.; Hahm, J. Y.; Jung, H.; Baek, H. J.; Kook, H.; Hahn, Y.; Kook, H.; Seo, S.-B., H3K9 methyltransferase G9a negatively regulates UHRF1 transcription during leukemia cell differentiation. *Nucleic Acids Res.* **2015,** *43* (7), 3509-3523.

87. Lehnertz, B.; Pabst, C.; Su, L.; Miller, M.; Liu, F.; Yi, L.; Zhang, R.; Krosl, J.; Yung, E.; Kirschner, J.; Rosten, P.; Underhill, T. M.; Jin, J.; Hebert, J.; Sauvageau, G.; Humphries, R. K.; Rossi, F. M., The methyltransferase G9a regulates HoxA9-dependent transcription in AML. *Genes Dev.* **2014,** *28* (4), 317-327.

88. Kondo, Y.; Shen, L.; Suzuki, S.; Kurokawa, T.; Masuko, K.; Tanaka, Y.; Kato, H.; Mizuno, Y.; Yokoe, M.; Sugauchi, F.; Hirashima, N.; Orito, E.; Osada, H.; Ueda, R.; Guo, Y.; Chen, X.; Issa, J.-P. J.; Sekido, Y., Alterations of DNA methylation and histone modifications contribute to gene silencing in hepatocellular carcinomas. *Hepatology Res.* **2007,** *37* (11), 974-983.

89. Chen, M.-W.; Hua, K.-T.; Kao, H.-J.; Chi, C.-C.; Wei, L.-H.; Johansson, G.; Shiah, S.-G.; Chen, P.-S.; Jeng, Y.-M.; Cheng, T.-Y., H3K9 histone methyltransferase G9a promotes lung cancer invasion and metastasis by silencing the cell adhesion molecule Ep-CAM. *Cancer Res.* **2010,** *70* (20), 7830-7840.

90. Maze, I.; Covington, H. E.; Dietz, D. M.; LaPlant, Q.; Renthal, W.; Russo, S. J.; Mechanic, M.; Mouzon, E.; Neve, R. L.; Haggarty, S. J.; Ren, Y.; Sampath, S. C.; Hurd, Y. L.; Greengard, P.; Tarakhovsky, A.; Schaefer, A.; Nestler, E. J., Essential Role of the Histone Methyltransferase G9a in Cocaine-Induced Plasticity. *Science* **2010,** *327* (5962), 213-216.

91. Subbanna, S.; Shivakumar, M.; Umapathy, N. S.; Saito, M.; Mohan, P. S.; Kumar, A.; Nixon, R. A.; Verin, A. D.; Psychoyos, D.; Basavarajappa, B. S., G9a-mediated histone methylation regulates ethanol-induced neurodegeneration in the neonatal mouse brain. *Neurobiol. Dis.* **2013,** *54*, 475-485.

92. Schaefer, A.; Sampath, S. C.; Intrator, A.; Min, A.; Gertler, T. S.; Surmeier, D. J.; Tarakhovsky, A.; Greengard, P., Control of Cognition and Adaptive Behavior by the GLP/G9a Epigenetic Suppressor Complex. *Neuron* **2009,** *64* (5), 678-691.

93. Benevento, M.; van de Molengraft, M.; van Westen, R.; van Bokhoven, H.; Nadif Kasri, N., The role of chromatin repressive marks in cognition and disease: A focus on the repressive complex GLP/G9a. *Neurobiol. Learn. Mem.* **2015,** *124*, 88-96.

94. Antignano, F.; Burrows, K.; Hughes, M. R.; Han, J. M.; Kron, K. J.; Penrod, N. M.; Oudhoff, M. J.; Wang, S. K. H.; Min, P. H.; Gold, M. J., Methyltransferase G9A regulates T cell differentiation during murine intestinal inflammation. *J. Clin. Investig.* **2014,** *124* (5), 1945-1955.

95. Chen, X.; El Gazzar, M.; Yoza, B. K.; McCall, C. E., The NF-κB factor RelB and histone H3 lysine methyltransferase G9a directly interact to generate epigenetic silencing in endotoxin tolerance. *J. Biol. Chem.* **2009,** *284* (41), 27857-27865.

96. Imai, K.; Togami, H.; Okamoto, T., Involvement of Histone H3 Lysine 9 (H3K9) Methyltransferase G9a in the Maintenance of HIV-1 Latency and Its Reactivation by BIX01294. *J. Biol. Chem.* **2010,** *285* (22), 16538-16545.

97. Dobson, T. H. W.; Hatcher, R. J.; Swaminathan, J.; Das, C. M.; Shaik, S.; Tao, R. H.; Milite, C.; Castellano, S.; Taylor, P. H.; Sbardella, G.; Gopalakrishnan, V., Regulation of USP37 Expression by REST-Associated G9a-Dependent Histone Methylation. *Mol. Cancer Res.* **2017,** *15* (8), 1073-1084.

98. Kumar, V.; Kumar, V.; McGuire, T.; Coulter, D. W.; Sharp, J. G.; Mahato, R. I., Challenges and Recent Advances in Medulloblastoma Therapy. *Trends Pharmacol. Sci.* **2017,** *38* (12), 1061-1084.

99. Hoang, D. H.; Pagnier, A.; Guichardet, K.; Dubois-Teklali, F.; Schiff, I.; Lyard, G.; Cousin, E.; Krainik, A., Cognitive disorders in pediatric medulloblastoma: what neuroimaging has to offer. *J. Neurosurg. Pediatr.* **2014,** *14* (2), 136-44.

100. Palmer, S. L., Neurodevelopmental impact on children treated for medulloblastoma: a review and proposed conceptual model. *Dev. Disabil. Res. Rev.* **2008,** *14* (3), 203-210.

101. Taylor, P.; Fangusaro, J.; Rajaram, V.; Goldman, S.; Helenowski, I. B.; MacDonald, T.; Hasselblatt, M.; Riedemann, L.; Laureano, A.; Cooper, L.; Gopalakrishnan, V., REST Is a Novel Prognostic Factor and Therapeutic Target for Medulloblastoma. *Mol. Cancer Ther.* **2012,** *11* (8), 1713-1723.

102. Das, C. M.; Taylor, P.; Gireud, M.; Singh, A.; Lee, D.; Fuller, G.; Ji, L.; Fangusaro, J.; Rajaram, V.; Goldman, S.; Eberhart, C.; Gopalakrishnan, V., The deubiquitylase USP37 links REST to the control of p27 stability and cell proliferation. *Oncogene* **2012,** *32*, 1691-1701.

103. Kaniskan, H. U.; Konze, K. D.; Jin, J., Selective inhibitors of protein methyltransferases. *J. Med. Chem.* **2015,** *58* (4), 1596-1629.

104. Greiner, D.; Bonaldi, T.; Eskeland, R.; Roemer, E.; Imhof, A., Identification of a specific inhibitor of the histone methyltransferase SU(VAR)3-9. *Nat. Chem. Biol.* **2005,** *1* (3), 143-145.

105. Iwasa, E.; Hamashima, Y.; Fujishiro, S.; Higuchi, E.; Ito, A.; Yoshida, M.; Sodeoka, M., Total Synthesis of (+)-Chaetocin and its Analogues: Their Histone Methyltransferase G9a Inhibitory Activity. *J. Am. Chem. Soc.* **2010,** *132* (12), 4078-4079.

106. Fujishiro, S.; Dodo, K.; Iwasa, E.; Teng, Y.; Sohtome, Y.; Hamashima, Y.; Ito, A.; Yoshida, M.; Sodeoka, M., Epidithiodiketopiperazine as a pharmacophore for protein lysine methyltransferase G9a inhibitors: Reducing cytotoxicity by structural simplification. *Bioorg. Med. Chem. Lett.* **2013,** *23* (3), 733-736.

107. Cherblanc, F. L.; Chapman, K. L.; Reid, J.; Borg, A. J.; Sundriyal, S.; Alcazar-Fuoli, L.; Bignell, E.; Demetriades, M.; Schofield, C. J.; DiMaggio, P. A.; Brown, R.; Fuchter, M. J., On the Histone Lysine Methyltransferase Activity of Fungal Metabolite Chaetocin. *J. Med. Chem.* **2013,** *56* (21), 8616-8625.

108. Yuan, Y.; Wang, Q.; Paulk, J.; Kubicek, S.; Kemp, M. M.; Adams, D. J.; Shamji, A. F.; Wagner, B. K.; Schreiber, S. L., A Small-Molecule Probe of the Histone Methyltransferase G9a Induces Cellular Senescence in Pancreatic Adenocarcinoma. *ACS Chem. Biol.* **2012,** *7* (7), 1152-1157.

109. Fuller, R. W.; Nagarajan, R., Inhibition of methyltransferases by some new analogs of S-adenosylhomocysteine. *Biochem. Pharmacol.* **1978,** *27* (15), 1981-1983.

110. Borchardt, R. T.; Eiden, L. E.; Wu, B.; Rutledge, C. O., Sinefungin, a potent inhibitor of S-adenosylmethionine: Protein O-methyltransferase. *Biochem. Biophys. Res. Commun.* **1979,** *89* (3), 919-924.

111. Schluckebier, G.; Kozak, M.; Bleimling, N.; Weinhold, E.; Saenger, W., Differential binding of S-adenosylmethionine S-adenosylhomocysteine and Sinefungin to the adenine-specific DNA methyltransferase M.TaqI. *J. Mol. Biol.* **1997,** *265* (1), 56-67.

112. Devkota, K.; Lohse, B.; Staerk, D.; Clausen, R. P.; Liu, Q.; Wang, M.-W.; Berthelsen, J., Analogues of the Natural Product Sinefungin as Inhibitors of EHMT1 and EHMT2. *ACS Med. Chem. Lett.* **2014,** *5* (4), 293-297.

113. Liu, Q.; Cai, X.; Yang, D.; Chen, Y.; Wang, Y.; Shao, L.; Wang, M.-W., Cycloalkane analogues of sinefungin as EHMT1/2 inhibitors. *Bioorg. Med. Chem.* **2017,** *25* (17), 4579-4594.

114. Kubicek, S.; O'Sullivan, R. J.; August, E. M.; Hickey, E. R.; Zhang, Q.; Teodoro, M. L.; Rea, S.; Mechtler, K.; Kowalski, J. A.; Homon, C. A.; Kelly, T. A.; Jenuwein, T., Reversal of H3K9me2 by a small-molecule inhibitor for the G9a histone methyltransferase. *Mol. Cell* **2007,** *25* (3), 473-481.

115. Chang, Y.; Zhang, X.; Horton, J. R.; Upadhyay, A. K.; Spannhoff, A.; Liu, J.; Snyder, J. P.; Bedford, M. T.; Cheng, X., Structural basis for G9a-like protein lysine methyltransferase inhibition by BIX-01294. *Nat. Struct. Mol. Biol.* **2009,** *16* (3), 312-317.

116. Liu, F.; Chen, X.; Allali-Hassani, A.; Quinn, A. M.; Wasney, G. A.; Dong, A.; Barsyte, D.; Kozieradzki, I.; Senisterra, G.; Chau, I.; Siarheyeva, A.; Kireev, D. B.; Jadhav, A.; Herold, J. M.; Frye, S. V.; Arrowsmith, C. H.; Brown, P. J.; Simeonov, A.; Vedadi, M.; Jin, J., Discovery of a 2,4-Diamino-7-aminoalkoxyquinazoline as a Potent and Selective Inhibitor of Histone Lysine Methyltransferase G9a. *J. Med. Chem.* **2009,** *52* (24), 7950-7953.

117. Chang, Y.; Ganesh, T.; Horton, J. R.; Spannhoff, A.; Liu, J.; Sun, A.; Zhang, X.; Bedford, M. T.; Shinkai, Y.; Snyder, J. P.; Cheng, X., Adding a Lysine Mimic in the Design of Potent Inhibitors of Histone Lysine Methyltransferases. *J. Mol. Biol.* **2010,** *400* (1), 1-7.

118. Liu, F.; Chen, X.; Allali-Hassani, A.; Quinn, A. M.; Wigle, T. J.; Wasney, G. A.; Dong, A.; Senisterra, G.; Chau, I.; Siarheyeva, A.; Norris, J. L.; Kireev, D. B.; Jadhav, A.; Herold, J. M.; Janzen, W. P.; Arrowsmith, C. H.; Frye, S. V.; Brown, P. J.; Simeonov, A.; Vedadi, M.; Jin, J., Protein Lysine Methyltransferase G9a Inhibitors: Design, Synthesis, and Structure Activity Relationships of 2,4-Diamino-7-aminoalkoxy-quinazolines. *J. Med. Chem.* **2010,** *53* (15), 5844-5857.

119. Liu, F.; Barsyte-Lovejoy, D.; Allali-Hassani, A.; He, Y.; Herold, J. M.; Chen, X.; Yates, C. M.; Frye, S. V.; Brown, P. J.; Huang, J.; Vedadi, M.; Arrowsmith, C. H.; Jin, J., Optimization of cellular activity of G9a inhibitors 7-aminoalkoxy-quinazolines. *J. Med. Chem.* **2011,** *54* (17), 6139-6150.

120. Vedadi, M.; Barsyte-Lovejoy, D.; Liu, F.; Rival-Gervier, S.; Allali-Hassani, A.; Labrie, V.; Wigle, T. J.; DiMaggio, P. A.; Wasney, G. A.; Siarheyeva, A.; Dong, A.; Tempel, W.; Wang, S.-C.; Chen, X.; Chau, I.; Mangano, T. J.; Huang, X.-p.; Simpson, C. D.; Pattenden, S. G.; Norris, J. L.; Kireev, D. B.; Tripathy, A.; Edwards, A.; Roth, B. L.; Janzen, W. P.; Garcia, B. A.; Petronis, A.; Ellis, J.; Brown, P. J.; Frye, S. V.; Arrowsmith, C. H.; Jin, J., A chemical probe selectively inhibits G9a and GLP methyltransferase activity in cells. *Nat. Chem. Biol.* **2011,** *7* (8), 566-574.

121. Sugeno, N.; Jackel, S.; Kahle, P. J.; Sugeno, N.; Jackel, S.; Kahle, P. J.; Voigt, A.; Voigt, A.; Wassouf, Z.; Schulze-Hentrich, J., α-Synuclein enhances histone H3 lysine-9 dimethylation and H3K9me2-dependent transcriptional responses. *Sci. Rep.* **2016,** *6* (36328).

122. Sato, T.; Cesaroni, M.; Chung, W.; Panjarian, S.; Tran, A.; Madzo, J.; Okamoto, Y.; Zhang, H.; Chen, X.; Jelinek, J.; Issa, J.-P. J., Transcriptional Selectivity of Epigenetic Therapy in Cancer. *Cancer Res.* **2017,** *77* (2), 470-481.

123. Wu, W.; Nishikawa, H.; Fukuda, T.; Vittal, V.; Asano, M.; Miyoshi, Y.; Klevit, R. E.; Ohta, T., Interaction of BARD1 and HP1 Is Required for BRCA1 Retention at Sites of DNA Damage. *Cancer Res.* **2015,** *75* (7), 1311-1321.

124. Krivega, I.; Byrnes, C.; de Vasconcellos, J. F.; Lee, Y. T.; Kaushal, M.; Dean, A.; Miller, J. L., Inhibition of G9a methyltransferase stimulates fetal hemoglobin production by facilitating LCR/γ-globin looping. *Blood* **2015,** *126* (5), 665-672.

125. Chen, X.; Skutt-Kakaria, K.; Davison, J.; Ou, Y.-L.; Choi, E.; Malik, P.; Loeb, K.; Wood, B.; Georges, G.; Torok-Storb, B., G9a/GLP-dependent histone H3K9me2 patterning during human hematopoietic stem cell lineage commitment. *Genes Dev.* **2012,** *26* (22), 2499-2511.

126. Renneville, A.; Van Galen, P.; Canver, M. C.; McConkey, M.; Krill-Burger, J. M.; Dorfman, D. M.; Holson, E. B.; Bernstein, B. E.; Orkin, S. H.; Bauer, D. E.; Ebert, B. L., EHMT1 and EHMT2 inhibition induces fetal hemoglobin expression. *Blood* **2015,** *126* (16), 1930-1939.

127. Srimongkolpithak, N.; Sundriyal, S.; Li, F.; Vedadi, M.; Fuchter, M. J., Identification of 2,4-diamino-6,7-dimethoxyquinoline derivatives as G9a inhibitors. *Med. Chem. Commun.* **2014,** *5* (12), 1821-1828.

128. San José-Enériz, E.; Agirre, X.; Rabal, O.; Vilas-Zornoza, A.; Sanchez-Arias, J. A.; Miranda, E.; Ugarte, A.; Roa, S.; Paiva, B.; Estella-Hermoso de Mendoza, A.; Alvarez, R. M.; Casares, N.; Segura, V.; Martín-Subero, J. I.; Ogi, F.-X.; Soule, P.; Santiveri, C. M.; Campos-Olivas, R.; Castellano, G.; de Barrena, M. G. F.; Rodriguez-Madoz, J. R.; García-Barchino, M. J.; Lasarte, J. J.; Avila, M. A.; Martinez-Climent, J. A.; Oyarzabal, J.; Prosper, F., Discovery of first-in-class reversible dual small molecule inhibitors against G9a and DNMTs in hematological malignancies. *Nat. Commun.* **2017,** *8* (15424).

129. Sweis, R. F.; Pliushchev, M.; Brown, P. J.; Guo, J.; Li, F.; Maag, D.; Petros, A. M.; Soni, N. B.; Tse, C.; Vedadi, M.; Michaelides, M. R.; Chiang, G. G.;

Pappano, W. N., Discovery and Development of Potent and Selective Inhibitors of Histone Methyltransferase G9a. *ACS Med. Chem. Lett.* **2014,** *5* (2), 205-209.

130. Wagner, T.; Greschik, H.; Burgahn, T.; Schmidtkunz, K.; Schott, A.-K.; McMillan, J.; Baranauskiene, L.; Xiong, Y.; Fedorov, O.; Jin, J.; Oppermann, U.; Matulis, D.; Schuele, R.; Jung, M., Identification of a small-molecule ligand of the epigenetic reader protein Spindlin1 via a versatile screening platform. *Nucleic Acids Res.* **2016,** *44* (9), e88.

131. Kaniskan, H. U.; Jin, J., Chemical probes of histone lysine methyltransferases. *ACS Chem Biol* **2015,** *10* (1), 40-50.

132. Abad-Zapatero, C., Ligand efficiency indices for effective drug discovery. *Expert Opin. Drug Discov.* **2007,** *2* (4), 469-488.

133. Hu, Y.; Stumpfe, D.; Bajorath, J., Recent Advances in Scaffold Hopping. *J. Med. Chem.* **2017,** *60* (4), 1238-1246.

134. Sun, H.; Tawa, G.; Wallqvist, A., Classification of scaffold-hopping approaches. *Drug Discov. Today* **2012,** *17* (7-8), 310-324.

135. Schneider, G.; Neidhart, W.; Giller, T.; Schmid, G., "Scaffold-Hopping" by topological pharmacophore search: a contribution to virtual screening. *Angew. Chem., Int. Ed.* **1999,** *38* (19), 2894-2896.

136. Evans, B. E.; Rittle, K. E.; Bock, M. G.; DiPardo, R. M.; Freidinger, R. M.; Whitter, W. L.; Lundell, G. F.; Veber, D. F.; Anderson, P. S.; et, a., Methods for drug discovery: development of potent, selective, orally effective cholecystokinin antagonists. *J. Med. Chem.* **1988,** *31* (12), 2235-2246.

137. Morris, G. M.; Huey, R.; Lindstrom, W.; Sanner, M. F.; Belew, R. K.; Goodsell, D. S.; Olson, A. J., AutoDock4 and AutoDockTools4: Automated docking with selective receptor flexibility. *J. Comput. Chem.* **2009,** *30* (16), 2785-2791.

138. Cosconati, S.; Forli, S.; Perryman, A. L.; Harris, R.; Goodsell, D. S.; Olson, A. J., Virtual screening with AutoDock: theory and practice. *Expert Opin. Drug Discov.* **2010,** *5* (6), 597-607.

139. Xiong, Y.; Li, F.; Babault, N.; Wu, H.; Dong, A.; Zeng, H.; Chen, X.; Arrowsmith, C. H.; Brown, P. J.; Liu, J., Structure-activity relationship studies of G9a-like protein (GLP) inhibitors. *Bioorg. Med. Chem.* **2017,** *25* (16), 4414-4423.

140. Barker, A.; Kettle, J. G.; Nowak, T.; Pease, J. E., Expanding medicinal chemistry space. *Drug Discov. Today* **2013,** *18* (5-6), 298-304.

141. Bellomo, F.; Medina, D. L.; De Leo, E.; Panarella, A.; Emma, F., High-content drug screening for rare diseases. *J. Inherited Metab. Dis.* **2017,** *40* (4), 601-607.

142. Naylor, L. H., Reporter gene technology: the future looks bright. *Biochem. Pharmacol.* **1999,** *58* (5), 749-757.

143. Bervoets, I.; Charlier, D., A novel and versatile dual fluorescent reporter tool for the study of gene expression and regulation in multi- and single copy number. *Gene* **2018,** *642*, 474-482.

144. Sdelci, S.; Lardeau, C.-H.; Tallant, C.; Klepsch, F.; Klaiber, B.; Bennett, J.; Rathert, P.; Schuster, M.; Penz, T.; Fedorov, O.; Superti-Furga, G.; Bock, C.; Zuber, J.; Huber, K. V. M.; Knapp, S.; Mueller, S.; Kubicek, S., Mapping the chemical chromatin reactivation landscape identifies BRD4-TAF1 cross-talk. *Nat. Chem. Biol.* **2016,** *12* (7), 504-510.

145. Breslin, H. J.; Kukla, M. J.; Ludovici, D. W.; Mohrbacher, R.; Ho, W.; Miranda, M.; Rodgers, J. D.; Hitchens, T. K.; Leo, G.; et, a., Synthesis and Anti-HIV-1 Activity of 4,5,6,7-Tetrahydro-5-methylimidazo[4,5,1-jk][1,4]benzodiazepin-2(1H)-one (TIBO) Derivatives. *J. Med. Chem.* **1995,** *38* (5), 771-793.

146. Fulopova, V.; Gucky, T.; Grepl, M.; Soural, M., Solid-Phase Synthesis of Trisubstituted Benzo[1,4]-Diazepin-5-one Derivatives. *ACS Comb. Sci.* **2012,** *14* (12), 651-656.

147. Santilli, A. A.; Osdene, T. S., 5H-1,4-Benzodiazepin-5-ones. Ring-closure reactions with substituted 2-aminobenzamides. *J. Org. Chem.* **1964,** *29* (7), 1998-2003.

148. Fray, M. J.; Cooper, K.; Parry, M. J.; Richardson, K.; Steele, J., Novel Antagonists of Platelet-Activating Factor. 1. Synthesis and Structure-Activity Relationships of Benzodiazepine and Benzazepine Derivatives of 2-Methyl-1-phenylimidazo[4,5-c]pyridine. *J. Med. Chem.* **1995,** *38* (18), 3514-3523.

149. Hradil, P.; Grepl, M.; Hlavac, J.; Soural, M.; Malon, M.; Bertolasi, V., Some New Routes for the Preparation of 3-Amino-2-phenyl-4(1H)-quinolinones from Anthranilamides. *J. Org. Chem.* **2006,** *71* (2), 819-822.

150. Quinn, J. F.; Bryant, C. E.; Golden, K. C.; Gregg, B. T., Rapid reduction of heteroaromatic nitro groups using catalytic transfer hydrogenation with microwave heating. *Tetrahedron Lett.* **2010,** *51* (5), 786-789.

151. Castellano, S.; Tamborini, L.; Viviano, M.; Pinto, A.; Sbardella, G.; Conti, P., Synthesis of 3-Aryl/benzyl-4,5,6,6a-tetrahydro-3aH-pyrrolo[3,4-d]isoxazole Derivatives: A Comparison between Conventional, Microwave-Assisted and Flow-Based Methodologies. *J. Org. Chem.* **2010,** *75* (21), 7439-7442.

152. Malet-Sanz, L.; Susanne, F., Continuous Flow Synthesis. A Pharma Perspective. *J. Med. Chem.* **2012,** *55* (9), 4062-4098.

153. Onopchenko, A.; Sabourin, E. T.; Selwitz, C. M., Selective catalytic hydrogenation of aromatic nitro groups in the presence of acetylenes. Synthesis of (3-aminophenyl)acetylene via hydrogenation of dimethylcarbinol substituted (3-nitrophenyl)acetylene over heterogeneous metallic ruthenium catalyst. *J. Org. Chem.* **1979,** *44* (8), 1233-1236.

154. Sashida, H.; Fujii, A.; Sawanishi, H.; Tsuchiya, T., New synthetic routes to fully unsaturated 1,4-benzodiazepines from quinolyl azides. *Heterocycles* **1986,** *24* (8), 2147-2150.

155. Sashida, H.; Fujii, A.; Tsuchiya, T., Studies on diazepines. XXVII. Syntheses of fully unsaturated 1H- and 3H-1,4-benzodiazepines from 4-quinolyl azides. *Chem. Pharm. Bull.* **1987,** *35* (8), 3182-3189.

156. Sashida, H.; Kaname, M.; Tsuchiya, T., The first examples of isolated N-unsubstituted 1H-1,4-benzodiazepines. *Chem. Pharm. Bull.* **1987,** *35* (11), 4676-4679.

157. Sashida, H.; Kaname, M.; Tsuchiya, T., Studies of seven-membered heterocycles. XXXII. Synthesis of N-unsubstituted 1H-1,4-benzodiazepines stabilized by intramolecular hydrogen bonding. *Chem. Pharm. Bull.* **1990,** *38* (11), 2919-2925.

158. Hölz, K.; Lietard, J.; Somoza, M. M., High-Power 365 nm UV LED Mercury Arc Lamp Replacement for Photochemistry and Chemical Photolithography. *ACS Sustain. Chem. Eng.* **2017,** *5* (1), 828-834.

159. Kuznetsov, D. M.; Mukhina, O. A.; Kutateladze, A. G., Photoassisted Synthesis of Complex Molecular Architectures: Dearomatization of Benzenoid Arenes with Aza-o-xylylenes via an Unprecedented [2+4] Reaction Topology. *Angew. Chem., Int. Ed.* **2016,** *55* (24), 6988-6991.

160. Kaname, M.; Tsuchiya, T.; Sashida, H., Thermal ring contraction of 3H-1,4-benzodiazepines into quinazolines. *Heterocycles* **1999,** *51* (10), 2407-2413.

161. Leyva, E.; Platz, M. S.; Persy, G.; Wirz, J., Photochemistry of phenyl azide: the role of singlet and triplet phenylnitrene as transient intermediates. *J. Am. Chem. Soc.* **1986,** *108* (13), 3783-3790.

162. Morwick, T.; Berry, A.; Brickwood, J.; Cardozo, M.; Catron, K.; DeTuri, M.; Emeigh, J.; Homon, C.; Hrapchak, M.; Jacober, S.; Jakes, S.; Kaplita, P.; Kelly, T. A.; Ksiazek, J.; Liuzzi, M.; Magolda, R.; Mao, C.; Marshall, D.; McNeil, D.; Prokopowicz, A., III; Sarko, C.; Scouten, E.; Sledziona, C.; Sun, S.; Watrous, J.; Wu, J. P.; Cywin, C. L., Evolution of the Thienopyridine Class of Inhibitors of IκB Kinase-β: Part I: Hit-to-Lead Strategies. *J. Med. Chem.* **2006,** *49* (10), 2898-2908.

163. Hann, M. M.; Oprea, T. I., Pursuing the leadlikeness concept in pharmaceutical research. *Curr. Opin. Chem. Biol.* **2004,** *8* (3), 255-263.

164. Rishton, G. M., Nonleadlikeness and leadlikeness in biochemical screening. *Drug Discov. Today* **2003,** *8* (2), 86-96.

165. Lennernäs, H.; Aarons, L.; Augustijns, P.; Beato, S.; Bolger, M.; Box, K.; Brewster, M.; Butler, J.; Dressman, J.; Holm, R.; Julia Frank, K.; Kendall, R.; Langguth, P.; Sydor, J.; Lindahl, A.; McAllister, M.; Muenster, U.; Müllertz, A.; Ojala, K.; Pepin, X.; Reppas, C.; Rostami-Hodjegan, A.; Verwei, M.; Weitschies, W.; Wilson, C.; Karlsson, C.; Abrahamsson, B., Oral biopharmaceutics tools – Time for a new initiative – An introduction to the IMI project OrBiTo. *Eur. J. Pharm. Sci.* **2014,** *57* (Supplement C), 292-299.

166. Kansy, M.; Senner, F.; Gubernator, K., Physicochemical high throughput screening: parallel artificial membrane permeation assay in the description of passive absorption processes. *J. Med. Chem.* **1998,** *41* (7), 1007-1010.

167. Ottaviani, G.; Martel, S.; Carrupt, P.-A., Parallel artificial membrane permeability assay: a new membrane for the fast prediction of passive human skin permeability. *J. Med. Chem.* **2006,** *49* (13), 3948-3954.

168. Di, L.; Kerns, E. H.; Fan, K.; McConnell, O. J.; Carter, G. T., High throughput artificial membrane permeability assay for blood–brain barrier. *Eur. J. Med. Chem.* **2003,** *38* (3), 223-232.

169. Sugano, K.; Takata, N.; Machida, M.; Saitoh, K.; Terada, K., Prediction of passive intestinal absorption using bio-mimetic artificial membrane permeation assay and the paracellular pathway model. *Int. J. Pharm.* **2002,** *241* (2), 241-251.

170. Könczöl, Á.; Müller, J.; Földes, E.; Béni, Z.; Végh, K.; Kéry, Á.; Balogh, G. T., Applicability of a Blood–Brain Barrier Specific Artificial Membrane Permeability Assay at the Early Stage of Natural Product-Based CNS Drug Discovery. *J. Nat. Prod.* **2013,** *76* (4), 655-663.

171. Merten, O.-W.; Hebben, M.; Bovolenta, C., Production of lentiviral vectors. *Mol. Ther. Methods Clin. Dev* **2016,** *3* (16017).

172. Tiscornia, G.; Singer, O.; Verma, I. M., Production and purification of lentiviral vectors. *Nat. Protocols* **2006,** *1* (1), 241-245.

173. Andersson, B. S.; Collins, V. P.; Kurzrock, R.; Larkin, D. W.; Childs, C.; Ost, A.; Cork, A.; Trujillo, J. M.; Freireich, E. J.; Siciliano, M. J., KBM-7, a human myeloid leukemia cell line with double Philadelphia chromosomes lacking normal c-ABL and BCR transcripts. *Leukemia* **1995,** *9* (12), 2100-2108.

174. Carette, J. E.; Guimaraes, C. P.; Wuethrich, I.; Blomen, V. A.; Varadarajan, M.; Sun, C.; Bell, G.; Yuan, B.; Muellner, M. K.; Nijman, S. M.; Ploegh, H. L.; Brummelkamp, T. R., Global gene disruption in human cells to assign genes to phenotypes by deep sequencing. *Nat. Biotechnol.* **2011,** *29* (6), 542-546.

175. Shen, J.; Woodward, R.; Kedenburg, J. P.; Liu, X.; Chen, M.; Fang, L.; Sun, D.; Wang, P. G., Histone Deacetylase Inhibitors through Click Chemistry. *J. Med. Chem.* **2008,** *51* (23), 7417-7427.

176. Coffin, A. R.; Roussell, M. A.; Tserlin, E.; Pelkey, E. T., Regiocontrolled synthesis of pyrrole-2-carboxaldehydes and 3-pyrrolin-2-ones from pyrrole Weinreb amides. *J. Org. Chem.* **2006,** *71* (17), 6678-6681.

177. Fuglseth, E.; Anthonsen, T.; Hoff, B. H., New chiral building blocks from acetovanillone using lipase A and B from Candida antarctica. *Tetrahedron: Asymmetry* **2006,** *17* (8), 1290-1295.

178. Chou, L.-C.; Tsai, M.-T.; Hsu, M.-H.; Wang, S.-H.; Way, T.-D.; Huang, C.-H.; Lin, H.-Y.; Qian, K.; Dong, Y.; Lee, K.-H.; Huang, L.-J.; Kuo, S.-C., Design, Synthesis, and Preclinical Evaluation of New 5,6- (or 6,7-) Disubstituted-2-(fluorophenyl)quinolin-4-one Derivatives as Potent Antitumor Agents. *J. Med. Chem.* **2010,** *53* (22), 8047-8058.

Cover Image 1 (Top left) is adapted from Task, F. et al., *Nature* **2008,** *454*, 711-715.